SYLVESTRE AURELIANO CARVALHO

STABILITY AND COMPLEXITY IN EMERGENT COMPLEX ECOLOGICAL NETWORKS

Thesis submitted to the Federal University of Viçosa, Brazil, in partial fulfillment of the requirements of the Physics Post-Graduate Program for the degree of *Doctor Scientiae*.

Adviser: Marcelo Lobato Martins

Co-advisers: Sílvio da Costa Ferreira Junior
Hallan Souza e Silva
Ugo Bastolla

VIÇOSA - MINAS GERAIS
2019

Ficha catalográfica preparada pela Biblioteca Central da Universidade Federal de Viçosa - Câmpus Viçosa

T
C331s
2019

Carvalho, Sylvestre Aureliano, 1989-
Stability and complexity in emergent complex ecological networks / Sylvestre Aureliano Carvalho. – Viçosa, MG, 2019.
131f. : il. (algumas color.) ; 29 cm.

Texto em inglês.
Inclui apêndices.
Orientador: Marcelo Lobato Martins.
Tese (doutorado) - Universidade Federal de Viçosa.
Referências bibliográficas: f. 99-111.

1. Ecologia - Modelos matemáticos. 2. Padrão de formação (Biologia). 3. Predação. 4. Mutualismo. 5. Alelopatia. 6. Estabilidade estrutural. I. Universidade Federal de Viçosa. Departamento de Física. Programa de Pós-Graduação em Física Aplicada. II. Título.

CDD 22 ed. 577

SYLVESTRE AURELIANO CARVALHO

STABILITY AND COMPLEXITY IN EMERGENT COMPLEX ECOLOGICAL NETWORKS

Thesis submitted to the Federal University of Viçosa, Brazil, in partial fulfillment of the requirements of the Physics Post-Graduate Program for the degree of *Doctor Scientiae*.

APPROVED: December 18th, 2019.

Assent:

Sylvstre Aureliano Carvalho
Author

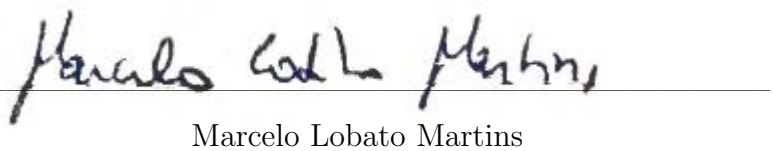

Marcelo Lobato Martins
Adviser

This thesis is dedicated to my mother Angela Aureliano and the memory of my grandma Maria Trindade, a strong and smart woman whom I still miss every day.

ACKNOWLEDGEMENTS

I would like to say a big thank you to my family. In special my mother (**Ângela**), my uncle (**Raimundo**) and my aunts (**Teca**, **Diva**, **Zita**, **Miza**) by all support at the crucial moment. A special thank you to my mother because always been supporting me in the decisions concerning the academic career. Regardless of anything, they are always there for me, and without them even knowing, they are the ones that make me strong enough to chase my dreams. Many thanks, **Dr. Lélis**, you are like my brother and a great example to me. I could not forget my grandma **Trindade** (*in memoriam*): you will always be remembered in my heart. His kindness and love have revealed to me something great; thank you very much. I wish you were alive today to celebrate this great moment of my life. I am very grateful to you for everything. Thus, thank you very much **Aureliano** family! If I had the chance of choosing my family, I would choose all of you again!

Next, I want to recognize the enormous influence of three of my former mentors, **Dra. Iraziet da Cunha Charret**, **Dr. Marcelo Lobato Martins** and **Dr. Ugo Bastolla Bufalini**. Many thanks, **Dra. Iraziet da Cunha Charret**, for introducing me to evolutionary theory, population dynamics, mathematical modeling and for showing me how cool it is to convey ideas using the language of mathematics. You directed me for guiding my first steps in theoretical ecology, and encouraging me to publish my first paper! Also, thank you for sparking my interest in biophysics and non-equilibrium thermodynamics. Because of you, I am doing what I do.

I want to express the deepest gratitude to **Dr. Marcelo Lobato Martins** for giving me the opportunity to work in his excellent research group during the past six years. I cannot imagine having a better supervisor than **Lobato**. With its free time monotonically decreasing, he read the n-th iterations of my manuscripts and engaged in long and late meetings. Thank you so much for the kindness of your priceless discussions that have taken place over the years where I have been able to learn a lot about biophysics and statistical physics. Thanks for the higher standards, for the openness to discuss off-topic but equally interesting subjects, for teaching me about political systems, and most importantly for making me focus on the important issues. And I must not forget all his patience and support regarding countless academic and non-academic matters.

Dr. Ugo Bastolla, I could have never imagined that someone important like you would be so nice and kind. You showed to me that we do not need to give up on things that we like to achieve our professional dreams, and how important is to have a balance between our professional and personal life. Without even realizing it, you taught me how discipline, time and organization are important to keep us going in the right direction. Thank

you very much for your kind words gave me great welcome, and help me with adaptation in Madrid. Also, I would like to speak thank you for your patience with the progress of the research project. I learned with you that we do not need to rush and that we always can make things better. Finally, thank you very much (grazie mille/muchísimas gracias) for all the opportunities that you gave me and, especially, thank you for making me feel welcome in your research group and in your house.

During my stay in Madrid, I made some very good friends that were important in the begging of my stay in Madrid. Thank you, friends, of lunchtime at Centro de Biología Molecular "Severo Ochoa"(CBMSO-UAM): **Ugo**, **David**, **Alex** and **Ana**. I would like to manifest here my sincere thank you to the friends of student house **César**, **Pedro** and **Janaína** for the great weekends we spend together. I had a super fun time with you, guys! I hope we can repeat it in the future.

Of course I also have to thanks all my friends from the "vicious city" (Viciosa/Viçosa), where everything was possible. Over these 6 years living in Viçosa is impossible do not think about a lot of big friends that are/were very important for every time. Thus, to represent all my "old friends" in Vicosa, I would like to say a special thank you to **Renan Loreto** and **Carlos Moreira Lima**. Thank you for being with me since my first years, for big matches of FIFA and for all setting up take-off for weekend! It does not matter how physically far we are, our friendship for each other is always the same; we will try to meet each other whenever possible. For the friends from my PhD program, I have to say thanks to people from "Salinha da Física" and "Galera do Almoço". In special, I would like to thanks my friends **Vivis**, **Leandro de Oliveira**, **Ulisses Moreira**, **Oscar Toro**, **Joaquim Gomes**, **Tiago Moura**, **Milton Lopes**, **Émerson Miranda**, **Hamilton Teixeira** and my older friends **Tatiane Podestá**, **Herman Fialho**, **Thiago Martins**, **Rafael Freitas**, and **Saulo Lima**. Thank you for being such amazing guys! All conversations/discussions/courses/projects/meetings/soccerGames/barbecues/beers were very important to me. I could not forget to thank the folks by the memorable trip to the Natal meeting: **Oscar**, **Tatiane**, **Ismael**, **Marlon**, **Eduardo**, **Cleidinéia**, **Anderson**, and **Aline**.

I would like to thank the Department of Physics and the Federal University of Viçosa for making this dream possible. I thank all the teachers who had the opportunity to take courses and learn from you. Also, I would like to thank those people who have been involved in event organizations, meetings or simple hall chat. You have always been helpful. I thank Professor **Márcio**, coordinator of the UFV graduate program, for all the support and assistance dedicated to students. Thank you also for opening the doors of your home for the memorable year-end barbecues for the Biological Physics group; those moments

will also be marked forever.

Finally, I also acknowledge to "**Brazilian Federal Agency for the Support and Evaluation of Graduate Education (CAPES)**" Finance Code 001, for the scholarships during both my doctorate at UFV - Viosa. Also, I would like to thank you to the funding agencies "**National Council for Scientific and Technological Development (CNPq)**" and "**Foundation for Research Support of the State of Minas Gerais (FAPEMIG)**" for the grants that partially supported the research activities of the thesis. I especially, acknowledge to CMBSO for ceding the infrastructure of the Bioinformatic Unit during the internship in Madrid.

"O homem não sabe mais que os outros animais; sabe menos. Eles sabem o que precisam saber. Nós não."

Fernando Pessoa (1888-1935)

ABSTRACT

CARVALHO, Sylvestre Aureliano, D.Sc., Universidade Federal de Viçosa, December, 2019. **Stability and complexity in emergent complex ecological networks**. Adviser: Marcelo Lobato Martins. Co-Advisers: Sílvio da Costa Ferreira Junior, Hallan Souza e Silva and Ugo Bastolla.

One of the main goals of theoretical ecology consists of determining the ecological forces that favor or not the maintenance of biodiversity in the face of species interactions and environmental perturbations. An approach to reach this goal is to describe the dynamics of the populations that form an ecological community through mathematical models of ecological interactions of different kinds (allelopathy, competition, mutualism, predation, etc), which are studied through numerical simulations and analytical approximations. In recent times, the evidence is mounting that the race of living organisms for adaptation to the chemicals synthesized by their neighbours may drive community structures. Particularly, some bacterial infections and plant invasions disruptive of the native community rely on the release of allelochemicals that inhibit or kill sensitive strains or individuals from their own or other species. On the other hands, the concept of structural stability, i.e., the maintenance of the model ecosystem under random changes in the parameters of the dynamical model, in particular, changes in the growth rates of the species that model environmental perturbations, has emerged as a key theoretical tool for characterizing the response of ecosystems to the fluctuations of the environment. In this thesis, an eco-evolutionary model and metacommunity pattern formation for community assembly through resource competition, allelopathic interactions, and evolutionary branching are presented and studied by numerical analysis. Our major findings are that stable communities with increasing biodiversity can emerge at weak allelopathic suppression, but stronger allelopathy is negatively correlated with community diversity. Furthermore, the heterogeneous patterns of these species emerge when diffusivity is low and the allelochemical network has cyclic interactions. The structural stability analysis of interactions as mutualism, competition, and predation shows that increasing biodiversity can be observed in mutualistic species (when the interspecific competition is weak), is impaired when the intragroup competition is considered, and predation interactions can increase or decrease the biodiversity (if the interspecific competition is weak or strong).

Keywords: Complex networks. Community structure. Ecological and evolutionary theory. Pattern formation. Competition. Predation. Mutualism. Allelopathy. Structural stability.

RESUMO

CARVALHO, Sylvestre Aureliano, D.Sc., Universidade Federal de Viçosa, dezembro de 2019. **Estabilidade e complexidade em redes ecológicas complexas emergentes**. Orientador: Marcelo Lobato Martins. Coorientadores: Sílvio da Costa Ferreira Junior, Hallan Souza e Silva e Ugo Bastolla.

Um dos principais objetivos da ecologia teórica consiste em determinar quais forças ecológicas favorecem ou desfavorecem a manutenção da biodiversidade em face das interações entre espécies e perturbações ambientais. Uma estratégia para alcançar esse objetivo, é representar a dinâmica de populações que formam uma comunidade ecológica por modelos matemáticos de interações ecológicas de diferentes tipos (alelopatia, competição, mutualismo, predação, etc.), que são estudados através de simulações numéricas e aproximações analíticas. Nos últimos anos, há evidências de que a corrida de organismos vivos para adaptação às substâncias químicas sintetizadas por seus vizinhos pode gerar estruturas comunitárias. Particularmente, algumas infecções bacterianas e invasões de plantas disruptivas da comunidade nativa dependem da liberação de aleloquímicos que inibem ou matam cepas sensíveis ou indivíduos de suas próprias espécies ou outras. Por outro lado, o conceito de estabilidade estrutural, ou seja, a manutenção do ecossistema sob mudanças aleatórias nos parâmetros do sistema dinâmico, em particular mudanças nas taxas de crescimento das espécies que modelam perturbações ambientais, emergiu como uma ferramenta teórica chave para caracterizar a resposta do ecossistema às flutuações do meio ambiente. Nesta tese, um modelo eco-evolucionário para a montagem de comunidades e a formação de padrões metacomunitários dirigidas pela competição por recursos, interações alelopáticas e ramificações evolutivas são apresentados e estudados por meio de análise numérica. Nossas principais descobertas são que comunidades estáveis com biodiversidade crescente podem emergir com supressão alelopática fraca, mas a alelopatia forte está correlacionada negativamente com a biodiversidade. Além disso, a formação de padrões heterogêneos dessas espécies alelopáticas emerge quando o coeficiente de difusão é baixo e a rede aleloquímica tem interação cíclica. A estabilidade estrutural de ecossistemas com interações do tipo mutualismo, competição e predação mostram que o aumento da biodiversidade pode ser observado em espécies mutualistas (quando a competição interespecífica é fraca), é desfavorecido quando a competição intragrupo é considerada, e pode aumentar ou diminuir a biodiversidade nas interações de predação (isso depende se a competição interespecífica for fraca ou forte).

Palavras-Chave: Redes complexas. Estutura comunitária. Teoria ecológica e evolucionária. Formação de padrões. Competição. Predação. Mutualismo. Alelopatia. Estabilidade estrutural.

LIST OF PUBLICATIONS

Scientific literature produced during the doctorate period is listed below.

- Jefferson Adriano Neves, Iraziet da Cunha Charret and Sylvestre Aureliano Carvalho. *Studying physics of greenhouse in 9th year:approach aimed meaningful learning.* **Experiências em Ensino de Ciências, 12(8)**, 66-87 (2017).

- S. A. Carvalho and M. L. Martins. *Invasion waves in the biochemical warfare between living organisms.* **Phys. Rev. E**, **97**, 042403 (2018).

- Carvalho, S. A; da Silva, S. O. and Charret, I. C. *Mathematical modeling of dengue epidemic: control methods and vaccination strategies.* **Theory Biosci, 138(223)**, 223-239 (2019) .

- CARVALHO, S. A. and MARTINS, M. L. *Biochemical Warfare Between Living Organisms for Survival: Mathematical Modelling.* **Reference Series in Phytochemistry. 1ed.: Springer International Publishing**, 1-38 (2019).

- Sylvestre Aureliano Carvalho and Iraziet da Cunha Charret. *Advances in the study of dengue epidemic spread: a brief overview.* **Journal of Vaccninology**, **1(1)**, 8-12 (2019).

- S. A. Carvalho and M. L. Martins. *Community structures in allelopathic interaction networks: An eco-evolutionary approach.* Submitted.

- Carvalho, S. A. and Martins, M. L. Pattern Formation in Allelopathic Species Networks. In preparation.

- U. Bastolla, A. Pascual-Garcia, S. A. Carvalho. *Mutualism favours the structural stability of complex ecological networks.* In preparation.

LIST OF ABBREVIATIONS

AB: Albert-Barabási
APE: Adapt/Persist/Evolve
ATP: Adenosine Triphosphate
BP: Branching Process
CCDF: Complementary Cumulative Distribution Functions
CDF: Cumulative Distribution Functions
DNA: Deoxyribonucleic Acid
E. coli: *Escherichia coli*
ER: Erdös-Rényi
FR: Functional Response
LRL: Little-Rock-Lake
LVM: Lotka-Volterra Model
NN: Nearest Neighbor
NNC: Nearest Neighbor Correlations
ODE: Ordinary Differential Equation
P. aurelia: *Paramecium aurelia*
P. caudatum: *Paramecium caudatum*
PDE: Partial Differential Equation
RB: Ravasz-Barabási
RPS: Rock-Paper-Scissor
RPSLS: Rock-Paper-Scissor-Lizard-Spock
SIE: Successive Invasion Events
WS: Watts-Strogatz

LIST OF FIGURES

LIST OF TABLES

CONTENTS

Chapter 1

General Introduction

1.1 Introduction

Earth Planet is changing with a speed that has never seen before. The technological advance since the industrial revolution and the disordered human growth after the First and Second World War generated environmental impacts that reflect in the organization of the living beings [1, 2]. Nowadays, species are more rapidly extinguishing than ever, transcending the five mass extinctions exhibited in the fossil record [2]. However, our lives are strongly dependent on resources dispensed by ecosystems. Thus the responses to global change of our natural heritage, habitat degradation of species and reduction of their biodiversity are of immediate concern and understanding the nature of extinction are relevant questions for guiding conservationist policies.

Even without the environmental impacts generated by humans, the interactions between species observed in nature are extremely complex. Extinctions, coexistence and biodiversity changing can be described by trophic webs and can be understood within the theoretical basis of complex networks, also used in other branches of science [3]. The mechanisms responsible for understanding the complexity, persistence and association in ecosystems was found essential to the stability and balance of the community structure [4, 5]. Previous studies [7, 6, 8] analyzed that increased complexity, measured by links among species, strength community stability. Within this proposal complexity has been related to richness, connectivity and interaction forces, whereas stability is related to strength and resilience. In contrast, several theoretical studies indicate that dynamical systems with random connections may be expected to be stable up to some critical level of the connectance, and become dynamically unstable for larger connectance [11, 12, 13]. Inspired by these studies, and applying results from random matrix theories [9, 10] showed analytically that the stability of model ecosystems connected through random interaction coefficients tends to decrease with the complexity of these interactions, in contrast with

the view reported above, founding the so-called "complexity-stability" debate.

Based on observational of several food webs analyzed through complex network theory [14] concluded that such relevant effects rarely propagate through food webs more than three links from the initial perturbation, displaying that the links among species are high. In complex system theory, this empirical evidence is known as small-world property and ecosystems with this property are highly complex and structurally stable. In the last years, Thilo Gross et al. [15] confirmed through the numerical study of food webs ensemble that the complexity of the networks is negatively correlated with dynamical stability. Relationships between complexity and stability still remain open. The "conventional wisdom" that more complex communities are more stable has been confirmed in some studies, but it is not possible to generalize the static view of communities to a scenario of dynamic balance.

Nowadays, there is mounting evidence that trophic interactions as resource competition and predator-prey are insufficient to explain the diversity in communities of macro and microbial organisms. Positive nontrophic interactions and war alliances between independent organisms in nature also play a major role in communities [16]. These interactions are mediated through changes in the abiotic environment or through other organisms. For instance, mycorrhizal networks facilitate and influence seedling in plant communities, by altering plant-plant interactions and by supplying and recycling nutrients [17]. The network of ecological interactions between species has a deep influence on the stability and balance of the community [4, 5]. On the other hand, the toxin uptake observed in communities of bacteria, fungi, plants, cells, and some animals highlight the need to address another type of interaction: allelopathy. This interspecific interaction consists of release secondary metabolic compounds in the environment that affect negatively survival or growth rate of the affected species.

The concept of structural stability, i.e., an external environmental perturbation in the parameter of dynamical model [120, 176], has been applied to study the relationship between structural stability of communities, their network structure and the nature of the ecological interactions connecting their species. This is one of the central themes of theoretical ecology. For instance, by exploring how the size of the community and the degree of connectivity between the species influences stability, it was found that the extinction of generalist species, which are the most connected in the community food chain, produces massive extinctions in the community [20].

Pattern formation in population dynamics has been studied both experimentally and theoretically. In experiments, the dynamics of insects, corals, lizards, plants and bacterial colonies, amongst others, have been observed [24, 23, 22, 21]. Some of them evidence certain species presents cyclic interactions mediated by toxins. However, is often difficult to control biological parameters such as initial concentration or mobilities of every individual type or external disturbances. Fortunately, there is a type of cyclic interactions

observed in communities composed of three strains of bacteria *Escherichia coli* that allows laboratory control of some parameters. *E. coli* are commonly found in human and animal intestines and its toxins have been applied to the development of antibiotics and food preservatives [25, 26]. The use of *E. coli* in the laboratory is facilitated by their rapid growth and simple nutritional needs [153]. Therefore, the outcome of different cultivation strategies can be evidenced in the laboratory. From the theoretical viewpoint, mean-field descriptions render macroscopic or mesoscopic approximations to describe the behavior of such complex systems, but to take into account spatial inhomogeneities, one may construct partial differential equation models [27, 28].

So, network models have become indispensable tools for helping understand the biological processes responsible for the stability and sustainability of biological systems [29]. The study of mechanisms capable of supporting greater biodiversity is interesting both for understanding how species interactions occur, as well as pointing out the factors in the environment that are important for the preservation of biodiversity. Within this context, it is ubiquitous and immediate to understand the relationship between complexity and stability of ecosystems is of key importance for the maintenance of the balance of human growth and the conservation of all the natural services that ecosystems provide [30].

In this work, we propose a model to study the allelopathic interaction dynamics between individuals considering successive invasion events and branching processes. Our goals are to analyze the effect of disturbances in the system's dynamics and how different allelopathic interaction networks can increase or decrease community diversity. The spatially extended version of the model was also studied for different networks of allelochemical interactions to determine the main dynamical aspects responsible for generating heterogeneous spatial patterns. Finally, the structural stability analysis for species interacting through mutualism, competition, and predation was made. We aim to verify which of these interactions are capable of reinforce structural stability or increase community diversity.

1.2 Thesis Objectives

The present thesis addresses the debate on the relationship between complexity and stability of biological communities driven by allelopathy, mutualism, competition and predation interactions. Specifically, our goals are understanding the network properties of communities assembled from allelopathic species and investigate the structural stability of ecosystems subjected to distinct types of interactions (mutualistic versus prey-predators).

1.3 Thesis Outline

Chapter 2 reviews the basic concepts on complex networks and its main topological properties such as degree, average connectivity, degree distribution, average path length, clustering coefficient, nearest neighbour correlation, centrality and entropy used to characterize the model for community assemble proposed here. Also, four paradigmatic network models namely Random (Erdös-Rényi), Small-World (Watts-Strogatz), Scale-Free (Barabási-ALbert), and Hierarchical (Ravasz-Barabási) models traditionally used as standards for comparison with other complex networks will be discussed. In addition, the main phenomenology of competition and allelopathic interactions that driven our community assembly models are highlighted. Finally, central debate on the relationship between complexity and stability in ecological theory and real ecosystems is considered.

In *Chapter* 3 a Lotka-Volterra competition model to describe the population dynamics of microorganisms and plants that synthesize and secrete secondary chemicals is proposed. The model contains $2\,N$ ODEs describing species and toxins time evolutions. Its main terms take into account toxin exudation, species mortality, toxins consume and natural degradation. The mortality due to allelopathy is described by Holling type I, II and III functional responses. We also tested distinct toxin uptake regimes. Analytical results for the two species competition involving one or two allelopathic species and for non-allelopathic, competing species are presented. Numerical results assembled through invasion and speciation events are shown for the topological properties of connectivity networks.

In *Chapter* 4 a spatially-explicit version of our Lotka-Volterra Model for a fixed number of allelopathic species competing for resources is considered. Pattern formation in spatially heterogeneous allelopathic models is the focus. Holling type I functional response was used and several allelochemical networks tested. Distinct patterns, from homogeneous to disordered or spiral waves were observed as diffusion coefficients were varied. Spiral patterns are formed when the number of species is odd and the allelopathic network exhibits cyclic dynamics. In contrast, when the species number is even, the spiral break up and form disordered spatial structures.

In *Chapter* 5, was considered a dynamical model with the within-group competition of Lotka-Volterra type and between-group mutualistic, competition or predation interactions using a functional response that saturate with the abundance. To study the relationship between the structural stability of species communities, and the network structure and nature of the ecological interactions that connect these species, initially considering the theory typically used on stability analysis. So, we can use the classical dynamical stability analysis, where the initial abundances and parameters of the dynamical system are perturbed, to an analysis where the growth rates are perturbed for a given feasible equilibrium.

Finally, a summary of the main results of this thesis and its contribution to debate complexity-stability in theoretical ecology compose *Chapter* 6.

Chapter 2

Fundamentals of Network Theory and Ecological Communities

Biological systems ranging from food webs in ecology to the molecular biology of the biochemical warfare between living organisms can benefit greatly from complex network analysis. Networks offer a quantitative description and play an important role in the characterization of various ecological systems, as for instance in understanding community structure, food webs, biomass, species-abundance distributions, spatial patterns of species and flows of energy and matter in ecosystems [31, 32, 7, 33]. In particular the race of plants, microbes, insects and even cells (e.g., within a tumor) for adaptation to the chemicals synthesized by their neighbors may drive species coexistence and community composition. These systems are well captured by network representations and for this reason, the basic concepts of complex networks and ecological communities are revised in this *Chapter*.

2.1 Complex Network Metrics

As a mathematical modeling tool, the definition of an interaction network for an arbitrary system is frequently not unique (see for example the case of interaction networks [9, 34, 35]). However, many topological properties appear to be independent of the definition of the network [36]. Moreover, some of those properties have emerged in the last years as universal features among systems otherwise considered very different from each other [3]. Here, the most basic network measures that allow us to compare and characterize different properties of complex networks will be defined. For a detailed overview of complex network theory, the readers can refer [3, 37, 38, 39].

(a) **Network**: A network is represented by a graph $G(n, l)$, where each element of this set is represented by a node (or vertex) n, and the relation between a pair of nodes is

represented by a connecting link (or edge) l. Edges can be weighty, directed, undirected or yet bi-directional. Vertex linked by a single edge is called nearest neighbours. Link in networks, i.e., those with symmetry or not and weighted or not edges are represented by a matrix known as the adjacency matrix. When two nodes i and j are neighbours, the adjacency matrix element is $\zeta_{i,j} = 1$ and $\zeta_{i,j} = 0$ otherwise. Standard metrics of interest that help to characterize the topology and complexity of networks include node degree, connectivity, degree distribution, clustering coefficient, nearest neighbor correlations, and centrality [40]. Here, solely these basic properties of complex networks will be revised.
(b) **Degree**: The most fundamental property of a vertex is its degree (or connectivity), k, which provides the number of links each node has to other nodes. For example, in the undirected network shown in Figure 2.1-(a), node D has degree $k = 6$. In directed networks (see Figure 2.1-(b)) there is an incoming degree, k_{in}, which denotes the number of links that point to a node, and an outgoing degree, k_{out}, which denotes the number of links that start from it. For example, node D in Figure 2.1-(b) has $k_{in} = 4$ and $k_{out} = 2$. An undirected network with n nodes and l links is characterized by an average degree $\langle k \rangle = 2\,l/n$ (where $\langle\rangle$ denotes the average) [31].

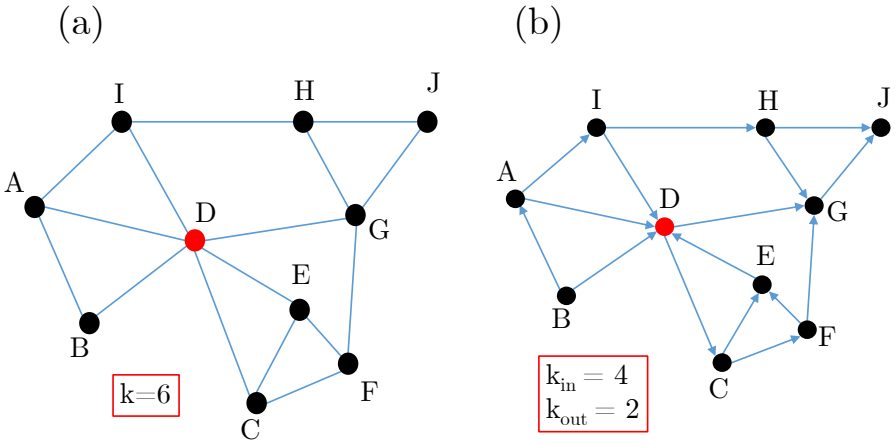

Figure 2.1: Schematic representation of (a) non-directed and (b) directed graphs with 10 nodes. The node D is highlighted in red because it is the node that has the highest connectivity.

(c) **Average Connectivity**: In a network of size n, the connectivity $C(n)$ is defined as the fraction of non-diagonal matrix elements different from zero. So considering a $n \times n$ adjacency matrix $\zeta_{i,j}$, the total connectivity is given by $C(n) = \frac{\sum_{i,j} \zeta_{i,j}}{n\,(n-1)}$. The connectivity of biological networks is often informative with respect to the network structure, like trophic relationships and food-web networks [41].
(d) **Degree Distribution**: The degree distribution, $P(k)$, gives the probability that a

selected node has exactly k links. The distribution $P(k)$ is obtained by computing the frequency of nodes with connectivity k, i.e., counting the number of nodes $n(k)$ with k links and dividing it by the total number of nodes n. The degree distribution allows us to distinguish between different classes of networks. For example, a peaked degree distribution, as seen in a random network (see section 2.2.1), indicates that the system has a characteristic degree and that the chance to find highly connected nodes (which are also known as hubs) is extremely small. In contrast, a power-law degree distribution indicates that the presence of a few hubs has a small but no negligible probability (see section 2.2.3). In some cases, there is interest in determining the Cumulative Distribution Function (CDF) or Cumulative Complementary Distribution Function (CCDF). For more details see appendix A.3.

(e) **Mean-Shortest Path Length**: This quantity is defined as the average of the minimum value of the distance $\delta(i, j)$ taken over all pairs of distinct vertices, $i, j \in n(G)$ which are connected by at least one path. More specifically, the average path length of a network is the average number of links between vertices which must be crossed in the shortest path between any two nodes. For non-directed networks it is calculated as $\langle l \rangle = \frac{2}{n(n-1)} \sum_{i=1}^{n} \sum_{j=1}^{n} \delta_{min}(i, j)$ and for directed networks the mean-shortest path length is $\langle l \rangle = \frac{1}{n(n-1)} \sum_{i=1}^{n} \sum_{j=1}^{n} \delta_{min}(i, j)$, where $\delta_{min}(i, j)$ is the minimum distance between nodes i and j.

(f) **Clustering Coefficient (Cc)**: To characterize neighbors network's structure, D. J. Watts e S. H. Strogatz [42] defined, in 1998, the clustering coefficient Cc_i of the node i as the ration between the number b_i of links connecting their neighbors and the maximum number of possible connections between these neighbors. For an undirected graph, the clustering coefficient is $Cc_i = 2b_i/k_i(k_i - 1)$. In effect, Cc quantifies the density of 'triangles' in a network having the node i as vertex, whereas $k_i(k_i - 1)/2$ is the total number of such triangles if all neighbors of node i are connected to each other. In the case of $k_i = 0$ or 1, then $Cc_i = 0$. The average clustering coefficient $\langle Cc \rangle$ gives the mean value of Cc_i; considering n nodes in a network, the average clustering coefficient is $\langle Cc \rangle = \frac{1}{n} \sum_{i=1}^{n} Cc_i$. The fully connected network has $\langle Cc \rangle = 1$. In a social network of friendships, if node i is connected to j, and j is connected to l, then there is a "good chance" that i also has a direct link to l. In other words, many of my friends are friends with each other. For many real networks $Cc(k) \sim k^{-1}$, which is an indication of a network's hierarchical character [43, 44] (see section 2.2).

In the same way, concerning directed networks, the clustering coefficient Cc_i for every node i has two components defined by [3]:

$$
\begin{aligned}
Cc_i^{in} &= \frac{(\zeta^T \zeta^2)_{ii}}{k_i^{in}(k_i^{in}-1)} \\
Cc_i^{out} &= \frac{(\zeta^2 \zeta^T)_{ii}}{k_i^{out}(k_i^{out}-1)}
\end{aligned}
\tag{2.1}
$$

where ζ is the network adjacency matrix.

(g) **Nearest Neighbors Correlation (NNC)**: A typical feature of networks is the tendency of nodes with a given degree to connect to nodes with similar or dissimilar degrees. Therefore, degree correlations capture the relationship between the degrees of nodes that link to each other [37]. One way to quantify the magnitude of degree correlations is to measure, for each node i, the average degree of its neighbors $k_{nn}(k_i) = \frac{1}{k_i}\sum_{j=1}^{n}\zeta_{i,j}\,k_j$ [45]. The behavior of the degree correlations is obtained averaging the degree of the nearest neighbors (NN), $k_{nn}(k)$, for vertices of degree k: $k_{nn}(k) = \sum_{k'} k' P(k'|k)$. Here $P(k'|k)$ is the conditional probability that following a link leaving a k-degree node we reach a k'-degree node [47]. If $P(k'|k)$ is just a function of k', then $k_{nn}(k)$ is a constant (see Figure 2.2-(a)) and degrees of neighboring vertices are uncorrelated. If vertices with higher or low degrees have the tendency to connect with vertices with similar degrees, k_{nn} increases with k (see Figure 2.2-(b)) and the network is called assortative. Conversely, if the vertices with a higher degree have a larger probability to connect with other low degree vertices then the network is called disassortative [48, 49], and k_{nn} decreases with k (see Figure 2.2-(c)).

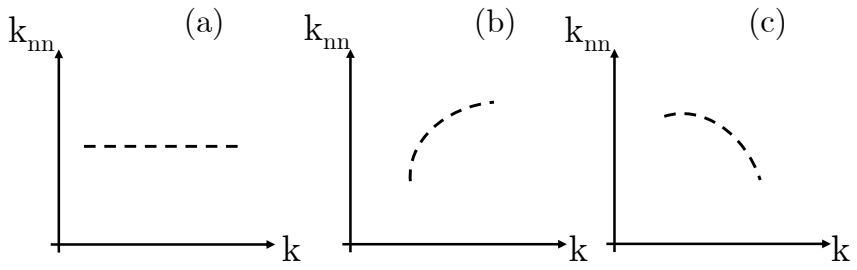

Figure 2.2: Schematic representation of nearest neighbors correlation functions: (a) $k_{nn}(k)$ is a constant and the nodes are uncorrelated. (b) $k_{nn}(k)$ increases with the degree indicating the presence of positive correlations between the nodes of the network (assortativity). Finally, in (c), $k_{nn}(k)$ has a decreasing trending, meaning that the network is negatively correlated (disassortativity).

(h) **Centrality**: In graph theory, a fundamental aspect of the analysis is to decide which are the most important (central) elements, i.e., those that, if eliminated, cause more damage to the network. A measure of the centrality of a node must be a function $c_x : n \to \mathbb{R}$ constructed in such a way that the order relation $c_x(n_i) > c_x(n_j)$ reflects the percep-

Properties	Random Network	Scale-Free Network	Small-World Network
Maximum Degree	10	21	10
Average Degree	4.0	3.94	4.0
Degree Distribution	Poisson	Power Law	Poisson-like
Average Path Length	3.38	3.08	4.0
Clustering Coefficient	0.045	0.156	0.544
Entropy	2.9	2.3	0.9

Table 2.1: Comparison of some properties of graphs ($n = 100$ nodes, $m = 200$ links and $p = 5\%$ - link probability) for distincts types of networks. Table adapteded from Ref. [51].

tion that i is more central than j in some sense. Several metrics have been proposed to measure the centrality of a node: *degree centrality*, *closeness centrality*, and *shortest path betweenness centrality*. Here, we highlighted the betweenness centrality, which measures the extent to which a node lies on paths of minimal length connecting to other nodes. Nodes with high betweenness centrality often have significant influence on the network dynamics. Mathematically, the betweenness centrality x_i of a node i is defined as $x_i = \sum_{j,k} n^i_{j,k}$, where $n^i_{j,k} = 1$ if the node i lies on the path of minimal length from node j to node k and $n^i_{j,k} = 0$ if i does not or if there is no such path.
(i) **Entropy**: The Shannon S-entropy [50] $S[P] = -\Sigma_k P(k)\, log\, P(k)$ can be used to quantify the disorder or uncertainty associated with a random variable or a random process. Here, $P(k)$ is the probability of a system to be in a cell k of the phase space. In some cases, log base 2 can be used, defining the Korner's entropy $H[P] = -\Sigma_k P(k)\, log_2\, P(k)$ [52].

On one hand, more random the graph is, that is, more homogeneous is its degree distribution, the greater is its entropy. On the other hand, the more structured the graph is, the smaller its entropy is, such that regular networks would have zero entropy [51]. For highly heterogeneous networks, such as scale-free networks, connectivity distribution asymptotically follow power laws and their entropies have intermediate values. Table 2.1 lists the typical values for some properties of networks. In particular, the entropy for scale-free networks is smaller than for random graphs, since scale-free networks are not completely unstructured due to the rule of preferential attachment (see *Chapter* 2.2).

2.2 Complex Networks Models

Several complex network models are crucial for shaping our understanding of natural and artificial networks observed in nature and help to describe characteristics and global structures of such networks [31]. There are four models that had a direct impact on biological network studies, and they are the four of this section.

2.2.1 Random Networks

The random network model [53] defined by Erdös-Rényi (ER) is built from n nodes and l edges which can connect randomly chosen node pairs with probability p. This model generates a graph with approximately $p\,n(n-1)/2$ randomly distributed edges (see figure 2.3-(a)), disregarding self-connection. The node degrees follow a binomial distribution, which in the limit ($n \to \infty$ and $\langle k \rangle$ fixed) becomes the Poisson distribution (see Figure 2.3-(b)). Therefore the probability of a vertex to have degree k is $P(k) \sim e^{-\langle k \rangle} \frac{\langle k \rangle^k}{k!}$, where $\langle k \rangle$ is the average connectivity of the network (see Appendix A.2). This indicates that the vertices have approximately the same number of edges (close to the average degree $\langle k \rangle$). The vertices with higher or lower degrees (tails of the distribution) are extremely rare because the degree distribution $P(k)$ in these regions deviating significantly from the average decreases exponentially. The clustering coefficient $Cc(k)$ is independent of the vertex's degree k, so $Cc(k)$ follow as a constant (see Figure 2.3-(c)). Finally, the mean path length is proportional to the logarithm of the network size, $l \sim logN$, indicating that random networks are characterized by the small-world property. This type of topology characterizes many biological networks, like food webs in which often happens that paths of few (three-four) interactions link most species [54]. As a consequence, local changes in species concentration by local perturbations in these networks will propagate throughout the entire network [53].

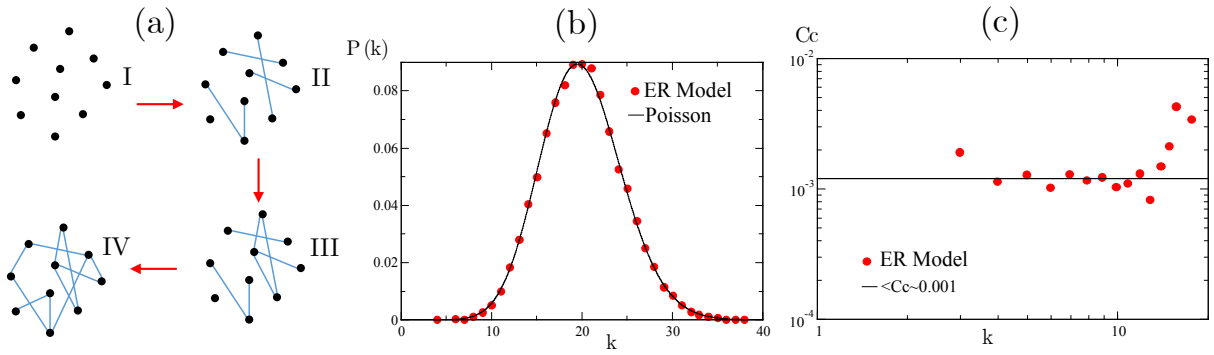

Figure 2.3: Random network model (ER): (a) Evolution of a random graph with 10 isolated nodes. Every pair of nodes were connected with probability (I) p=0, (II) p=0.1, (III) p=0.15 and (IV) p=0.25, respectively. (b) Degree distribution of the random graph. The red circles show the degree distribution, or n_k/n, the fraction of nodes with k links as a function k, for a single instance of the binomial random graph $G(n,p)$ with $n = 2 \times 10^4$ nodes and the probability $p = 10^{-3}$ for a link connect two nodes. The continuous black line is a plot of the Poisson distribution $P(k)$ with $\langle k \rangle = p\,n = 20$. (c) The clustering coefficient Cc is independent of node degrees. For the parameters used in (b), $Cc \sim 0.001$ is obtained. Figure built from Ref. [53]

2.2.2 Small-World Networks

The small-world model (WS) was introduced to describe networks that follow the small-world topology [42] and can be generated by the following algorithm: i) Start with a ring lattice with n vertices. Initially, every vertex is connected to its first k neighbors ($k/2$ on either side). In order to always have a sparse but connected network, consider $n \gg k \gg ln(n) \gg 1$. ii) Randomly rewire each edge of the lattice with probability p such that self-connections and duplicated edges are excluded. Within this context, rewire a link means leave the first vertex unchanged and choose the second vertex at random. This process doesn't allow self-loops or more than one link connecting the same two vertices. Also, it introduces $p\,n\,k/2$ long-range edges linking nodes that otherwise would be part of different neighborhoods. By varying p one can closely monitor the transition between order $p = 0$ and randomness $p = 1$. Figure 2.4-(a) shows a schematic representation of graphs with $n = 20$, $k = 4$, and a range of values of p. When $p = 0$, the graph is a ring lattice (regular structure). For increasing randomness, the graph' structure exhibit small-world properties, while for $p = 1$, it is completely random. The degree distribution generated by WS model varies. When p is 0, all the nodes have the same degree, k, hence the degree distribution is just a Dirac-delta function centered on k: $\delta(x - k)$. However, when p increases, the degree distribution changes and becomes a picked distribution, typical of random networks (see Figure 2.4-(b)). In addition, in the region (highlighted) where the clustering coefficient Cc is high enough and the average path length l is short enough (see Figure 2.4-(c)) in comparison to their values for random and regular' networks, one finds the emergent small-world characteristics of organisms/organizations that persist and resonate over space and time. It is only within this narrow band that systems adapt/persist/evolve (APE) [55].

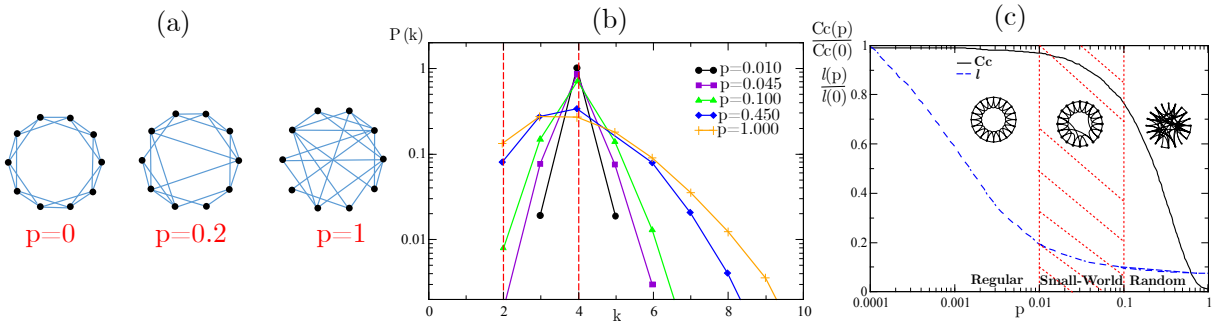

Figure 2.4: Small-world network model (WS): (a) Schematic representation of graphs with $l = 20$ and $k = 4$ for: completely regular network $p = 0$ (left), small-world network $p = 0.2$ (middle), and random network $p = 1$ (right). (b) Degree distribution of WS network for $n = 2000$, $k = 4$ and distinct p values. This plot shows curves only for connectivity values greater than $k/2$ and the mean degree is $\langle k \rangle = 4$. (c) Clustering coefficient (Cc) for WS graphs with $n = 2000$, $k = 4$, as a function of p and normalized for the regular case. Figure build from Ref. [42]

2.2.3 Scale-Free Networks

To explain the origin of the power-law degree distribution, Barabsi and Albert (BA) proposed another network model [56, 57]. The BA model of scale-free networks (see Figure 2.5) can be constructed by iteratively performing two steps of self-organization: growth and preferential attachment. The generation scheme of a BA scale-free model is the algorithm: i) Growth: start with a small number m_0 of nodes; at every time point, a new node is introduced and is connected to $m \leq m_0$ already-existing nodes. ii) Preferential Attachment: The probability Π_i that a new node will be connected to an already existing node i (one of the m already-existing nodes) depends on its degree k_i and is given by $\Pi_i = k_i / \sum_j k_j$, where the sum extends over all the networks nodes j. After t time steps, this algorithm results in a network with $N = t + m_0$ nodes and $m\,t$ edges (see scheme in the Figure 2.5-(a)). The networks generated by this growth process have a power law degree distributions $P(k) \sim k^{-\gamma}$, with degree exponents $\gamma < 3$ for a wide range of scales (see Figure 2.5-(b)). For finite size networks, a cutoff appears for some maximum degree k_{max}; and the degree distribution is generally well described by $P(k) \sim k^{-\gamma} e^{-k/k_{max}}$ [58, 59]. In the BA model, the networks present an inhomogeneous structure (see Appendix A.2), and thus the probability that a node is highly connected is statistically more significant than in a random network. The networks generated by the BA model do not exhibit a neat scaling of the clustering coefficient, for $Cc(k)$ appears to be a constant (see Figure 2.5-(c)), meaning no inherent modularity. Moreover the average path length scales as $l \sim loglogN$, which is significantly shorter than $logN$ that characterizes random small-world networks.

2.2.4 Hierarchical Networks

The hierarchical network model introduced by Ravasz-Barabási (RB)[43, 44] aims to describe the multi-layered organization of systems in which a few top-level elements are related to many elements on intermediate levels, which are in turn related to an even greater number of bottom-level elements. To explain the origin of the coexistence between modularity, local clustering, and scale-free topology, the RB model starts from a graph with a small cluster of four densely connected vertices (see the first graph in Figure 2.6-(a)). The second step is to create three replicas of this initial module and link the three external vertices of the replicated clusters to the central vertex of the old cluster. The result is a large 16-vertex module (see the second graph in Figure 2.6-(a)). Recursively, three replicas of this 16-vertex module (red) are generated and each one of their

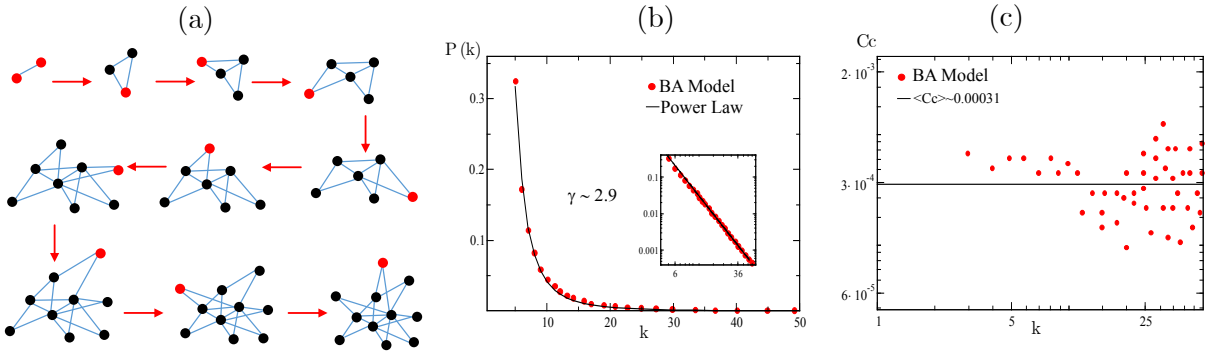

Figure 2.5: Scale-free network model (BA): (a) Iteration steps in the recursive construction of the scale-free network model (BA). Initially, the network is comprised of two nodes (red) and successive additions of a new node (red) are performed at each time step. (b) Degree distribution for the Barabási-Albert model, with $N = m_0 + t = 300\,000$ and $m_0 = m = 5$. The slope of the red full line is $\gamma \sim 2.9$, providing the best fit to the data. The inset shows the log-log distribution for the same scenario; (c) The clustering coefficient Cc is a constant as predicted by the black full-line and provides $Cc \sim 0.00031$. Figure build from Ref. [56, 57]

16 peripheral nodes is connected to the central node of the old module. The result is a new module of 64 nodes shown in the third graph in Figure 2.6-(a). This iterative process can proceed *ad infinitum*. The RB model presents a topology whose degree distribution follows $P(k) \sim k^{-\gamma}$, with $\gamma = 1 + ln4/ln3 \approx 2.26$ (see Figure 2.6-(b)); the clustering coefficient scales as a power-law $C(k) \sim k^{-\beta}$, with β taking values close to one (see Figure 2.6-(c)); and the average clustering coefficient $\langle Cc \rangle \sim 0.6$. This has been interpreted as an evidence for a modular structure organized in a hierarchical way.

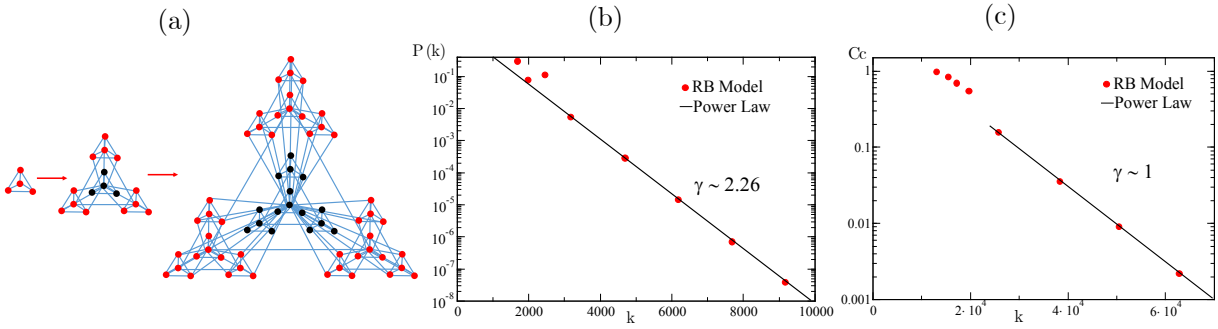

Figure 2.6: Hierarchical network model (RB): (a) A schematic illustration to generate a hierarchical, scale-free network with modularity, showing the first three steps of the iterative process. The stages of evolution are represented starting from a graph with 4 nodes and by adding at successive stages new groups of red nodes. (b) The degree distribution obtained for a network size with $n = 5^7$ follows a power law (full line) with slope whose exponent is $\gamma = 1 + ln4/ln3 = 2.26$. (c) Clustering coefficient for this model, demonstrating that it follows $Cc \sim k^{-1}$ and provides $\langle Cc \rangle \sim 0.6$. Figure build from Ref. [44]

2.3 Ecological Interactions

Different forms of local interaction between living organisms are observed in ecological communities. These interactions can be characterized by either mutual benefit, or the benefit of just one of them, or yet by the damage to both interacting species. Broadly speaking, mutual damage is called competition and can be defined as an interaction in which the survival and reproduction of individuals are negatively affected by the presence of other individuals. In many cases, competitors do not interact by coming in direct contact. Instead, they affect each other indirectly by exploiting common resources, like nutrients, light, water, etc [46].

Current ecological community theory postulate that stabilizing mechanisms are essential for species coexistence [60]. These mechanisms rely on negative intraspecific interactions, stronger than interspecific interactions, that cause species to limit themselves more than they limit others. Without stabilizing mechanisms, the inhibitory effects of competition on inferior competitors will ultimately lead to their extinction. Classically, such stabilizing interactions have been thought to result from resource partitioning [61]: competing species can coexist provided they are most limited by different resources and, also, they consume that resource they are most limited by a higher rate than do other species.

Several important examples of competitive interactions are present in nature. In special, in the case of plants, the competition plays an important role that affects plant fitness and structures plant communities [62]. The competition experienced by individual plants can vary greatly in many regards including the spatial distribution of their roots, reduction the total amount of roots that plants have available to place in soil, the spatial range over which they are active, the conditions that generate their emission, the tissues they target, how quickly they move, and often impairs plant growth more than competition for light [63].

A lot of experimental evidence suggests that plants are able to integrate communication between roots in the rhizosphere (the active soil zone in which plant roots compete for space, water, and mineral nutrients) to make allocation decisions [63, 64, 65]. For instance, Cahill et al. [66] showed that plants can adjust root location depending on nutrient availability and the presence of competitors' plants (see Figure 2.7). If an *Abutilon theophrasti* individual grows alone, their roots are distributed without a strong dependence on the distribution of soil nutrients. However, if individuals grow with neighbors, they adjusted their placement of roots and foraged less widely. With the presence of competitors, root growth was also more sensitive to the directions of nutrients and neighbors [66].

Other common mechanisms of damage interference observed in some species is allelopathy. While competition is characterized by the removal of environmental resources

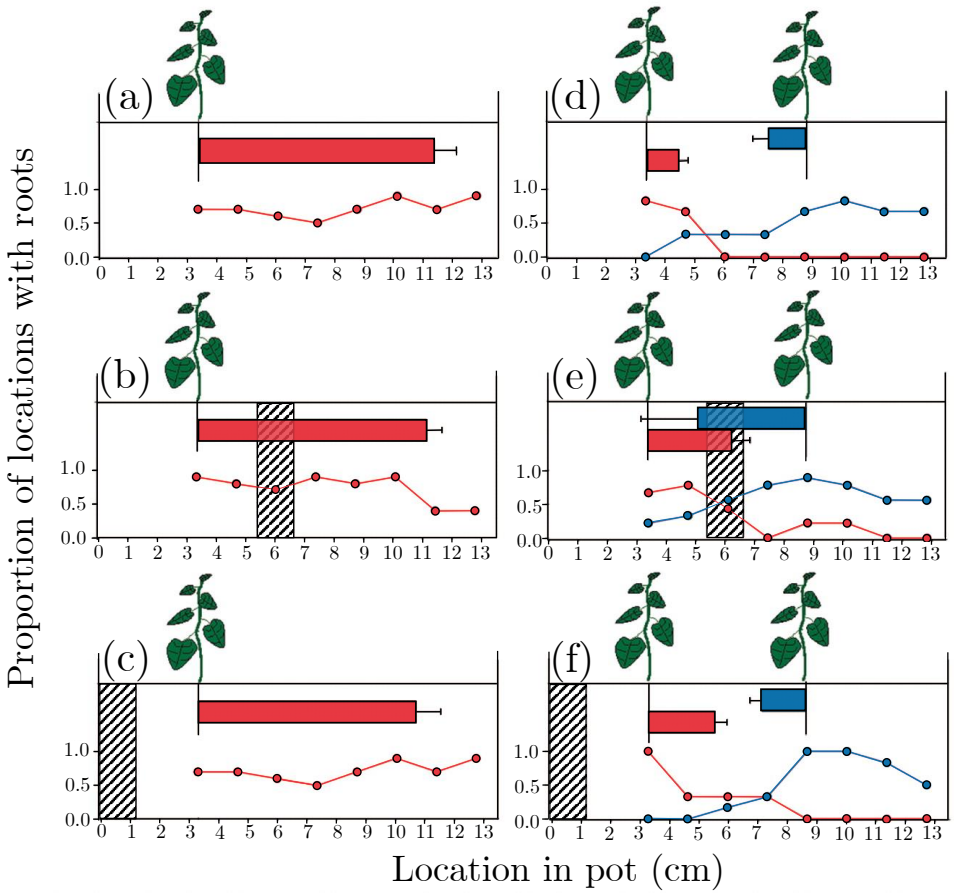

Figure 2.7: Six combination where *Abutilon theophrastias* were planted and grown during 8 weeks alone (a, b, c) or with a neighbor (d, e, f) in a uniform soil (a, d) or heterogeneous soil with nutrients rich patches $(b, c, e, f$ - shaded bar) and root distribution analyzed. In uniform soil with the competition, roots avoided each other, resulting in spatial soil segregation among the two plants. But the plants proliferate in a nutrient-rich patch, in spite of their neighbor (d). In the patch-center treatment with a competitor, plants had a broader root distribution (e), where plant roots over-lapped in the patch and thus were not segregated. In the patch-edge treatment with competition, the root distribution of the focal plant roots was intermediate in breadth (f). The Figure is taken from Ref. [66].

that are required for survival, the allelopathic phenomenon is characterized by the release of toxic substances in the environment which may inhibit or kill other species [46, 35, 108].

The allelopathic interactions are observed in several groups of microorganisms, such as bacteria [67], yeasts [68], and other fungi [69], which frequently secrete antibiotic compounds that kill or inhibit the growth of sensitive strains from their own genotypes or different species. Similarly, plants commonly exude secondary metabolites (phytotoxins) that suppress the germination or growth of neighboring plants [93]. Amazingly, glycolytic carcinoma cells excrete large amounts of lactic acid toxic to the surrounding normal cells. The resulting tissue acidification fosters tumor growth and invasion [71]. These examples suggest that interference competitions mediated by the production of toxic chemical compounds - antibiotic, phytotoxins, lactate, etc. - are ubiquitous in biological communities

[46, 35, 108].

In the case of bacteria, for instance, the toxin release and absorption processes involve specialized channels and receptors present in the cell membrane [72, 46]. These toxins or allelochemicals are synthesized and released under cellular stress, diffuse into the extracellular medium and bind to the membrane receptors in other cells that direct the toxin to the cellular DNA [73, 46]. Figure 2.8-A shows a scheme that describes the process of bacteriocin uptake by the membrane receptor channels until the degradation of cellular DNA. Moreover, the cells producing toxic substances provide immunity for themselves, i.e., there is no self-poisoning [46].

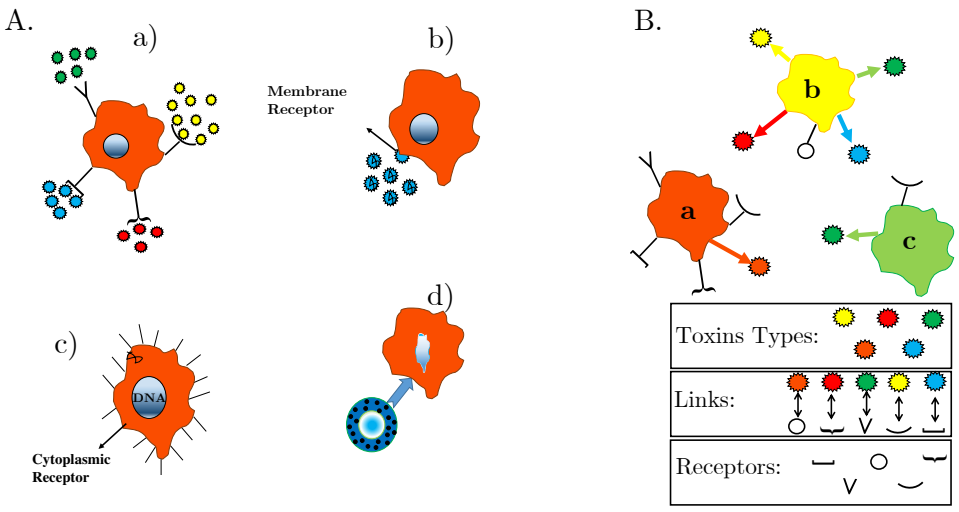

Figure 2.8: Bacteriocin producing and receptor channel: A. Absorbing process of bacteriocin and one of the damage effects it brings to the cell. a) Cell and its receptors receiving different types of bacteriocin. b) Process of cell infection upon receipt of the "blue circle" bacteriocin. c) Targeting the toxin to the cell nucleus from cytoplasmic receptors. d) Infection, deformation of the genetic material and cell death caused by the activation of the DNA-disrupting nuclease. B. Schematic representation of three cells a, b and c that produce different types of bacteriocins (colored circles) and have different types of receptors on cell membranes. Each type of bacteriocin links to a different receptor, according to the explanatory table. Figure adapted from Ref. [46]

Cells secreting bacteriocins can be separated into producer, receptor (sensitive), resistant groups, and those that show combinations of these characteristics (see Figure 2.9-(a,b)). Cells that produce a certain toxin poison sensitive cells. Resistant cells can resist bacteriocins from producer cells because they are unaffected by bacteriocin and can take advantage of surviving some of the producer cells that die by releasing the toxin. Therefore, some toxin-producing cells are at a disadvantage when interacting with resistant cells [74]. Figure 2.8-B contains a schematic description of some of the different types of receptors and bacteriocins produced by cells.

Among the most diverse types of bacteriocins produced, those from *Escherichia coli* (*E. coli*) have great practical applicability. The antimicrobial agents produced by *E. coli*

have been largely used in a wide range of food and pharmacy research, for the development of food preservation products and the manufacture of antibiotics [26]. This species of bacteria and others of the family *Enterobacteriaceae* can produce different types of bacteriocin. However, two are the most common: colicins and microcins. Colicins are produced under stress conditions and may lead to the elimination of neighboring cells [75]. In general, the releasing process of these toxins into the environment stems from the process of cell lysis [76]. Microcines, when released, do not lead to the death of the producing cell, and the possible explanations for these phenomena are not yet fully known [77]. Evidence shows that usual culturing conditions of these species might not adequately represent the stress associated with low resource levels and intense competition, which are common in natural microbial ecosystems [78, 79, 80], and for this, the mutation rate and diversity may enhance [81, 82]. Experimental results reveal that bacterial evolution under stress conditions (concerning batch cultures with limited resources [83, 84, 85, 86]) results in periodic selection and high levels of strain diversity (see Figure 2.9-(c)) [25, 87].

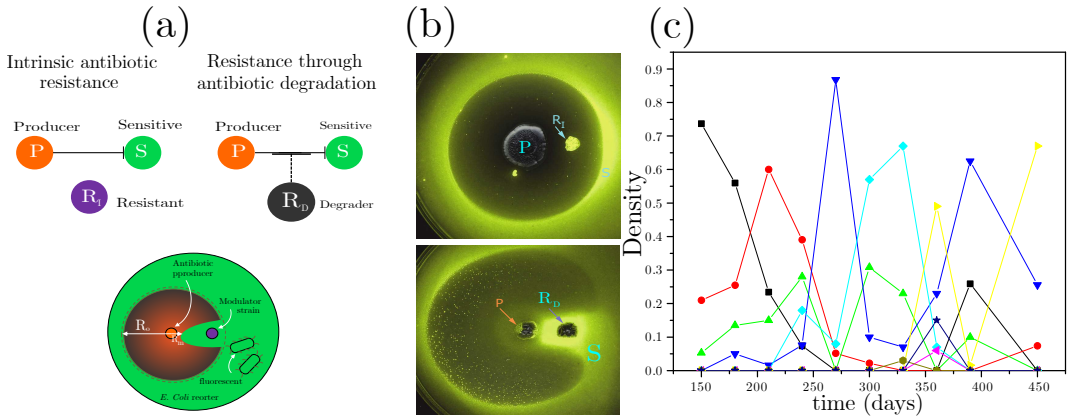

Figure 2.9: Examples of interaction among *E. coli*. a) Diagram of interaction among antibiotic-producing (P), - sensitive (S) and intrinsically resistant (R_I) species and the same scenario where the sensitive species can be protected by an antibiotic degrading species (R_D); schematic representation illustrating that measuring the antibiotic inhibition zone of *E. coli* around a producer strain enables quantification of three-species interactions caused by a modulator strain. b) Images of a yellow fluorescent protein of *E. coli* strain (S, yellow-green) growing in the presence of two *Streptomyces* colonies. The inhibition of the probe strain by a producer (dark area around P) is unaffected by an intrinsically resistant species (R_I, left), but is strongly attenuated around an antibiotic-degrading species (right, yellow-green halo around R_D colony). Images are representative of cases without and with three-way interactions among 54 *Streptomyces* pairs tested. c) Coexistence of different colony morphotypes, indicated by colors, during long-term incubation of an initially isogenic strain of *E. coli* (i.e. produced by sibling crossbreeding for 20 or more generations). Figures adapted from Refs. [25, 87].

Also, a major problem in public health is the invasion of the human organism by some of their symbiont microbes eventually causing serious diseases, as is the case of *Ente-*

rococcus faecalis, a leading cause of hospital-acquired infections [88, 89]. The inter- and intraspecies competition among the *Enterobacteriaceae* in the inflamed gut is mediated by microcins [90]. Moreover, microcins can act as narrow-spectrum therapeutics to inhibit enteric pathogens and reduce enterobacterial blooms [90].

In glioblastoma, the most aggressive brain tumor, glioma cells release ATP to the tumor microenvironment. The extracellular ATP itself has a small cytotoxic effect on normal cells, but adenosine formed from ATP degradation by ectonucleotidases overexpressed on the membrane of glioma cells induces significant apoptosis of the adjacent normal cells [91, 108].

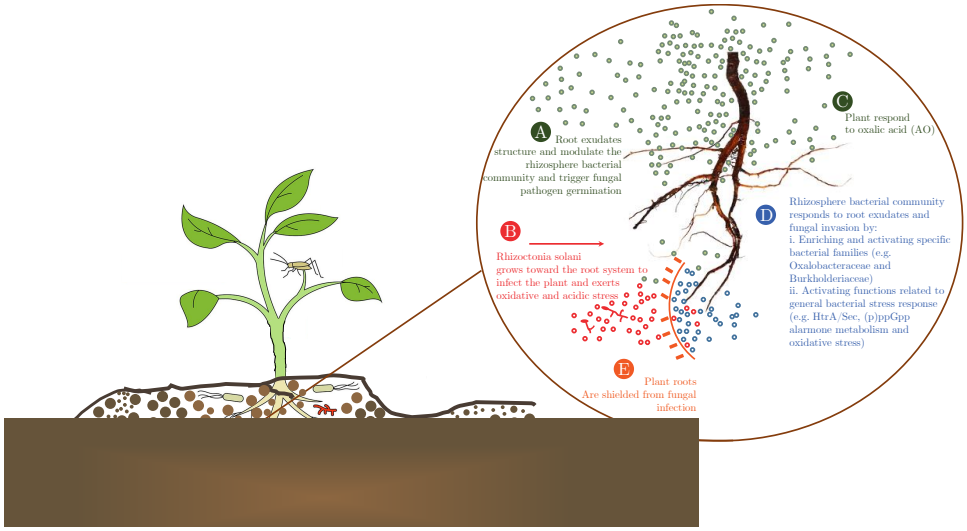

Figure 2.10: Conceptual illustration of sequential events (A - E) in the microbial community assembly and functional traits in the bulk soil taking place in the rhizosphere of plants grown in a chemical suppressive soil during the fungal invasion. Depicted are the changes in microbial community composition and activities that restrict fungal growth and plant infection.

Instead of being passively shaped by fluctuations in the resources they require, plant communities can emerge from direct chemical interactions between the species [92, 93]. Root exudates initiate and regulate biological and physical root-root and root-microbe interactions within the plant rhizosphere (see Figure 2.10). Since plant species differ in their reaction to individual microbe species, the density and/or composition of the soil community rapidly changes in response to plant identities. These changes, in turn, alters significantly the outcome of plant-plant interactions, resource partitioning, resource sharing through common mycorrhizal networks, and soil community feedback. Consequently, the relative growth rates and fitness of individual species are affected. Indeed, microbial mediated resource partitioning and negative soil community feedback are stabilizing mechanisms for the maintenance of diversity, whereas resource sharing through a common mycorrhizal network is a fitness equalizing mechanism. It is worthy to mention that these

three mechanisms, not mutually exclusive and that can possibly occur simultaneously, are regulated by the plant root-secretion system. The amazing array of bioactive-proteins and secondary metabolites it synthesizes, many of which appear to be species-specific [94], actively protect the plant against infection by soil-borne pathogens, encourage mutualistic and beneficial bacterial and fungal associations and affect other plants by their phytotoxic or antimicrobial actions [93].

If plants have species-specific responses to different chemicals released from particular neighbors, then the identity of neighbors may have an essential effect on the development of allelopathically homeostatic conditions in natural communities. In other words, the race of plants and microbes for adapting to the chemicals synthesized by their neighbors may drive species coexistence and community composition. In addition, communities normally come about by a succession of one or a few species arrivals at a time and the disappearance of resident ones. Hence, community and invasion ecology are naturally interconnected because both the persistence of a species in a community or its invasion success abroad its native habitat primarily depends on its ability to increase from low-density [95, 96, 101]. Figure 2.11-(a) shows typical invasion patterns corresponding to a homogeneous native plant community with a low resistance to the phytotoxin radially secreted by the alien species, while Figure 2.11-(b) show the morphology of the invasion patterns for high resistance to the phytotoxin. This worldwide phenomenon represents a major threat for ecosystem functioning and biodiversity conservation, water availability, and agricultural production [97, 98, 99, 100, 101].

Figure 2.11: Satellite images of typical invasion effects in a homogeneous native plant community with (a) low-*Vochysia sp.*(*Vochysiaceae*) and (b) high-*Myracrodruon urundeuva* (*Anacardaceae*) resistance to the phytotoxin secreted by the alien plant in Brazil. Figure adapted from Ref. [101].

Beyond its paramount relevance, ecological theory approaches competition from its effects on populations. For a long time, competitive interactions were modeled by means

of Lotka-Volterra equations [102, 103]. On the other hand, despite its ecological relevance, the allelopathic phenomenon is currently poorly understood at a quantitative level. Durret and Levin studied a model for allelopathy in spatially distributed populations of bacteria [104] involving linear functional response. They found that the coexistence between colicin producers and colicin-sensitive strains is possible only in a structured environment if a third strain, expending less on colicin production but resistant, is present. Similarly, Souza, Martins, and Carmo [101], analyzing a multiscale and hybrid agent-based model for allelopathic plant invasion, also found that the success and invasion speed decrease in the presence of resistant native plants. Szabó, Czárán, and Szabó [105] proposed a lattice model for the population dynamics of allelopathically competing bacterial strains. These authors demonstrated that cyclically dominated spatial species associations may produce very diverse and complex coexistence patterns of the distinct strains. In turn, Weber et al. [106] showed that cyclic dominance between strains is not necessary for bacterial coexistence in competitive expansions. Instead, a balance between replication rates and either a low initial density of the toxin-producing strain or a short enough toxin range is demanded to establish a robust three-strain coexistence. More recently, Fassoni and Martins [107] proposed and analyzed a spatially explicit model for the biological warfare involving allelopathic species that also compete for common environmental resources. In this work [107], they improved and extended previous results describing the population dynamics of two competing plant species in which one of them is an invader and produces a phytotoxin affecting the other. Preventing biological invasions and predicting their spreading patterns emerge as imperative tasks in an ecologically sustainable world [108].

2.4 Complexity-Stability and Ecological Structure

The study of the relationship between stability-complexity of species communities and the network structure and nature of the ecological interactions that connect these species is one of the central themes of theoretical ecology. For instance, by exploring how the size of the community and the degree of connectivity between the species influences stability, it was found that the extinction of generalist species, which are the most connected in the community food chain, produces massive extinctions in the community [20].

The network of ecological interactions between species has a deep influence on the stability and balance of the community [4, 5]. Early empirical and theoretical studies [7, 6] suggested that increased complexity, measured by the connections between species, fortify ecosystem stability. According to that empirical evidence, stable ecosystems are highly complex. Later, experiments of aquatic and terrestrial food webs analyzed through complex network theory [54, 14], suggested that environmental perturbations rarely propagate through food webs for more than three links away from the initially affected species,

consistent with the idea that real ecosystems are structurally stable.

The empirical network showed in Figure 2.12 describes a detailed representation of a real food web for Little Rock Lake (LRL) that is compiled explicitly to test food web theory and patterns [54]. The food web is structured as a series of trophic levels including 181 taxa (11 fishes, 110 invertebrates, 59 autotrophs, 1 detritus) with 92 trophic-species such as fishes, copepods, cladocera, rotifers, diptera, and other insects, mollusks, worms, porifera, algae, and cyanobacteria (corresponding to vertical layers). This vertical axis of interaction with 997 links describes four types of consumer-resource interactions: herbivorism, primary consumer, secondary consumer and cannibalism (self-loops) [109].

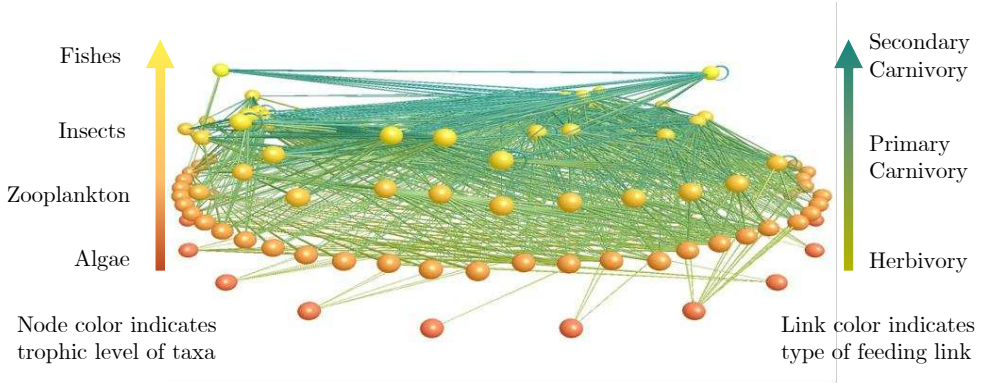

Figure 2.12: Food web of trophic interactions for Little Rock Lake (LRL), Wisconsin [54]. This picture summarizes 92 trophic species (nodes) and 997 feeding links in a freshwater lake in the northern United States. The vertical position includes node colors representing trophic level (algae, zooplankton, insects, and fishes) and links run by coloured links between predator-prey species pair describing herbivory, primary and secondary carnivory and cannibalism is shown with self-loops. The Figure was created by Richard Williams and Neo Martinez and provided by the Pacific Ecoinformatics and Computational Ecology Lab [2][109].

The LRL data obtained by Martinez [54] have shown that trophic webs tend to follow common functional patterns such as asymmetric degree distribution (see Figure 2.13-(a)), i.e., few species concentrate many interactions, and many contain few. The LRL network exhibits fluctuating degree distribution with very high variance, but no obvious recognizable standard shape, although it is also skewed, with a prominent peak of 21 species (involving a coarse-grained cluster of cyanobacteria and green algae predated by pelagiccladocera, copepods, and rotifers) [54, 125]. Moreover, the insets contain CDF ($F(k)$) and CCDF ($G(k)$) that follow a model of exponential decrease with $\langle k \rangle \sim 26$ [111, 110]. It differs from the expected standard in scale-free networks, whose function is described by power-law [59, 56]. Therefore, most species have a small degree (k) and the CDF shows a rapid ascendancy and stabilization near 1. In this way, it is difficult to compare

[2] www.foodwebs.org

different communities and models. Using the CCDF, the curve starts at 1, and decreases more slowly, which facilitates comparison between communities and models. In a semi-logarithmic scale, the exponential model is characterized by a linear decay, and the power function, by an elongated curve to the right (see the curve of $G(k)$ inset the Figure 2.13-(a)). Connectivity decrease considerably with increasing species richness but remained relatively similar at web sizes above 70 species (see Figure 2.13-(b)). The connectivity behavior shown in Figure 2.13-b can be explained by the observation that a huge amount of species in food webs is followed by an increase in the total variety of body sizes in the community. This increased size discrepancy may render direct trophic links less likely between species at the two extremes, contributing to a decline in connectance [112].

Although most real networks have scale-free properties that lead to a power-law distribution [31]. Ecological networks may exhibit exponential or uniform, power-law, or exponentially distributions truncated power-law. A fundamental characteristic that differs heterogeneous from homogeneous' networks (see Appendix A.2) is the size and form of connectivity. Scale-free networks are much larger and sparsely connected than most homogeneous networks [110].

The ecological network models generated to describe networks with exponential or uniform distributions may be the result of two simple assumptions: (i) random immigration to local webs from a randomly linked regional set of taxa, and (ii) random extinctions in the local webs [113]. Power-law degree distributions is a feature associated to the level specialist-generalist in ecological communities: a large number of species with few interactions coexists with a relatively small number of super-generalist species [114]. If the network did not fit this power-law distribution (see scale-free network), then a single value of k would characterize the distribution, thus having a characteristic scale (single scale) [115]. In networks exhibiting a distribution of node degrees that fits a truncated power-law regime, the prevalence of specialists and the rarity of super generalists is suggested. Indeed, in random networks, a super generalist, that is, a strongly connected node, simply does not exist [116].

Available data for plant-pollinator and plant-frugivore networks in mutualistic webs reveal some general patterns in the node degree distributions of ecological networks. The observed degree distributions can be adequately described by power laws (animals in Figure 2.14-b), exponentially truncated power laws (plants in Figure 2.14-(a) and (b)) and exponentials (animals in Figure 2.14-(a) and (c)) [117, 118, 119]. Furthermore, power-law distributions were also obtained to fit the distributions of node degrees distribution in mutualistic networks [116]. The measure of heterogeneity associated with node degree distributions, $\kappa = \langle k^2 \rangle / \langle k \rangle$, with $\kappa \gg \langle k \rangle$, was discovered years later to be a primary factor that interferes negatively the local stability of mutualistic networks [115].

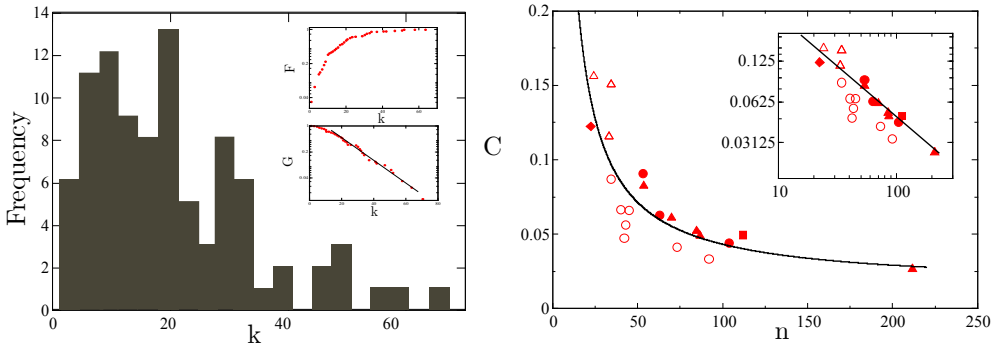

Figure 2.13: Degree distribution and connectivity in LRL network: a) Absolut frequency distribution, CDF, and CCDF as a function of degree k. Insets shows CDF and CCDF, where the CCDF G(k) follows an exponential model. b) Connectivity as a function of individual number in LRL network $C \sim n^{-1}$. Figure built from Refs. [110, 112].

Despite the fact that network size and links between nodes partially determine the complexity of the network, they neglect important information concerning individual species connectivity as well as degree distribution among species. Theoretical studies indicate that dynamical systems with random connections may be coming stable up to some critical level of the connectivity, becoming dynamically unstable for larger connectances [11]. Years earlier, MacArthur showed that ecosystem stability increases with complexity [7]. Inspired from these studies, and applying results from random matrix theories, May [9, 10] demonstrated analytically that the stability of model ecosystems connected through random interaction coefficients tends to decrease with the complexity of these interactions. This result is in marked contrast with the view reported above and founded the so-called "complexity-stability" debate. The May's stability line ($C(n) \sim n^{-1}$) can be obtained for network sizes up to $\sim 10^6$.

Years latter, Thilos Gross et. al. [15] through the numerical study of several essays of food webs, confirmed that food web complexity is negatively correlated with dynamical stability. It is worth mentioning that the behavior $C(n) \sim n^{-(1+\epsilon)}$ has been obtained in several self-organized ecological systems [120]. In Figure 2.14-(d)-(f), is plotted the connectivity for different ecological networks across three orders of magnitude of network size scales, using data collected from the literature [110, 121, 122]. In all cases, ubiquitous pattern emerges scaling inversely proportional to the system size, very well fitted by a single power-law $C(n) \sim n^{-(1+\epsilon)}$, in nice agreement with the $\epsilon = 0$ or 0.2 in food webs and mutualistic networks. This result shows that species connect choosily even when they coexist at small distances and most of the links are deactivated. However, there are other works that show constant connectance in food webs [124, 125, 126, 127].

In addition, other properties such as path length, clustering coefficient, and neighbor correlations also have been studied in different ecological networks. In many ecological networks, it is observed that the clustering coefficient of a node with degree k follows the scaling law $Cc(k) \sim k^{-\beta}$, with β taking values close to one. This has been interpreted

as evidence for a hierarchically organized modular structure [43]. In turn, ecological networks have shown strong disassortativity properties, i.e., highly connected nodes tend to be preferentially connected to nodes with low degree and *vice-versa* [128]. Such disassortativity may be associated to a finite-size effect in ecology, where the species have limits of connections with each other. Nevertheless, in food webs, it may also be consequence of the stabilizing effects of having feeding specialists connected to feeding generalists, as has been observed in a large number of plant-pollinator- and frugivory (fruit-eating) networks [117]. Concerning path length, food webs display short path lengths that are similar to what is seen in random webs [110]. On average, taxa are about two links from other taxa in a food web ("few degrees of separation"), and path length decreases with increasing connectance [14].

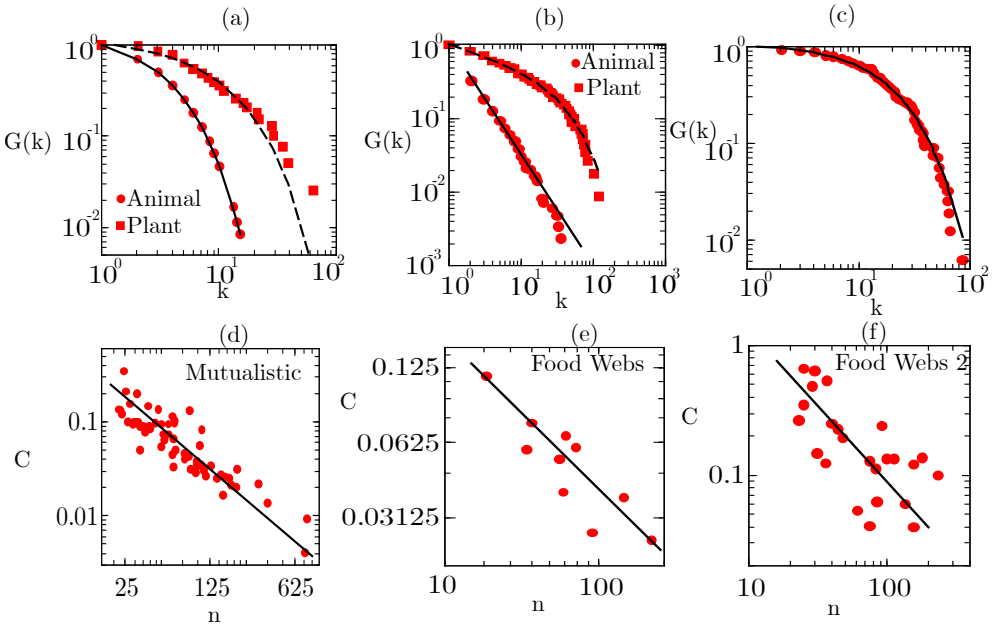

Figure 2.14: Experimental degree CCDF (squares and circles) and best fits (lines) for: a) frugivore-plant web [118], b) pollinator-plant web [119], c) food web from El Verde rainforest [131]; and average connectivity for d) mutualistic [121], e) host-parasites and plants-herbivors [121], and f) distinct food webs [132, 110]. In a) and b), for red circles, k is the number of plants species visited by an animal, and for red squares, k is the number of pollinator species visiting each plant species. In c) the sum of prey-predator links and predator-prey links for each species was used. Best fits to the data in a-c are as follows: a), animals, exponential, $G(k) \sim e^{-k/3.998}$; plants, truncated power law, $G(k) \sim k^{-0.013}\, e^{-k/11.22}$; b), animals, power law, $G(k) \sim k^{-1.512}$; plants, truncated power law, $G(k) \sim k^{-0.2822}\, e^{-k/42.55}$; c), exponential, $G(k) \sim e^{-k/8.861}$ [133]. (d-f) The connectivity in all cases show a clear emergent pattern of sparsity in empirical ecological networks with $C \sim n^{-(1+\epsilon)}$, where $\epsilon = 0$ in (c) and (d), and $\epsilon = 0.2 \pm 0.1$ ($R^2 = 0.92$) in (e-f) [122]. Figure build from Ref. [59].

In recent times, there has been a shift of interest from the concept of dynamical sta-

bility to the concept of structural stability. In this new approach, instead of constructing a random system and asking with which probability the system is dynamically stable, as in May's approach, theoreticians consider a system that is by construction dynamically stable and with positive equilibrium abundance of all species. Then they simulate environmental perturbations, and investigate how large is the maximum perturbations that typically maintains the coexistence of all species, which quantifies the structural stability of the model ecosystem. In this way, Bastolla et. al. showed that mutualistic interactions enhance structural stability when the direct competition between plants and between pollinators is weak [129] and when the ecological overlap (number of shared ecological interactions) between plants and between pollinators is strong [130]. Such overlap, a concept that has been denominated nestedness, is a widespread property of mutualistic networks. Nested mutualistic interactions induce indirect positive interactions between plants and between pollinators that reduce their direct competition and enhance the structural stability of the ecosystem. In this regime of low direct competition, the complexity of the mutualistic interactions favors the structural stability, providing a possible solution of the complexity-stability debate.

Chapter 3

Eco-Evolutionary Dynamics in Allelopathic Communities

Biological diversity depends on the interplay between evolutionary speciation and ecological mechanisms allowing species to coexist [123]. To understand the origin and maintenance of biological diversity, it is necessary to explore the integrated effects of evolutionary and ecological processes. Here, inspired in previous papers on biological invasion through allelopathic suppression [101, 107], the perspectives acting of two distinct timescales of ecology and evolution are theoretically explored. Specifically, a species community in which the species sustain intra- and interspecific competition, alellopathic interactions and in which new species are randomly introduced via mutations of the resident species is considered. The negative effects on offspring and mortality of resident species generated by the toxins (phytotoxin, microcin, lactate, etc) constitute the primary stabilizing mechanism. In truth, the effective toxins model for species-species interactions emerges from the battery of bioactive secondary metabolites and surfactants that mediate and regulate the complex ecological processes involving allelopathic species. The aim is to understand the conditions under which species communities can be stabilized by allelopathic interactions. The results present in this *Chapter* were partially published in [35, 108, 146].

3.1 Ecological Model for Allelopathic Suppression

To model the community dynamics, a set S of $l \in \mathbb{N}$ biological species with populations given by $\mathbf{N}= (N_1, N_2,\dots, N_l)$ is considered. The interactions among these species occurs only via intra- and interspecific resource competition and allelopathic suppression. Thus, every species in S synthesizes and releases toxic secondary chemical compounds (microcins, fitotoxins, lactate, etc.) that enhance the mortality of other species. The strengths of such interactions depends on the toxin concentration $\mathbf{B}= (B_1, B_2,\dots, B_l)$ and

vary in time because **B** depends on the abundance of the species. Furthermore, the community assembly proceeds from an initial subset $S_0 \subseteq S$ by randomly adding new species through mutations fixed in a fraction of resident species' offspring.

The evolution in time of the biological community in a homogeneous environment is described by the coupled ordinary differential equations

$$\begin{aligned} \frac{\mathrm{d}N_i}{\mathrm{d}t} &= r_i \left(1 - \sum_{j=1}^{l} \nu_{ij} N_j\right) N_i - \sum_{j \neq i}^{l} \mu_{ij} \Phi_{ij}^{(k)} N_i \\ \frac{\mathrm{d}B_i}{\mathrm{d}t} &= \beta_i N_i - \delta_i B_i - \sum_{j \neq i}^{l} \gamma_{ji} N_j B_i. \end{aligned} \tag{3.1}$$

Here, N_i stands for the population density of the species i that produces the allelochemical concentration B_i, respectively. Also, r_i, β_i and $\delta_i, i = 1, 2, \ldots, l$, respectively, are the reproduction, toxin release and natural degradation rates associated to the competing species. A classical interspecific competition for the environmental resources is assumed. The term $r_i(t) = r_i(1 - \sum_{j=1}^{l} \nu_{ij} N_j)$ describes the offspring number generated by the strain i in time, so that growth is reduced by the competition for resources between i and j's species, where parameters ν_{ij} are the competition coefficients that measure the extent to which each species presses upon the resources used by the others. The term $-\sum_{j \neq i} \mu_{ij} \Phi_{ij}^{(k)}$ represent species decreases induced by the allelochemicals released by their allelopathic suppressors, in which μ_{ij} is the mortality rate of the species i induced by the toxin released by its suppressor j. Finally, the quantity $\gamma_{ji} N_i B_j$ represents the overall consumption of the toxin i by the species j, $i \neq j$, with per capta absorption rate γ_{ji}. These quantities depend on the toxin's levels in a linear way.

Different Holling types I, II, and III functional responses were assumed:

$$\Phi_{i,j}^{(k)} = \begin{cases} \frac{B_j}{B_0} & (k = 1) \\ \frac{B_j}{c_i + B_j} & (k = 2) \\ \frac{B_j^2}{c_i + B_j^2} & (k = 3) \end{cases} \tag{3.2}$$

where the parameters $B_0 \equiv 1$ is the slope of the linear response used to make it dimensionless and c_i control the toxins efficiencies in poison their competing species. All these response functions assume null thresholds for toxin effects, but those with $k > 1$ impose saturation to the allelopathic suppression. Also, all the response functions involve the total toxin concentration. The effect of consider mortality only due to toxins absorption consists in introduce the term $\gamma_{ji} N_i B_j$ in the functional responses, equation (3.2). These cases are reported on the Section 3.3 and Appendix B.

The interacting parameters ν_{ij}, γ_{ji}, and μ_{ij} define networks in which the species are the

nodes. These parameters can be expressed as $\nu_{ij} = \nu_{ij}\,\epsilon_{ij}$, $\gamma_{j,i} = \gamma_{j,i}\,\zeta_{ji}$, and $\mu_{ij} = \mu_{ij}\,\zeta_{ij}$, in which $\epsilon_{ij} = 1$ ($\zeta_{ij} = 1$) if species i competes with (poisons) species j, but $\epsilon_{ij} = 0$ ($\zeta_{ij} = 0$) if i does not compete with (poisons) j. Every ϵ_{ij},$\zeta_{ij} = 1$ is a link connecting two species. The set of values ϵ_{ij} and ζ_{ij} define two matrices ϵ and ζ which characterize the competition and allelochemical interaction networks, respectively. These matrices are examples of the adjacency matrix, central in network theory [3, 37, 38, 39]. The diagonal elements of ϵ are $\epsilon_{ii} = 1$ and represent intraspecific competition, with all $\nu_{ii} = 1$ by definition. In turn, we set all $\zeta_{ij} = 0$ in order to avoid allelopathic-self suppression.

The ecological interactions (competition and allelopathy) drive the dynamics, equation (3.1), towards an stationary state ($\mathbf{N}^*$,$\mathbf{B}^*$) in a short time scale. This stationary state depends on the species initially present and their interaction networks. Eventually, even in the weak interspecific competition (coexistence) regime, some populations are led to extinction by competition and/or allelopathic suppression and the community diversity (species richness) decreases.

3.2 Competition for Resources

In the absence of allelopathic interactions ($\zeta_{ij} = 0$; $\forall\ i, j$) the system's dynamics is described the Lotka-Volterra Model (LVM), for the competition among several populations:

$$\frac{\mathrm{d}N_i}{\mathrm{d}t} \;=\; r_i \left(1 - \sum_{j=1}^{l} \nu_{ij} N_j\right) N_i. \tag{3.3}$$

In summary, equation (3.3) shows that the *per capita* growth rate of the species i is decreasing linearly with the density of each population. In the absence of competitors ($\nu_{ij} = 0$) or very low population densities ($N_j \to 0$), the dynamics of each species follows the exponential growth model with intrinsic rate *per capita* r_i.

The competition coefficients ν_{ij} are parameters that quantify how strongly the *per capita* growth rate of species i is affected by the presence of species j. In the presence of competitors ($\nu_{ij} > 0$), the competition can be classified into two types: intra- and interespecific. In the intraspecific competition, as the population density of species i increases, there is a reduction in its growth rate to achieve an equilibrium density or "carrying capacity". In interspecific competition the growth rate also decreases due to the presence of other species. In this case, the stationary population density ends below the carrying capacity.

The individual carrying capacity of each species is now determined by the coefficient of its own self-limitation (ν_{ii}), such that $k_i = \frac{1}{\nu_{ii}}$. Moreover, if $\nu_{ij} > \nu_{ii}$, the effect of species j on i is stronger tan the effect of species i on itself or vice-versa. If all $\nu_{ij} > 0$ then the multispecies LVM describes a community with only competitive, i.e., without mutualistic

or predator-prey relations between species. Mutualistic parameters are characterized by $\nu_{ij} < 0$ whereas prey-predator has $\nu_{ij} < 0$ and $\nu_{ji} > 0$ (here species i is a predator of species j).

To analyze the emergence of stable topologies in competitive ecological systems, we start assuming a simpler community matrix with symmetrical and uniform intra- and interspecific competitive pressures, i.e., $\nu_{ii} = \nu_{ij} = \nu \; \forall \; i, j$. In this case, the parameters r_i don't change stationary equilibrium population and the equilibrium points are determined by the competition parameter (ν) and initial conditions. The system exhibit stable coexistence between populations for all $\nu > 0$, as can be shown in the Figure 3.1-(a).

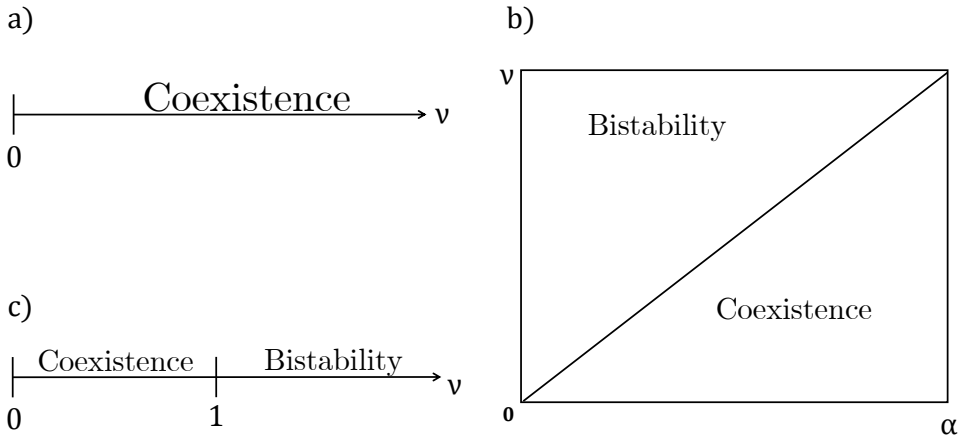

Figure 3.1: Regions of stable coexistence and bistability among populations for three scenarios whose matrices of competition are: a) $\nu_{ij} = \nu > 0 \; \forall \; i, j$; b) $\nu_{ij} = \nu > 0 \; \forall \; i \neq j$ and $\nu_{ii} = \alpha > 0 \; \forall \; i$; c) $\nu_{ii} = 1$ and $\nu_{ij} = \nu > 0 \; i \neq j$.

If all species have equal initial conditions, then populations may increase (see Figure 3.2-(a)) or decrease (Figure 3.2-(b)) to the same steady state $N_i(\infty) = \frac{1}{l\nu}$. If the initial conditions are different, the species with the highest initial condition will reach a higher stationary density. Thus, different initial conditions produce different levels for saturation densities. If the initial conditions are smaller than the carrying capacity, the species present sigmoidal growth curves (see Figure 3.2-(c)). If the initial conditions are greater than the individual carrying capacity, then the species' populations decay until reaching equilibrium densities (see Figure 3.2-(d)). In all cases the equilibrium population densities satisfy the equation $\sum_{i=1}^{l} N_i(\infty) = \frac{1}{\nu}$. Therefore, the stability of an ecosystem formed by these types of competitive interactions is associated to the initial condition and the competition parameter.

Considering the case of uniform and symmetrical competition between members of a community interacting via competition, the Figure 3.3-(a) shows the variation of the species number initially present and abundances of population densities upon reaching steady state with the competition coefficient (ν). Concerning the increase of competition coefficient and/or the number of species initially present in the community, there is a

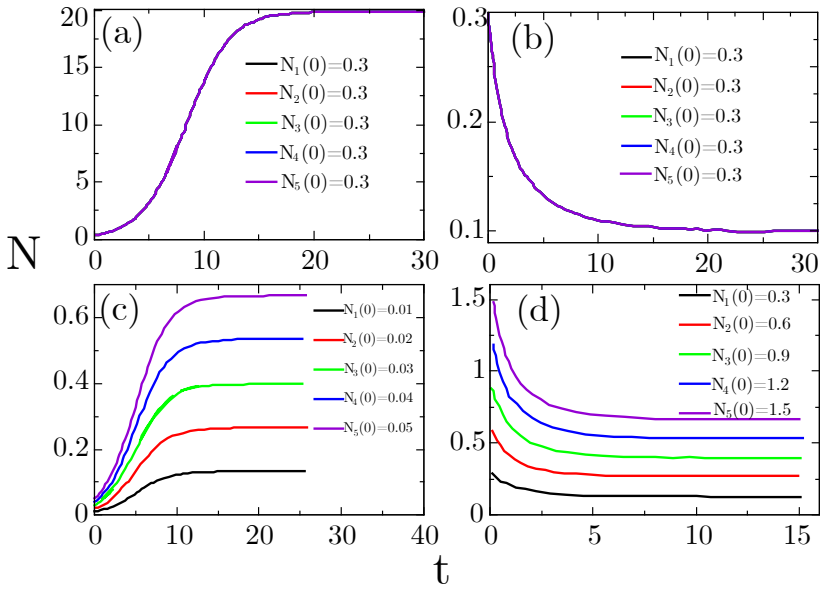

Figure 3.2: Temporal evolution of populations in a community formed by $l = 5$ species. It was considered in each case uniform and symmetrical competition $\nu_{ij} = \nu \ \forall \ i, j$. a) $\nu = 0.01$; b) $\nu = 2$; c) and d) $\nu = 0.5$ with distinct initial conditions.

reduction in the equilibrium density of the populations.

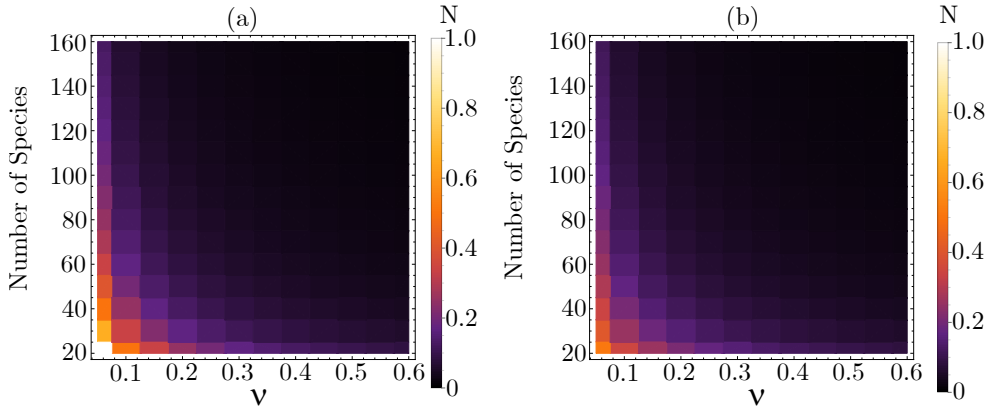

Figure 3.3: Variation of the number of resident species as a function of competition parameter ν: a) $\nu_{ij} = \nu \ \forall \ i, j$ and b) $\nu_{ij} = \nu \ \forall \ i \neq j \ \nu_{ii} = \alpha = 1$; the color scale represent the stationary population density. The density plot were according to the LVM 3.3. The initial populations considered are $N_i(0) = 0.3$, and growth rate $r_i = 1 \ \forall \ i = 1, 2, \ldots, 160$.

Generally, in a competitive interaction the competition coefficients are not equal. This is due to the fact that the species do not have the same ecological niche[1], i.e., they do not use the same available resources. Thus, as a first step forward it will be considered a matrix of competitive interaction that is described by interspecific competition parameters ($\nu_{ij} = \nu$) different of the intraspecific competition parameters ($\nu_{ii} = \alpha$). Thus equation

[1]Species that interact in the same way, need the same nutrients, live in the same habitat at the same time, and so on.

(3.4) is rewritten as

$$\frac{\mathrm{d}N_i}{\mathrm{d}t} = r_i \left(1 - \nu_{ii}\, N_i - \sum_{j \neq i}^{l} \nu_{ij} N_j\right) N_i. \tag{3.4}$$

In this case, the phase plane ($\nu \times \alpha$) exhibit two regions: coexistence and bistability (see Figure 3.1-b). If the interspecific competitive pressure is weak ($\nu < \alpha$), then coexistence between species is possible. However, if interspecific competition is stronger than the intraspecific effect ($\nu > \alpha$), bistability is observed, i.e., the asymptotic state depends on initial conditions. The stationary abundance of surviving species in the bistability region is given by $N_i(\infty) = \frac{1}{\alpha}$. Furthermore, the region of bistability ($\nu > \alpha$) can become a region of coexistence if the initial conditions of all species are equal. In this case, the stationary density of the species satisfy the equation $N_i(\infty) = \frac{1}{\alpha+(l-1)\nu}$ and, therefore, $\sum_{i=1}^{l} N_i(\infty) = \frac{l}{\alpha+(l-1)\nu}$ for all parameter space ($\nu \times \alpha$).

In particular, a case that has been discussed extensively throughout history is one in which intra-specific competition coefficients are scaled to a unit $\nu_{ii} = 1$ (such as the carrying capacities of all species). The interspecific competition may be considered the same in all pairs of species ($\nu_{ij} = \nu_{ji} = \nu$, $i \neq j$), via equation (3.4). This type of interaction is called "diffuse competition" [134].

In this case, the phase space is represented by the semi-axis $\nu > 0$ which is partitioned into two parts: coexistence and bistability (see Figure 3.1-c). If $\nu < 1$, then the species coexist independently of the initial conditions. In the bistability region ($\nu > 1$), species can coexist since the initial conditions are equal. In this condition the species reach the same stationary level $\left(\frac{N_i(\infty)}{N_j(\infty)} = 1\right)$ and the individual stationary abundance is given by $N_i(\infty) = \frac{1}{1+(l-1)\nu}$. If the initial conditions are different in the region $\nu > 1$ the one with the largest population will overcome the competitive dynamics and its abundance will be given by $N_i(\infty) = 1$.

Concerning the cases $\nu_{ij} = \nu \; \forall \; i \neq j$ and $\nu_{ii} = 1$, the Figure 3.3-b) show the species number and stationary abundance as functions of the competition parameter ν in the regime ($\nu \leq 1$). For both cases the stationary population decrease densities with the increase of the number of species and/or competitive pressure.

Specifically, Figure 3.4 show the case of two species competing for resources with different competitive strengths. There are four qualitatively different regions in phase space (ν_1, ν_2): extinction of one species, stable coexistence and bistability. If two species are under weak competition (ν_1 ,$\nu_2 < 1$), the only asymptotically stable fixed point corresponds to the coexistence. If competition between species is unequal ($\nu_1 > 1 > \nu_2$ or $\nu_1 < 1 < \nu_2$) only the fixed point representing the survival of the fittest will be asymptotically stable. If $\nu_1, \nu_2 > 1$ we have the phenomenon of bistability. The hyperbola $\nu_1\, \nu_2 = 1$ tells that competitors occupy the same ecological niche and characterizes the principle of competi-

tive exclusion[2], is forbidden for this model.

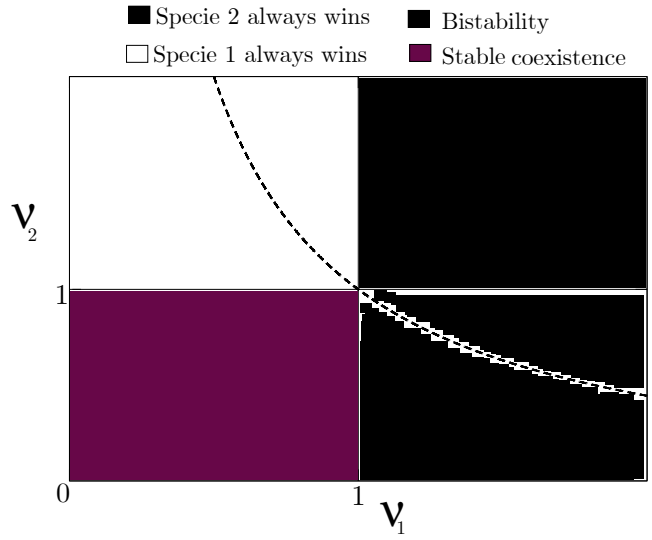

Figure 3.4: The different outcomes for competing populations in the parameter space - (ν_1, ν_2) plane. The parameters ν_1 and ν_2 are the competition coefficients that measure the extent to which each species presses upon the resources used by the other. It includes regions of species coexistence, bistability (in which the initial conditions determine the surviving species), and one species eradication. The species coexistence is forbidden onto the hyperbola $\nu_1\,\nu_2 = 1$. Figure taken from [108].

Figure 3.5 shows a typical curve of population growth under competition of two species of protozoa when they are separated or mixed. Considering the case where the species are separated, as the population density increases, intraspecific competition slows down the rate of growth until an equilibrium density or "carrying capacity" is achieved. In the presence of the other species, the growth rate also slows down due to interspecific competition, and the final density ends below the carrying capacity. Gause found the numbers of *P. caudatum* always declined up to extinction, leaving *P. aurelia* the only survivor. This occurred because *P. aurelia* was able to better use the limited available resources and hence grow six times faster than its competitor, *P. caudatum* [135].

Figure 3.6 shows the characteristic phase space of an experiment that considers competition between two types of algae. It is possible to identify three typical regimes of competition between these two species: coexistence and survival of only one of those species. Similar experiments make it possible to empirically forecast the environmental conditions that allow both species to coexist. Also, it is possible to introduce into the model explicit characteristics of resources and environment [137]

Hitherto it was considered the simplest cases of uniform competition matrices (ν_{ij}) in the LVM. Accordingly, each species competes with all others and itself with equal

[2]This principle states that if two species are competing for a resource, the species that uses the resource more efficiently will eventually eliminate the other locally – no two species with the same niche can coexist.

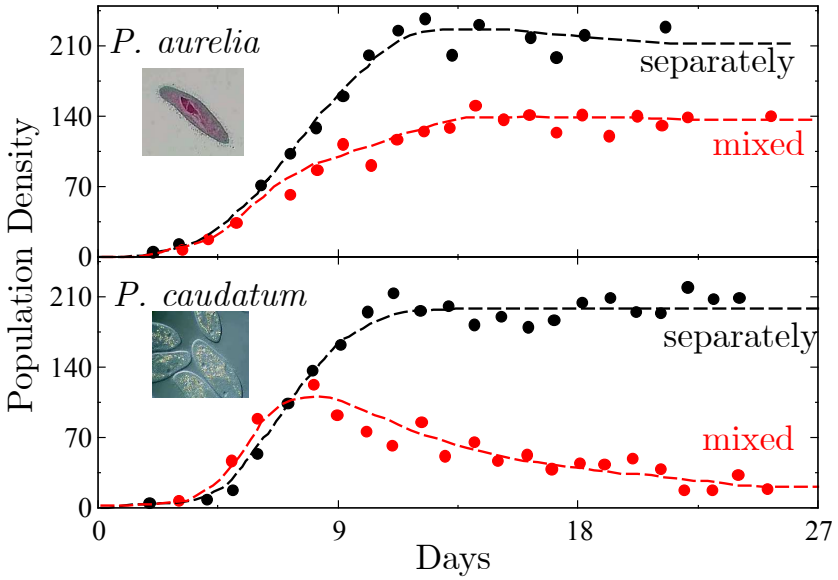

Figure 3.5: Competition between the protist *Paramecium aurelia* and *Paramecium caudatum* under resource limitation conditions. If the species grow separately, they attain stable population densities. If they are mixed, competition causes that the numbers of *P. caudatum* always declined to extinction, leaving *P. aurelia* the only survivor. The growth curves were fitted according to the LVM (3.4) for $l = 2$. After [135].

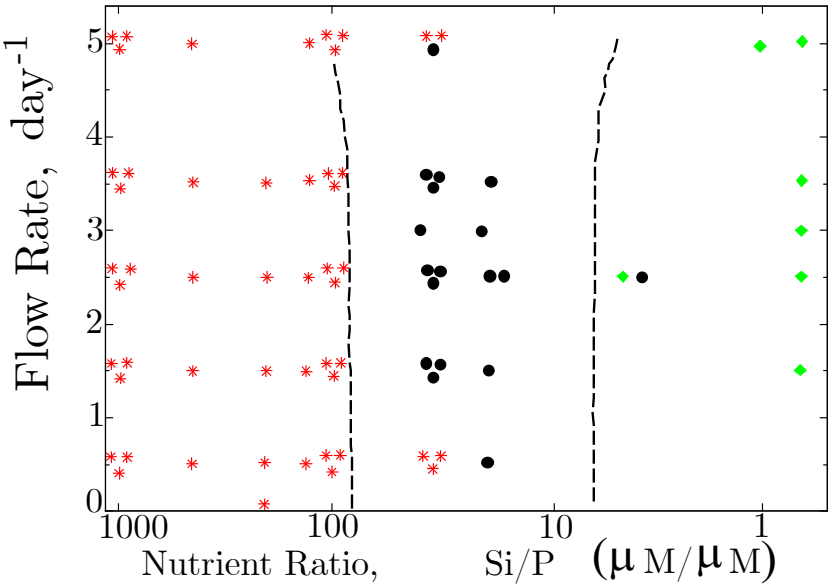

Figure 3.6: Competition between the algae *Asterionella formosa* (*A.f.*) and *Cyclotella meneghiniana* (*C.m.*) for two mineral resources: silica (Si) and phosphorous (P). The competition equations for resources can be used to predict the index of resources offer ($S_1/S_2 = Si/P$) for which *A.f.* wins (left region), *C.m.* wins (right region), or both species coexist (middle region). This diagram was constructed on the basis of experimental results in which *A.f.* wins ($*$), *C.m.* wins ($\blacklozenge$), or both coexist ($\bullet$). Figure adapted from [136].

($\nu_{ij} = \nu_{ji} = \nu$) or distinct ($\nu_{ij} = \nu$ and $\nu_{ii} = \alpha \; \forall \; i, j$) resistance. These two scenarios allow us to explore the effects of competition without secondary extinctions caused by competitive exclusion in the context of a competitive network. To introduce more realistic characteristics, the limited uniform model can be altered incorporate stochastic fluctuations that act to structurally perturb the interaction network [138, 139, 140, 141, 142, 143]. The diffuse and asymmetric competition network topology can be specified by a large set of competing community architectures when the interspecific interaction matrix ν_{ij} is generated by drawing $N \times N$ random numbers from a uniform distribution into $[0, 1]$ and $\nu_{ii} \in (0, 1]$.

At last, it is worthy to call attention to the following "phylosofical" point. The LVM is purely phenomenological; it does not refer to any explicit mechanism underlying competition, and there is no *a priory* reason to assume that the presence of other species should have a linear effect on a species per capita growth rate. Indeed the competition coefficients ν_{ij} cannot be derived from first principles but only measured *a posteriori*, e.g., after having performed a competition experiment. Accordingly, the Lotka-Volterra model is mainly a conceptual tool and it has very limited predictive power in real-world scenarios [144].

3.3 Allelopathic Suppression

The effects of allelopathy emerge when $\zeta_{ij} \neq 0$ are considered for multispecies competition in LVM, the system of equation (3.1). These allelopathic networks can be described by the parameters μ_{ij} (mortality of species i due to toxin j) and γ_{ij} (uptake of toxin j by species i). Thus, studying the competitive dynamics mediated by the production of toxic chemical compounds is important to understand the formation and establishment of biological communities.

The simplest case of a competitive and allelopathic dynamic is that involving two species. Specifically, will be reported here the case toxin absorption described by a Holling type III functional response, as in equation (3.2), with a threshold for toxin effects and saturation of the allelopathic suppression: $\Phi(x_i) = \frac{(x_i-1)^2}{c_i+(x_i-1)^2}$ for both species. Their threshold concentrations are 1 and $x_i = \gamma_i \, N_i \, B_j$ represents the consumption of the toxin j by the species i, $i \neq j$, with *per capta* absorption rate γ_i. When at least one of the interacting species releases toxins in quantities greater than its poisoning threshold, the regions of coexistence, bistability, and eradication of a species by interspecific competition (see Figure 3.4) are changed by allelopathic suppression as shown in Figure 3.7. Summarizing, if species 1 uptake the toxin released by species 2 at levels below the poisoning threshold, the region in the plane (ν_1, ν_2) with the prevalence of species 2 increases, whereas the region characterized by the dominance of species 1 decreases (see Figure 3.4-(a)). Similar

results are obtained for the inverse situation, i.e., species 1 produces allelochemicals in a high concentration while species 2 produces at a low concentration (see Figure 3.4-(b)) [108].

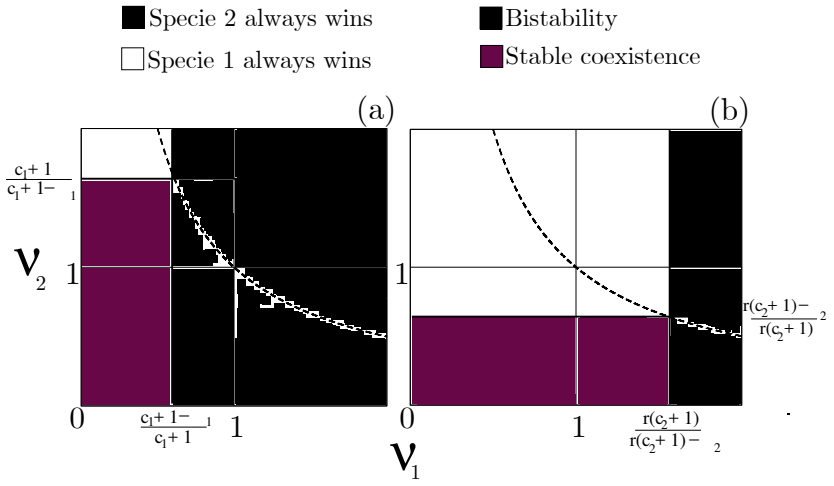

Figure 3.7: The effect of allelopathy on the outcomes for two competing populations. In (a) the species 2 can allelochemically suppress species 1 ($x_1 \leq 1$ and $x_2 > 1$) and the converse in (b) ($x_2 \leq 1$ and $x_1 > 1$). In comparison with pure interspecific competition (see Figure 3.4), the regions of coexistence, bistability, and one species eradication are changed. The main result is that a weak, but allelopathic, a competitor can eradicate or coexist with a stronger competitor for resources. Figure is taken from [108].

At last, the case $x_1 > 1$ and $x_2 > 1$ in which the two competing species uptake toxins at levels beyond their poisoning thresholds were analyzed. So, each competing species is subjected to the allelopathic suppression induced by the other. In this case, we were unable to derive analytical inequalities $\nu_i < f_i(\mu, c, r)$, involving the competition coefficients, replicative rates, and the parameters characterizing the functional responses to the toxins, that limit the regions of coexistence, bistability, and one species eradication onto the plane ν_1, ν_2 plane. In Figure 3.8-(a) these regions are shown for a system in which species 1 has an advantage over its competitor in their biochemical warfare ($c_1 < c_2$ and $\mu_1 < \mu_2$). *Mutatis mutandis*, the scenario is qualitatively the same observed in Figure 3.7. Again, a weak competitor can eradicate a strong competitor if endowed with more lethal biochemical weapons. Additionally, the dominance of the stronger allelopathic species is enhanced by the invasion of coexistence and bistability regions. In Figure 3.8-(b) the converse case is illustrated.

3.3.1 Evolutionary Dynamics

The origin and maintenance of biological communities depend on the interplay between evolutionary processes and ecological interactions that allow species coexistence [123]. Ecological and evolutionary processes are integrated in our model by assuming that mu-

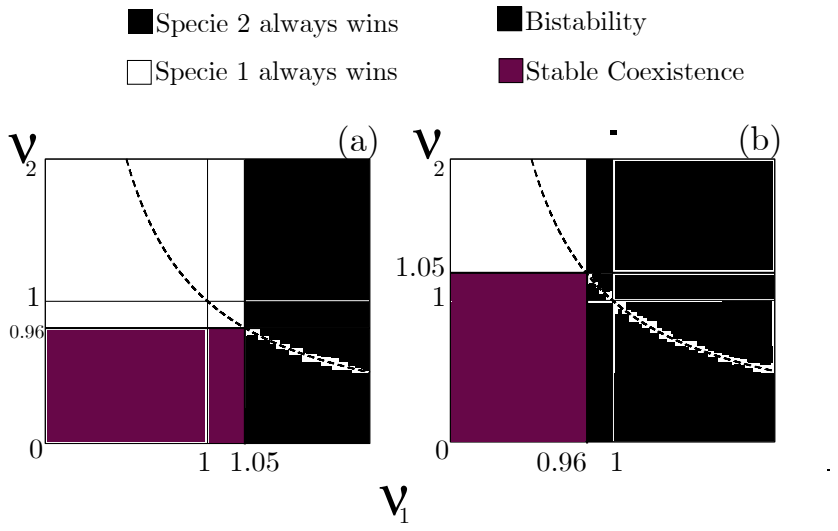

Figure 3.8: The outcomes for the allelochemical warfare between two competing species. The value $r = 1$ was used in order to ensure equal species replication rates. Differences in allelopathic suppression rely on toxin release β and degradation rates δ, lethality μ and efficacy c. In (a) the values $\beta_1 = 0.7$, $\beta_2 = 0.3$, $\delta_1 = 0.2$, $\delta_2 = 0.3$, $c_1 = 0.5$, $c_2 = 0.7$, $\mu_1 = 0.3$ and $\mu_2 = 0.4$ were fixed, providing an advantage to species 1 in the allelochemical warfare against species 2. Numerically, the lines $\nu_1 \lesssim 1.05$ and $\nu_2 \lesssim 0.96$ were found to limit the coexistence, bistability, and one species eradication regions. In (b) all the parameters fixed in (a) are interchanged in order to invert the species allelochemical traits. Figure is taken from [108].

tations in one of the competing species present at the current stationary state of the ecological dynamics generate a new species. This fresh species must survive and evolve in response to novel conditions, and the old species in the community must, in turn, evolve in response to the new species. Ultimately, the ecological dynamics are driven to another stationary state characterized by distinct populations and interaction networks. After that, additional genetic diversity is generated by adding different species to the current community, and so on. Two mechanisms for species introduction were tested, which we namely call: sequential invasion events (SIE) and branching process (BP).

Numerical integration

The previously described eco-evolutionary processes were investigated through numerical integration using the fourth-order Runge-Kutta method. Distinct distributions for the values of the competition and allelochemical parameters ϵ_{ij} and ζ_{ij} were employed. Also, 200 independent evolutionary histories were generated for the SIE and BP dynamics, in the latter case for each initial graph shown in Figure 3.9. From the numerical integrations, the adjacency matrix at the successive stationary states for each evolutionary history were obtained. Then, the community structures (interaction network topologies) and species

richness was determined for both SIE and BP dynamics.

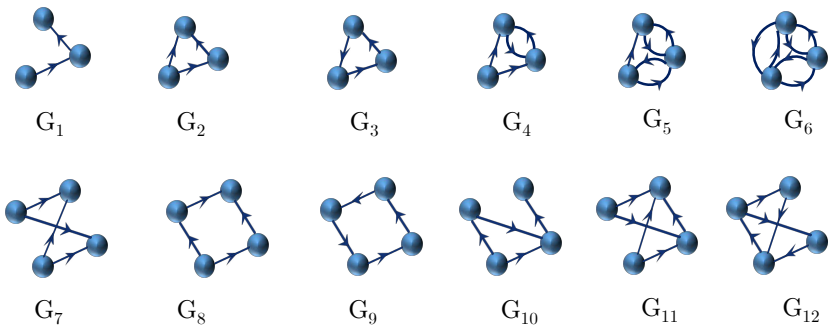

Figure 3.9: Allelopathic networks used as starting structures for the BP dynamics. The species interactions are indicated by arrows. In numerical integrations, the population densities $N_i\ (0) = 0.7$ and toxin concentrations $B_i\ (0) = 0$ were fixed.

Sequential Invasion Events (SIE)

To describe sequential invasion events consider that an alien species, the node $n+1$, is added to a stationary state currently containing n species. It is assumed that the alien species compete for resources with all the n pre-existing ones. Thus $\varepsilon_{n+1,i} = \varepsilon_{i,n+1} = 1$ for $i = 1, \ldots, n$. Concerning allelochemical suppression, the alien species affects k_{n+1}^{out} of the old ones and is affected by k_{n+1}^{in} of them. So, k_{n+1}^{out} elements $\zeta_{n+1,i}$ in the row $n+1$ of the enlarged adjacency matrix ζ are fixed in 1 and the remaining in 0. To do this, an integer i is randomly chosen in the interval $[1, n]$, and we set $\zeta_{n+1,i} = 1$, with a probability $p = 1 - n^{out}/n$, or $\zeta_{n+1,i} = 0$, with a probability $1 - p = n^{out}/n$. Then, a new distinct i is randomly selected and the protocol repeated until k_{n+1}^{out} elements in the $(n+1)$-th row of ζ are set to 1. The value $n^{out} \in [1, n]$ defines the probability p and, again, is an integer random number chosen with equal change. In average, n^{out} determines the fraction of species in the community which do not interact with the alien species. Analogously, k_{n+1}^{in} elements $\zeta_{i,n+1}$ in the column $n+1$ of the enlarged adjacency matrix are fixed in 1 and the remaining in 0. The same protocol is used to determine the k_{n+1}^{in} nodes i that suppress the node $n+1$ (i. e., $\zeta_{i,n+1} = 1$). But now the probability used is $p = 1 - n^{in}/n$. Finally, the initial toxin concentration of the alien species is $B_{n+1} = 0$ and its population density is $N_{n+1} = 0.01N_i^*$, with N_i^* corresponding to the stationary population density of one species chosen at random between the n current members of the community. Regarding the initial community structure, the SIE evolutionary dynamics starts from a single species.

The SIE dynamics were analyzed for three distinct scenarios considering functional responses (3.2). In the first one, called homogeneous, the original and all introduced species have equal competition and allelopathic traits: $r_i = 1\ \forall i$, $\nu_{ij} = 0.1$ and $\epsilon_{ij} = 1$,

$\forall i, j$ and $\gamma_{ij} = 0.1$, $\forall i, j$, $c_i = 0.1$, $\beta_i = 0.1$, and $\delta_i = 0.2$, with weak ($\mu_{ij} = 0.1$) or strong ($\mu_{ij} = 0.5$) alellopathic suppression $\forall i$. In the second scenario, called heterogeneous competition, the allelochemical traits are equal, as before, but the competition coefficients ν_{ij} are disordered, i.e., randomly drawn from a uniform distribution on the interval $(0, 1]$. Thus, the species can have different competition, but the same allelochemical capabilities. Finally, in the third scenario, called completely heterogeneous, it is supposed that both competition and allelochemical traits are disordered and independently drawn from uniform distributions on the interval $(0, 1]$. Only the toxins' degradation and uptaken rates, $\delta_i = 0.2$ and $\gamma_{j,i} = 0.1$, are the same for all species. Results concerning the absorption effect in the response functions, equation (3.2) are reported on the Appendix B.

In Figure 3.10-(a) and -(b) the average diversity as a function of the number n_{SIE} of SIE is shown. The diversity or species richness is defined as the fraction of species that survive at the community stationary state. As expected, weak ($\mu = 0.1$) allelopathic suppression allows the assembly of communities exhibiting large diversities. This is true for all response functions tested and, as expected, the diversity decreases as the response to toxins increases. For instance, in our simulations, $\Phi^{(1)}(x) < \Phi^{(3)}(x) < \Phi^{(2)}(x)$ except for small ($x < 0.11$) or large ($x > 0.89$) toxin concentrations. In contrast, community diversity is drastically reduced at strong allelopathy ($\mu = 0.5$) for all response functions. As an example, the number of surviving species decreases from ~ 100, at weak, to ~ 9 at strong allelopathic suppression and response function $\Phi^{(1)}$. In this strong regime, diversity seems to decrease slowly after reaches a maximum as the number of invasion events increases. In Figure 3.10-(c) it is plotted the diversity as a function of the strength of allelopathic suppression for homogeneous competition and allelopathy. Again, the larger the interaction strength μ is, the smaller is community diversity. Indeed, diversity decays exponentially beyond a threshold value dependent on the response function. This decay is much faster than the inversely proportional to the strength of interaction suggested by May's stability line [9].

In Figure 3.11, the average connectivity of allelochemical networks is illustrated as a function of the number n of surviving species observed at the stationary state reached after a SIE. Our results indicate that the average connectivity is similar for both weak ($\mu = 0.1$) than strong ($\mu = 0.5$) allelopathy. Furthermore, the connectivity saturates to a constant value. This behavior is very distinct from the power-law scaling for large n values observed in random networks, $C(n) \sim n^{-1}$ [9], and a model for growing random networks based on global stability, $C(n) \sim n^{-1.2}$ [34]. In contrast to previous works in which the number of interactions decreases linearly with the number of species [9], Martinez [124] found a constant connectance for some food webs. Therefore, our results indicate that the communities generated by the SIE dynamics markedly differ from random networks involving positive and negative interactions.

The degree distributions $P(k)$ for allelochemical interaction networks generated by

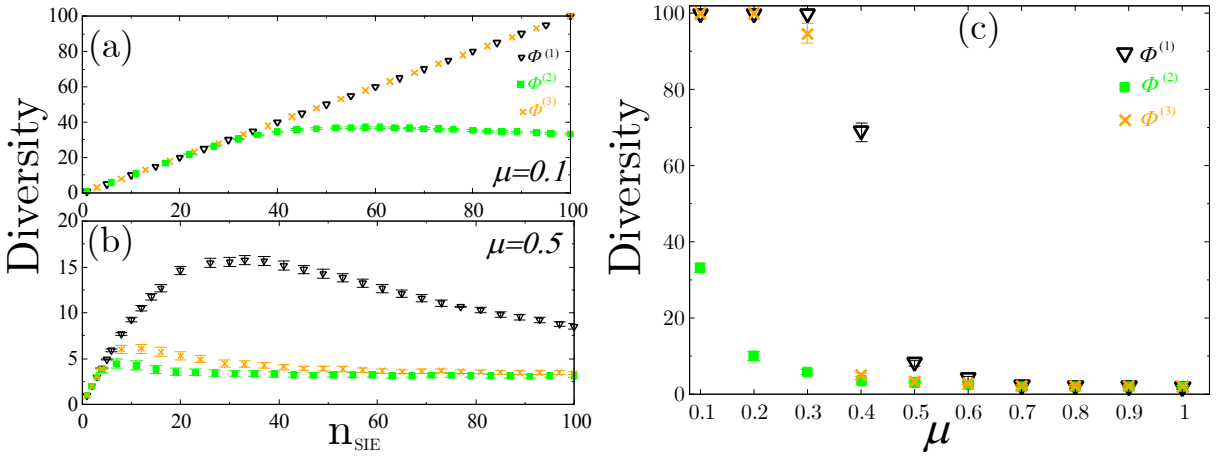

Figure 3.10: Average diversities for 200 independent eco-evolutionary histories as functions of the number n_{SIE} of surviving species observed after successive invasion events (SIE). In (a) weak ($\mu = 0.1$) and in (b) strong ($\mu = 0.5$) allelopathic effect were tested. Average diversity after $l = 100$ SIE as a function of μ. All plots refer to homogeneous parameters $r_i = 1$, $\nu_{ij} = \gamma_{ij} = 0.1$, $c_i = \beta_i = 0.1$, and $\delta_i = 0.2$ $\forall i, j$. The community always starts from a single species.

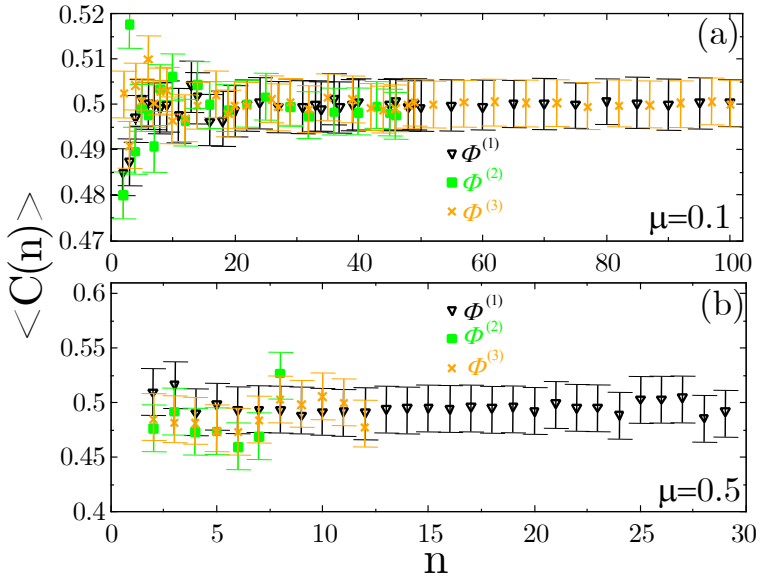

Figure 3.11: Average connectivities as functions of the number of surviving species after SIE dynamics considering (a) weak and (b) strong allelopathic mortality. Both plots refer to parameters $r_i = 1$, $\nu_{ij} = \gamma_{ij} = 0.1$, $c_i = \beta_i = 0.1$, and $\delta_i = 0.2$ $\forall$ i, j. Averages were performed over 200 independent samples.

the SIE dynamics are shown in Figure 3.12. Normal (Gaussian) and Weibull distributions were observed for in- and out-degree distributions $P(k^{in})$ and $P(k^{out})$ (data not shown) depending on the mortality μ induced by allelopathy. For strong ($\mu = 0.5$) allelopathic suppression, $P(k^{in})$ is a Weibull distribution. In contrast, at weak ($\mu = 0.1$) allelopathic suppression, $P(k_{in})$ is a Gaussian. The apparent anisotropies observed in the insets for $\Phi^{(1,2,3)}$ are very weak, as supported by skewness $S \sim 0$ and kurtosis $K \sim 3$. The ratio $\kappa = \langle k^2 \rangle / \langle k \rangle \sim \langle k \rangle$ is obtained for either weak or strong allelopathic suppression μ, indicating that the SIE allelochemical networks are homogeneous [3] (see Table B.1 in Appendix B).

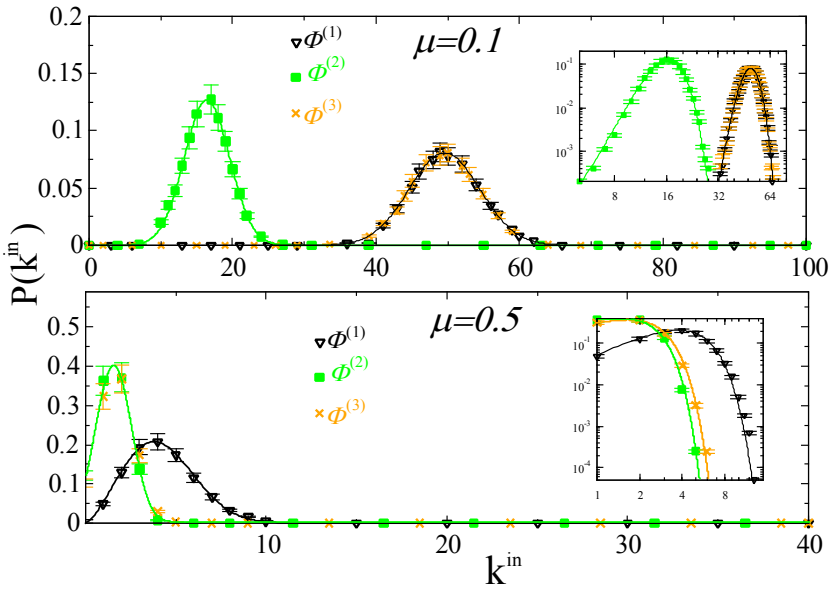

Figure 3.12: Degree distributions $P(k^{in})$ for SIE allelochemical interaction networks in which the competition and allelochemical traits are the same for all species. The green and black solid curves correspond, respectively, to Gaussian and Weibull fittings to the data. The parameters were fixed in $r_i = 1$, $\nu_{ij} = \gamma_{ij} = 0.1$, $c_i = \beta_i = 0.1$, and $\delta_i = 0.2$ $\forall$ i, j. Insets: log-log plots of the in-degree distributions. The parameters and properties of these distributions are reported in Table B.1 Appendix B.

In Figure 3.13, the average betweenness centrality $\langle x_i \rangle$ is plotted for every node i present at the stationary allelochemical network after $l = 100$ SIE. It can be noticed that $\langle x_i \rangle$ decreases dramatically as the strength of allelopathic suppression increases. Also, stronger is the responses to toxins ($\Phi^{(2)}$ for $\mu = 0.1$ and $\Phi^{(2,3)}$ for $\mu = 0.5$), smaller is the $\langle x_i \rangle$. Furthermore, the average centrality is almost constant at weak allelopathic suppression indicating a homogeneous connectivity pattern for every node and the absence of hubs, bridges joining distinct modules, and star graphs in the network. This feature is consistent with the typical network structures seen in the $\mu = 0.1$ plot. In contrast, at strong allelopathy (see Figure 3.13-(b)), the average centrality fluctuates probably due to the emergence of modules in the network, as suggests the typical structures for $\Phi^{(1)}$ and $\mu = 0.5$, but the behavior is typically constant. In addition, the small values for $\langle x_i \rangle$ are

a consequence of very small and sparsely connected network structures.

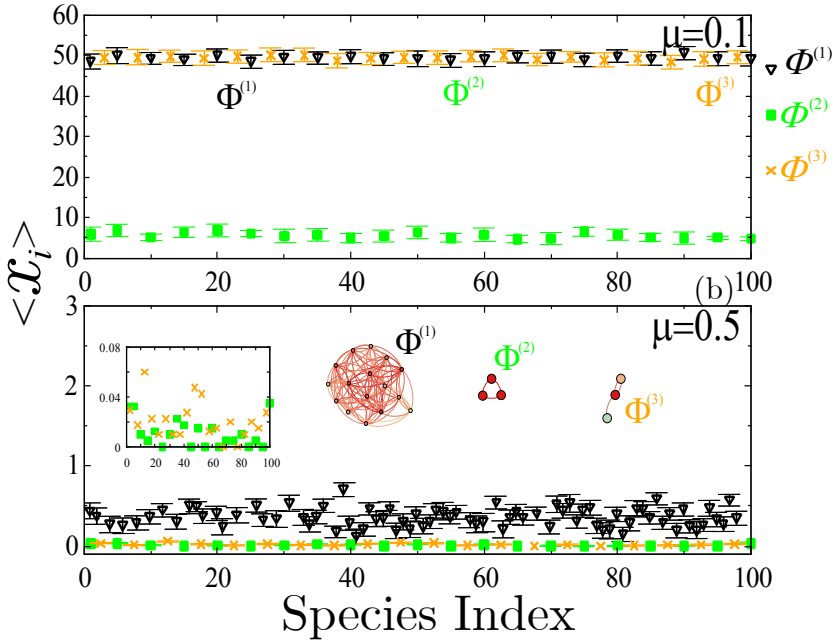

Figure 3.13: Average betweenness centrality for each node (surviving species) in communities generated from a single initial species through successive invasion events for weak $\mu = 0.1$ and strong $\mu = 0.5$ allelopathic suppression. Typical network structures associated with each functional response are also included. Homogeneous competition and allelopathy are assumed ($r_i = 1$, $\nu_{ij} = \gamma_{ij} = 0.1$, $c_i = \beta_i = 0.1$, and $\delta_i = 0.2$ $\forall i, j$). Inset: very small, but non-vanishing centralities for the response functions $\Phi^{(2)}$ and $\Phi^{(3)}$ at strong $\mu = 0.5$ allelopathic suppression.

The community structure was also investigated for scenarios in which only the competition, in addition, allelopathy are heterogeneous, so that the coefficients ν_{ij} and μ_{ij} are drawn from random distributions. The results are qualitatively the same as those obtained for the homogeneous cases reported earlier, but the introduction of heterogeneity in competition coefficients has stronger effects as shown, for instance, in Figure 3.14. In comparison with Figure 3.10, a drastic reduction in diversity is observed even under weak allelopathy $\mu = 0.1$ and for all response functions. Disorder (heterogeneities) in the allelochemical traits further reinforce this tendency.

Lastly, typical allelochemical networks or community structures generated by the SIE dynamics are illustrated in Figure 3.15. The nodes in these networks represent species present in the community and the directed edges between them represent allelopathic interactions. As the allelopathic strength increases, the number of nodes (surviving species) decreases, the network topology seems to changes from random to modular structures, and the corresponding connectivity distributions change from normal (or Gaussian) to Weibull distributions.

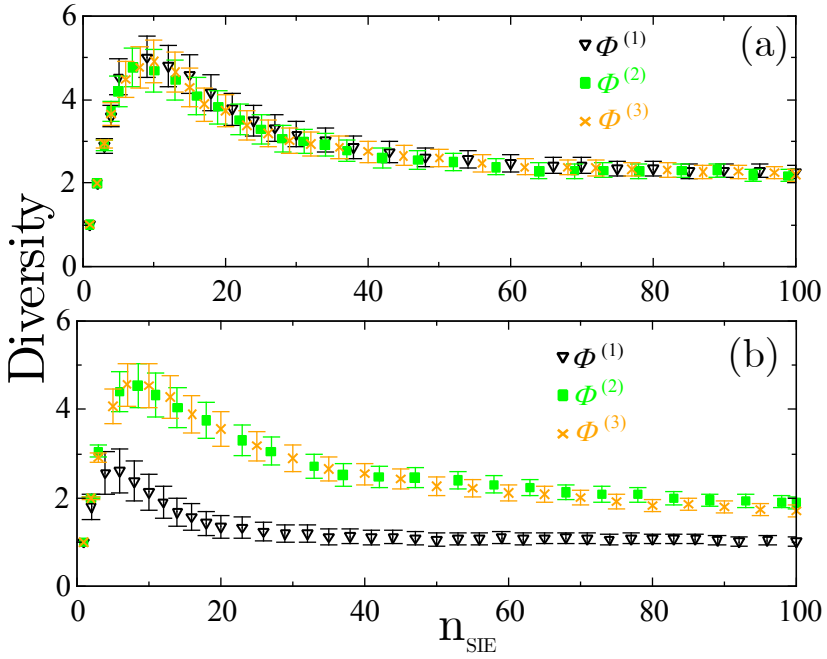

Figure 3.14: Average diversity for 200 independent eco-evolutionary dynamics observed after successive invasion events. The initial community is always composed of a single species. In (a) the competition parameters are heterogeneous, i. e., ν_{ij} are randomly chosen from uniform distributions in $(0, 1]$, but the allelochemical traits ($r_i = 1$, $c_i = \beta_i = 0.1$, $\delta_i = 0.2$ and $\gamma_{ij} = 0.1\ \forall\ i, j$) are homogeneous. The value of $\mu = 0.1$ was used (weak allelopathy). In (b) both competition coefficients and allelopathic traits are heterogeneous with $\gamma_{ij} = 0.1$ and $\delta_i = 0.2\ \forall\ i, j$.

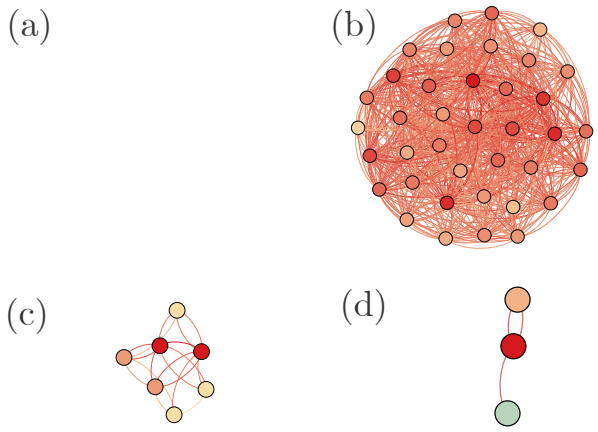

Figure 3.15: Typical allelochemical networks generated after $l = 100$ SIEs for (a) weak ($\mu = 0.1$) and (b) strong ($\mu = 0.5$) allelopathic suppression for homogeneous competition and allelochemical traits ($r_i = 1$, $\nu_{ij} = \gamma_{ij} = 0.1$, $\beta_i = c_i = 0.1$ and $\delta_i = 0.2\ \forall\ i, j$). (c) Heterogeneous competition ($\nu_{ij} \in (0, 1]$ randomly chosen), but weak and homogeneous allelopathy ($\mu_{ij} = 0.1\ \forall\ i, j$). (d) Both, competition and allelopathy heterogeneous (ν_{ij}, μ_{ij}, c_i and $\beta_i \in (0, 1]$ randomly chosen). The functional response $\Phi^{(1)}$ was used.

Branching Process (BP)

The new species $n+1$ introduced in the network descends from one of the n species present at the community stationary state. The ancestor species i is randomly chosen and only their allelochemical traits are mutated in its descendant species $n+1$. Specifically, all the k_i^{in} input and k_i^{out} output connections of the ancestor node i are inherited by the new node $n+1$, except one of them. With equal chance, either a randomly chosen input $\zeta_{j,i}$ or output $\zeta_{i,j}$ of the node i will be activated ($\zeta_{j,n+1} = 1$) in node $n+1$ if inactive ($\zeta_{j,i} = 0$) in i, or vice-versa. Since it is supposed here that the resource competition traits are not changed by mutations, $\varepsilon_{i,j} = \varepsilon_{n+1,j}$ and $\varepsilon_{j,i} = \varepsilon_{j,n+1}$ for $j = 1, \ldots, n$. Again, the initial toxin concentration of the new species is $B_{n+1} = 0$ and its population density is $N_{n+1} = 0.01N_i^*$. Finally, concerning the initial community structure, the BP evolutionary dynamics start from a network with $n_0 < l$ nodes. Different starting graphs for the BP dynamics are shown in Figure 3.9.

The BP dynamics were analyzed for three distinct scenarios. In the first one, called homogeneous, all the original and introduced species have equal competition and allelopathic traits: $\nu_{ij} = 0.1$ and $\epsilon_{ij} = 1 \; \forall \; i, j$, $\mu_{ij} = \gamma_{ij} = 0.1$,$\forall \; i, j$, $c_i = \beta_i = 0.1$ and $\delta_i = 0.2$ $\forall \; i$. In the second scenario, called heterogeneous competition, the allelochemical traits are equal, as before, but the competition coefficients ν_{ij} are disordered, i. e., randomly drawn from a uniform distribution on the interval $(0, 1]$. Thus, the species can have different competition, but the same allelochemical capabilities. Finally, in the third scenario, called completely heterogeneous, it is supposed that both competition and allelochemical traits are disordered and independently drawn from uniform distributions on the interval $(0, 1]$. Only the toxins' degradation and uptaken rates, $\delta_i = \delta = 0.2$ and $\gamma_{ji} = \gamma = 0.1$, are assumed the same for all species.

The average diversity as a function of the number n of "speciations" is shown in Figure 3.16. The middle and bottom plots evidence that heterogeneous competition and allelochemical traits strongly decrease community diversity in comparison to homogeneous traits (upper plot).

In Figure 3.17, the average centrality is plotted for every node i present at the stationary allelochemical network after $l = 100$ speciation events. It can be noticed that $\langle x_i \rangle$ decreases dramatically as the strength of allelopathic suppression increases. Indeed, even at weak suppression ($\mu = 0.1$, upper plot), strong responses to toxins ($\Phi^{(2)}$) lead to small average centrality. However, in contrast to the SIE dynamics for which a constant $\langle x_i \rangle$ is observed (see Figure 3.13), the centrality is higher for the first species introduced in the community and monotonously decreases for those species attached later.

The in- and out-degree distributions, $P(k^{in})$ and $P(k^{out})$, for the allelochemical interaction networks generated by the BP dynamics are shown in Figure 3.18. In all the tested scenarios, these degree distributions are fitted by power-laws truncated by

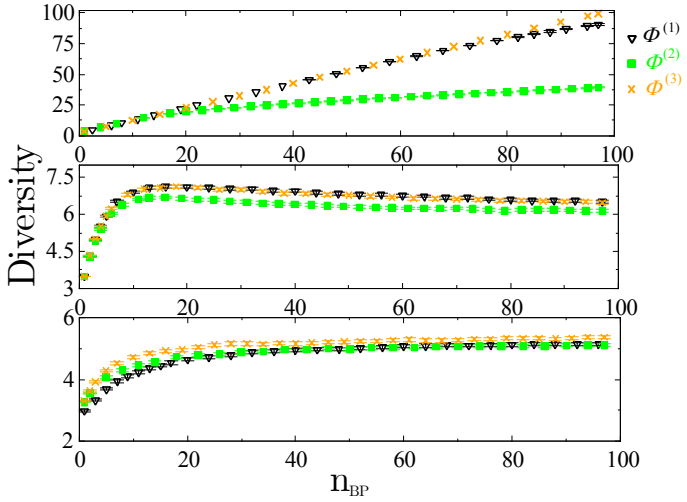

Figure 3.16: Average diversity for 200 independent BP eco-evolutionary histories as a function of the number n_{BP} of speciation events. The initial communities are the graphs shown in Figure 3.9. The upper, middle, and bottom plots refers, respectively, to homogeneous ($r_i = 1$, $\nu_{ij} = \mu_{ij} = \gamma_{ij} = 0.1$, $c_i = \beta_i = 0.1$, and $\delta_i = 0.2$, $\forall\ i, j$), heterogeneous competition ($\nu_{ij} \in (0, 1]$, randomly drawn), and completely heterogeneous scenarios (both competition ν_{ij} and allelopathic μ_{ij}, β_i and c_i parameters randomly chosen in $(0, 1]$ with $\delta_i = 0.2$ and $\gamma_{ij} = 0.1\ \forall\ i, j$).

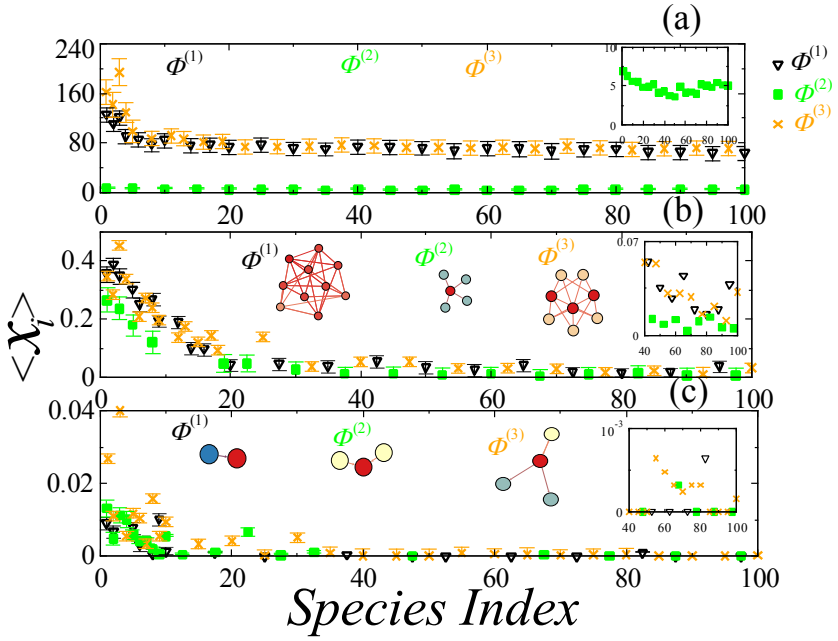

Figure 3.17: Average betweenness centrality for each node (surviving species) in communities generated from the initial graphs shown in Figure 3.9 for (a) homogeneous, (b) competition heterogeneous, and (c) completely heterogeneous scenarios. The model parameters are those used in Figure 3.16. Typical network structures associated with each functional response are also included. Insets: zooms for small $\langle x_i \rangle$ values.

stretched exponentials $P(k) \sim k^{-\alpha}\, exp(-\eta\, k^{\lambda})$ (Weibull-like distributions). The ratio $\langle k^2 \rangle / \langle k \rangle \sim \langle k \rangle$ is observed only for both competition and allelopathy homogeneous and weak ($\nu < 1$ and $\mu = 0.1$), indicating the homogeneous nature of such networks. In contrast, $\langle k^2 \rangle / \langle k \rangle \ll \langle k \rangle$ was found for the remaining cases: (i) weak homogeneous competition ($\nu < 1$) and strong homogeneous allelopathy ($\mu = 0.5$); (ii) weak heterogeneous competition ($\nu_{ij} \in (0, 1]$ randomly chosen) and weak homogeneous allelopathy ($\mu = 0.1$); and (iii) heterogeneous competition and allelopathy (ν_{ij}, μ_{ij}, c_i and $\beta_i \in (0, 1]$ chosen at random). In these regimes, the emergence of heterogeneous networks is expected. The values obtained for the ratio $\langle k^2 \rangle / \langle k \rangle$ and the exponents characterizing the degree distributions for SIE and BP dynamics are listed in Table B.2 in Appendix B.

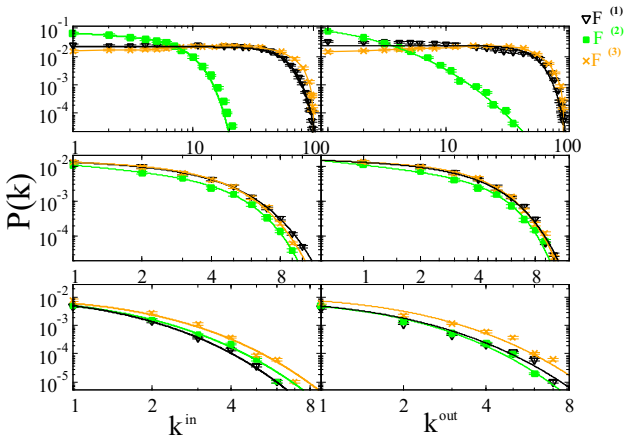

Figure 3.18: In- and out-degree distribution functions in directed BP allelochemical networks. The upper, middle, and bottom plots refer, respectively, to homogeneous, heterogeneous competition, and completely heterogeneous scenarios. The model parameters are those used in Figure 3.16. In all plots, a typical power-law truncated by a stretched exponential fit (solid curve) is shown whose parameters and distribution properties are listed in Table B.2 in Appendix B.

The BP dynamics generate diverse community structures as illustrated in Figure 3.19. At weak allelopathic suppression ($\mu = 0.1$), Figures 3.19-(a) and -(b), the hierarchical and modular character of such networks emerges. This trait seems to be reflected on the larger values of $\langle k \rangle$ for small k, but smaller and almost constant for large k. In turn, for heterogeneous competition and allelopathy, Figures 3.19-(c) and -(d), the networks are very small and sparsely connected. The model parameters are those used in Figure 3.17.

In order to further characterize these BP networks, the clustering coefficient and the average degree among nearest neighbors of a node with degree k were also determined. Figure 3.20 shows the average local clustering as a function of in-and out-degree. Our results reveal that both $Cc^{in}(k)$ and $Cc^{out}(k)$ increases slowly for small degrees, but exhibit stretched exponential cut-offs for large degrees, i. e., $Cc \sim k^{-\alpha}\, exp(-\eta\, k^{\lambda})$ and $\eta > 0$.

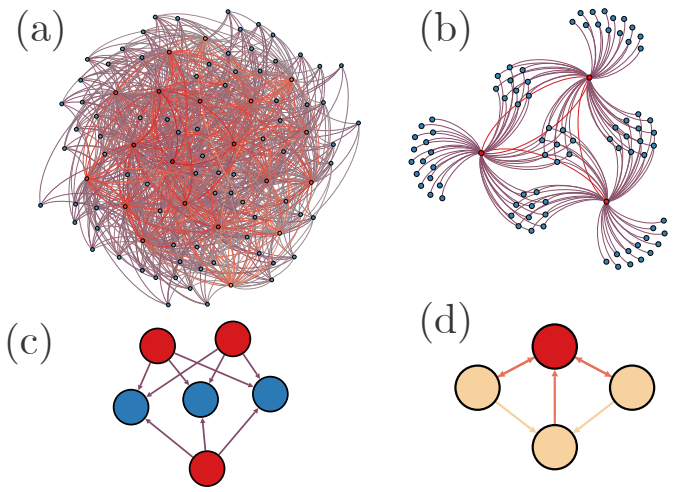

Figure 3.19: Examples of allelochemical networks generated after $l = 100$ speciations. (a) Homogeneous scenario (constant and equal competition $r_i = 0.1$, $\nu_{ij} = 0.1$ and allelopathic $\gamma_{ij} = \beta_i = c_i = 0.1$, $\delta_i = 0.2$ parameters for all species) at weak allelopathy ($\mu = 0.1$). The heterogeneous competition scenario (randomly chosen competition coefficients ν_{ij} but equal allelopathic parameters) at (b) weak ($\mu = 0.1$) and (c) strong ($\mu = 0.5$) allelopathic suppression. (d) Completely heterogeneous scenario (randomly chosen competition and allelopathic parameters except for $\gamma_{ij} = 0.1$ and $\delta_i = 0.2$) fixed. The starting community structures are those shown in Figure 3.9. The response functions $\Phi^{(1)}$ (in (a) and (b)), $\Phi^{(2)}$ (in (c)), and $\Phi^{(3)}$ (in (d)) were used.

The stretched exponential decays of both Cc^{in} and Cc^{out} for large degrees are faster than power lay decays, $Cc(k) \sim k^{-\alpha}$ with $\alpha \sim 1$, characteristic of modular structures with a hierarchical organization [43]. Also, for homogeneous and weak competition and allelopathy, the average clustering coefficient has the same magnitude as those for random networks with the same n, $\langle k^2 \rangle$, and $\langle k \rangle$. However, heterogeneity in competition or strong allelopathic suppression leads to the average clustering coefficient smaller than those for random networks. Since the behavior of Cc is associated with the dynamical mechanisms controlling which newly attached node survives or extinguishes, this result indicates that allelochemical networks grow primarily by adding nodes with few links.

The allelochemical network entropy was determined. Specifically, the degree distribution entropy H for networks with size n was calculated. This Shannon entropy [50] is larger more homogeneous is the degree distribution and communities with greater diversities tend to be more homogeneous. As illustrated in Figure 3.21, the entropy decreases as the allelochemical suppression increases. Particularly, $H[P(k^{out})]$ is more affected. Also, peaks at the initial community structures G_2, G_6, and G_{11} are neatly observed in $H[P(k^{in})]$ for almost all response functions in the heterogeneous regimes. Peaks in the entropy $H[P(k^{out})]$ are less evident and restricted to few response functions, e. g., in G_9 for $\Phi^{(4)}$ and G_4 for $\Phi^{(6)}$ at the homogeneous and heterogeneous competition scenarios, respectively.

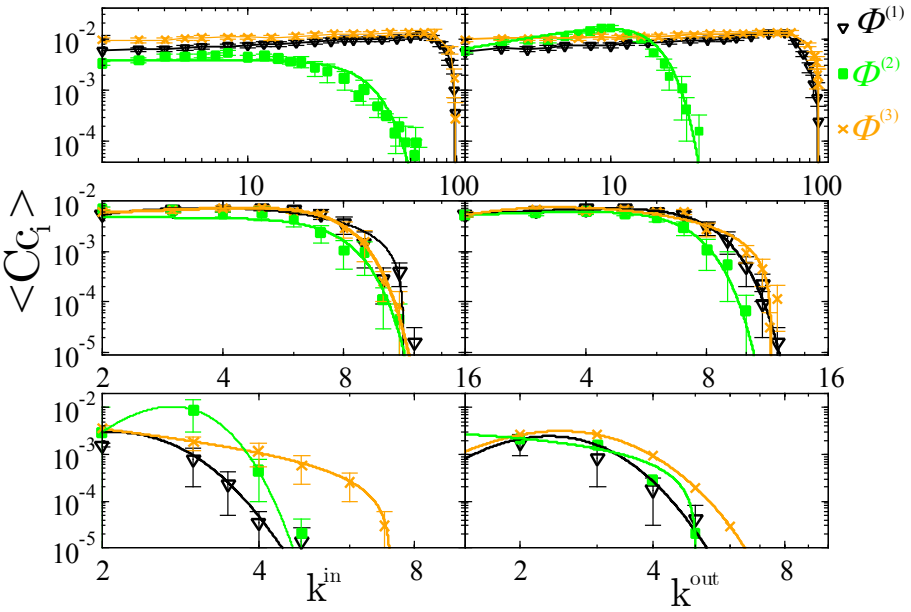

Figure 3.20: Average local clustering coefficient as a function of in- and out-degree. The upper, middle, and bottom plots correspond, respectively, to the homogeneous, heterogeneous competition, and completely heterogeneous scenarios. The initial networks were all those graphs shown in Figure 3.9. The model parameters are those used in Figure 3.16. In all plots, a typical power-law truncated by a stretched exponential fit (solid curve) is shown. The parameters of this fit are listed in Table B.3 in Appendix B.

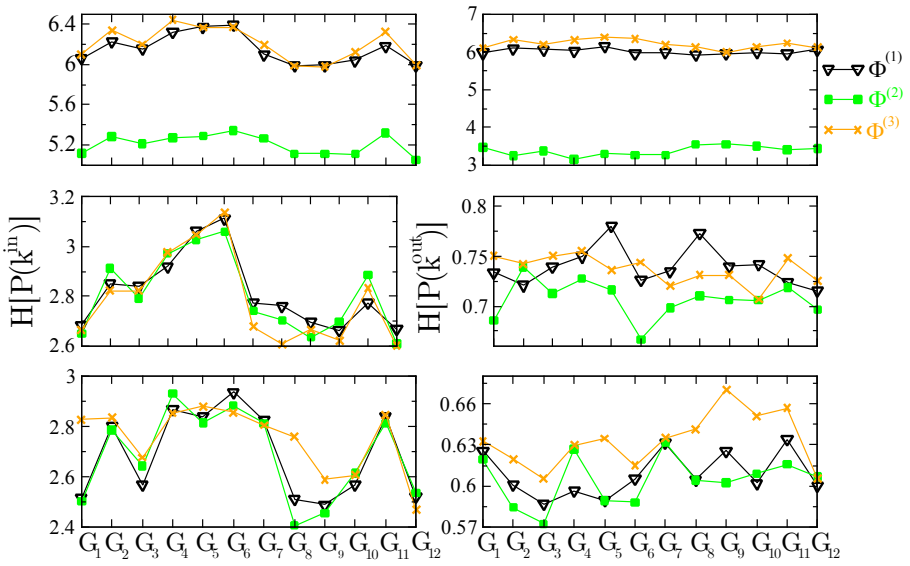

Figure 3.21: In- and out-degree distribution entropies for networks generated after $l = 100$ speciation events starting from each initial community structure shown in Figure 3.9. The upper, middle, and bottom plots correspond to the homogeneous, heterogeneous competition, and completely heterogeneous scenarios, respectively. Averages were taken over 200 independent histories.

Finally, the average degree K_{nn} among the nearest neighbors of a node with degree k was determined. K_{nn} measures the mixing by degree properties of networks, i. e. quantifies if there is a tendency of nodes with high degrees to connect to others with high degrees, and similarly for low degrees. If this is the case, the network is assortative; in contrast, if nodes with high degrees tend to connect to others with low degrees, the network is disassortative. In Figure 3.22, it can be seen that K_{nn} decays for large node's degree k^t even at weak homogeneous allelopathy in a clear disassortative behavior. Such a result is consistent with the observation that assortative mixing by degree makes a network more unstable [145].

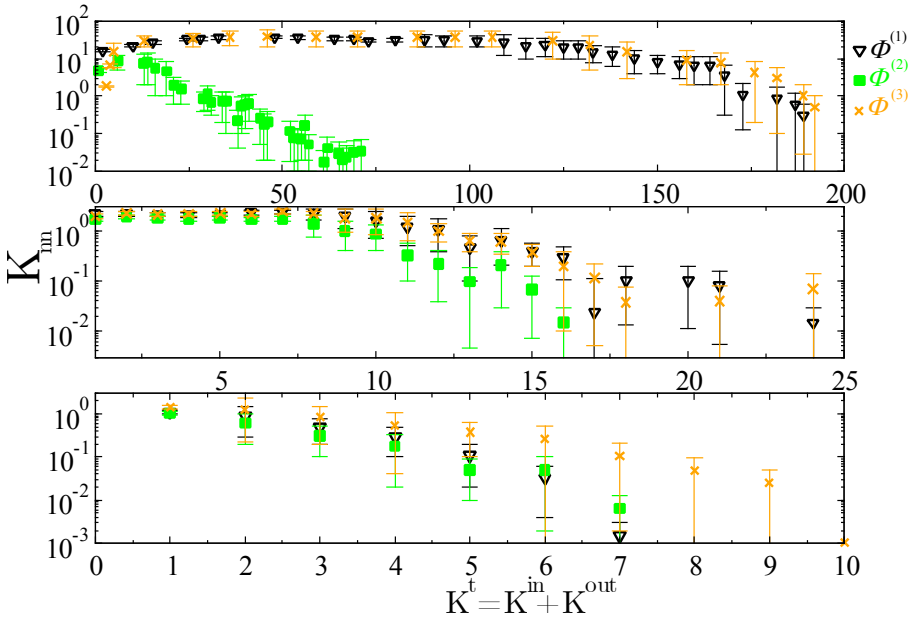

Figure 3.22: Average nearest neighbors degree $K_{nn}(k)$ of a node with total degree k^t for the homogeneous (upper), heterogeneous competition (middle), and completely heterogeneous (bottom) scenarios. The model parameters are those used in Figure 3.16 and the initial networks were all graphs in Figure 3.9.

3.4 Discussion

In this *Chapter*, a mathematical model was proposed to study the multispecies population dynamics that, in addition to competing for common resources, engage in chemical warfare based on toxins released against each others. The spatially homogeneous version of the model were studied through analytical methods and numerical integration. Here, we will discuss the main results under the light of the classical competition theory, complex network ecological interactions, and other models for allelopathy [107].

Concerning the study of two species population dynamics, the present model behaves qualitatively like the classical interspecific competition model. The dynamic outcomes–

bistability (for two strong competitors), coexistence (for two weak competitors), and the extinction of the weaker by the stronger competitor–are the same. However, the borders between these regimes are altered by allelopathic interactions. On one hand, the dominance of the stronger allelopathic species is enhanced at the expense of the coexistence and bistability regions. On the other hand, a weak competitor can eradicate a strong one if endowed with more lethal biochemical weapons. These changes are primarily determined by the model parameters that control the species' functional responses to the secreted allelochemicals (toxin's sensitivities and efficacies). Such a scenario is entirely consistent with the one described in Ref. [107] in which a model for plant invasion mediated by allelopathy is considered.

The extension of this model for multispecies was proposed and studied, through numerical methods and with a focus in network approach, to describe eco-evolutionary dynamics for community assembly involving two coupled processes. The first one is a fast ecological dynamics in which species compete for common resources and suppress each other allelopathically. The second is slow evolutionary events in which new species are added to the biological community at its ecological stationary state. Clearly, our study addresses a basic question: the relation between stability and complexity in the ecology of many interacting species.

All the results obtained in Section 3.3.1 must be analyzed bearing in mind the scenario for pure intra- and interspecific competition. In the coexistence regime and homogeneous competition ($\nu_{ij} = \nu < 1 \ \forall i, j$), diversity increases linearly with the number l of introduced species, but all their stationary densities, which are inversely proportional to l, vanish as $l \to \infty$. Fully connected communities with high diversity are the rule. In turn, weak ($\nu_{ij} < 1 \ \forall i, j$) and disordered competition can lead several of the introduced and/or resident species to extinction. Therefore, community diversity tends to be smaller than the number of invasion or speciation events. Yet, all the surviving species at every stationary state constitute fully connected competition networks, as assumed in our models. This scenario change considerably in the presence of inhibitory species-species interactions mediated by toxins.

In the SIE dynamics, ecological networks grow through a succession of species immigration. These alien species allelochemically suppress and are suppressed by resident species at random, eventually leading to the eradication of either the invader or some resident species. The results presented in Section 3.3.1, shown in Figures 3.10-a,b, 3.14 and B.2, reveal that communities exhibiting large diversities can be assembled at weak allelopathy, but diversities are drastically reduced at strong allelopathy for all response functions. In the weak allelopathic regime, the diversity either increases linearly or saturates, depending on the response function (see, e.g., Figure 3.10-a,b). For the response functions $\Phi^{(1,3)}$, competition overcomes toxin-mediated suppressions. The reason is that all stationary species densities decrease after each invasion event, consequently reducing

the toxin concentrations to very low levels ($B \sim 0$ and $B < c$) for which the response functions are small. This is the reason why we do not expect community diversity saturation, even for more than $n_{SIE} > 100$. In contrast, for the functional form $\Phi^{(2)}$ the strength of the response to toxins is stronger for very small concentrations in comparison to $\Phi^{(1,3)}$ ($\mathrm{d}\,\Phi^{(i)}(0)/\mathrm{d}B = 1, 1/c, 0$, $i = 1, 2, 3$ and $c < 1$). In this case, diversity saturation is expected because the chemical warfare is enhanced with the introduction of new species. So, the initial increase in diversity for all response functions occurs until a certain number of new introduced species causes a significant allelopathic suppression.

Furthermore, in the strong suppression regime, species richness either saturates or decreases slowly after reaches a maximum. The maxima occur after $\sim 10 - 30$ invasion events, depending on the response function to toxins. At the maxima, the average number of species in the communities never exceeds $16 - 18$ [95]. So, the system of interacting species becomes unstable and the networks stop to grow, consistent with the limit found by May [9]. Beyond these upper bounds, the number of surviving species decreases continuously after each SIE until the rest only one (a successful invasion) or very few species. Accordingly, network topologies evolve towards marked hierarchical structures, as seen in Figure 3.15, and the corresponding connectivity distributions change from normal (or Gaussian) to Weibull distributions (Figures 3.12,B.4). Moreover, almost constant average centralities indicate homogeneous connectivity patterns for every node and the absence of hubs, bridges joining distinct modules, and star graphs in the network generated at weak allelopathic suppression. In contrast, at strong allelopathy, networks are very small and sparsely connected, leading to small centrality values (see Figure 3.13). Maybe, fluctuations in the small average centralities for strong allelopathic suppression suggest the emergence of modules in the network. Regardless of the regime, such networks comprise a subset of almost null measure in a random ensemble which can only be generated through a constrained growth process.

For BP dynamics (see Figure 3.16) diversity seems to saturate independently on response functions. Indeed, every introduced species has suppressive interactions highly correlated to those of its ancestor, in contrast to the random choice of targets in the SIE dynamics. Thus, chemical warfare is enhanced after each speciation event against a particular subset of target species. The fundamental distinction between the SIE and BP dynamics is that new species are attached to the community with either random or correlated connectivity patterns in the former and the latter case, respectively. Accordingly, species diversity and centrality for BP communities are greater than those for SIE networks (see Figures 3.16 and 3.17). Indeed, each attached species in BP dynamics has, due to its connectivity pattern strongly correlated to that of its ancestor, a smaller chance to destabilize the network. Also, this is the reason why the founders or first species in BP communities have large centrality values in comparison to those almost constant for SIE dynamics (Figure 3.17). Additionally, these connectivity correlations

foster the emergence of hierarchical and modular structures in BP community networks, as seen in Figures 3.20,3.22. These networks have a clear disassortative behavior even at weak homogeneous allelopathy since the average nearest neighbors degree K_{nn} decays for large node's degree (Figures 3.22,B.8). Such a result is consistent with the observation that assortative mixing by degree makes a network more unstable. Accordingly, the local clustering coefficients for nodes with high degrees k are very small (Figures 3.20,B.7) indicating that species which interact strongly should do so with a few ones, a corollary of May's stability criterium for multi-species communities [9]. Here, the growth process favors the attachment of nodes with few links, since they modify the interaction matrix stability much less than new nodes with many links.

Concerning the main ecological question on the complexity-stability relationship, our findings reveal that high species diversities and dynamical stability of growing ecological networks are very constrained under a widespread biochemical warfare between the interacting species. Indeed, the rate in which species abundance decreases as the number of strong allelopathic interactions increases is faster than those predicted by May's classical analysis [9]. Also, at strong allelopathy, the emerging community networks exhibit average connectivity, degree distributions and clustering coefficients described by stretched exponentials tails. The clear disassortative behavior of the interaction networks, observed even at weak homogeneous allelopathy, generates strongly hierarchical and modular community structures. In contrast, Perotti *et al.* [122] analyzing a model in which new attached nodes to an existing community have interaction coefficients randomly chosen, both positive and negative, found a power-law scaling for such network metrics (connectivity, degree distribution, and clustering coefficient). So, interspecific positive interactions are essential to enhance species persistence, diversity, and community stability. This intuitive expectation was recently demonstrated by Pascual-García and Bastolla [129] who pointed out that mutualism can lead to highly connected and diverse networks when the direct interspecific competition is weaker than a critical value.

Considering our results, the species coexistence in unstructured environments remains unexplained unless the negative allelopathic interactions are weak. A possible alternative to enable the long-term coexistence of complex communities was proposed by Kelsic *et al.* [25]. Analyzing a theoretical model for microbial communities, these authors showed that the combined effect of antibiotic production and degradation can sustain biodiversity. Coexistence depends on the presence of an antibiotic-degrading species which attenuates the inhibitory interactions between two other species. At least two antibiotics are required for stability, but more complex communities and dynamical behaviors emerge for greater numbers of antibiotics. Accordingly, Cordero *et al.* [67] revealed that environmental bacteria are organized into socially cohesive units in which antagonism occurs between rather than within ecologically defined populations. Within populations, few species produce broad-range antibiotics, whereas all others are resistant, suggesting co-

operation between conspecifics.

Summarizing, our major result is that, in allelochemical networks generated either by SIE or BP dynamics, species with strong and negative (inhibitory) interactions are part of systems with a small number of species. Moreover, the interactions tend to be arranged in modules or hierarchies with low clustering coefficients, disassortative behavior, and homogeneous degree distributions in order to ensure community stability. So, species-rich communities can be assembled in a homogeneous environment only at weak allelopathy and even in this regime species interact with a few others. The plankton paradox stands in the context of total biochemical warfare between organisms. Of course, natural ecosystems are extremely complicated, containing additional interactions at the level of resource competition, metabolic cross-feeding, predator-prey relationships, etc. Maybe, the coexistence of positive (or activatory) and negative (or inhibitory) interactions is necessary to generate stability and diversity in homogeneous, unstructured environments. But this will be the focus of future works.

Chapter 4

Pattern Formation in the Biochemical Warfare

Chemical compounds mediating interactions between allelopathic species may interfere in community structures, species survival and, consequently, also in species' spreading or persistence leading to interesting spatial patterns of species. Moreover, since species can move, there is a great interest in understanding how the diffusive processes are related to competition and allelopathy. Understanding the interaction networks between and spatial distribution of different species in a community is an important issue to help, manage and protect populations in real ecosystems. The aim of this *Chapter* is to study the self-organized pattern formation processes leading to species coexistence, a fundamental problem in ecology and evolutionary biology. The results discussed in this chapter were partially published in references [108, 146].

4.1 Spatially Extended Model Applied to Allelopathic Networks

In this section, will be presented a model of community structure considering a network describing the dynamics of l species through competition and playing m distinct allelopathic strategies in a spatially heterogeneous environment consisting of n patches. The spatial distribution of each species and toxin are modelled using $2\,l$ partial differential equations (PDE). The system's dynamics emerges from specific per capita birth rates of species (which include intra - and interspecific competition) and deaths induced by allelochemical compounds whose concentrations are, dependent on the set of species densities,

$\{N\}$. The resulting set of dynamical equations is

$$\begin{aligned}\frac{\partial N_i}{\partial t} &= D_i^{(N)}\,\nabla^2 N_i + \bar{r}_i\,N_i - \sum_{j\neq i}^{l}\mu_{ij}\,\Phi_{ij}N_i \\ \frac{\partial B_i}{\partial t} &= D_i^{(B)}\,\nabla^2 B_i + \beta_i\,N_i - \delta_i\,B_i - \sum_{j\neq i}^{l}\gamma_{ij}\,N_j\,B_i \end{aligned} \tag{4.1}$$

where $N_i(t,x,y)$ and $B_i(t,x,y)$ are, respectively,the population density and toxin's concentration associated to species i. So, both processes, dispersal and local dynamics, are described by reaction-diffusion equations. The mobility of species is described as a normal diffuse process characterized by $D > 0$ diagonal matrix of diffusion coefficients. The other terms take into all the local nonlinear ecological interactions.

The model considers three ecological interactions, namely, reproduction, competition and allelopathy, the last one constrained by specific network interactions. The competition for resources $\bar{r}_i = r_i\,(1 - \sum_{j=1}^{l}\nu_{ij}\,N_j)$, assumes intraspecific competition equal to 1 (i.e. $\nu_{ii} = 1\ \forall i$) and weak interspecific competition $0 < \nu_{ij} < 1\ \forall\ i,j$. The parameters r_i describe the maximal growth rates, supposed constants and the interactions between species are defined by the parameters ν_{ij}, μ_{ij}, and Φ_{ij}, which describe the effect of species j on species i. If $\nu_{ij} > 0$ then the species j inhibits the growth of species i. Then, the term $\bar{r}_i = r_i\,(1 - N_i - \sum_{j\neq i}^{l}\nu_{ij}\,N_j)$ describes decreasing reproduction rate due to competition for resources. The biochemical dynamics contains, respectively, release and natural degradation rate described by β_i and δ_i. The term $-\gamma_{i,j}\,N_j\,B_i$ represents toxin uptaken by the i species. Finally, the term $-\mu_{ij}\,\Phi_{ij}^{(k)}$ represents species mortality induced by the allelochemical B_j. Holling type I functional responses are assumed:

$$\Phi_{ij}^{(k)} = \begin{cases} \frac{B_j}{B_0} & \text{if } k = 1 \\ \gamma\,N_i\,B_j & \text{if } k = 2 \end{cases} \tag{4.2}$$

The functional responses associated to $k = 1$ assume that mortality is induced by the total mount of allelochemicals locally available, whereas the $k = 2$ imposes that only the consumed toxins contribute for mortality. The parameters $B_0 \equiv 1$ is the slope of the linear response and make it dimensionless. The absorption and mortality rates can be written as $\gamma_{ij} = \gamma\,\xi_{ji}$ and $\mu_{ij} = \mu\,\xi_{ij}$, where

$$\xi_{ij} = \begin{cases} 1, & \text{if j poison i} \\ 0, & \text{othewise.} \end{cases}$$

The spatially homogenous dynamics of this model was proposed and studied in the *Chapter* 3.

The system (4.1) is integrated numerically by discretizing in a square lattice of size L^2. For each lattice point, the densities of every population and its respective toxin concentration are calculated using a finite difference method [147, 148]

4.2 Biochemical Warfare Between Two Species

We start by studying, instead of only one species endowed with allelochemical weapons, the arm race involving two allelopathic organisms in a spatially heterogeneous environment. Then, as particular case of system (4.1), the following set of dimensionless partial differential equations was proposed:

$$\begin{cases} \partial_t N_1 &= \nabla^2 N_1 + (1 - N_1 - \nu_1 N_2)N_1 - \mu_1 \Phi_1(y_2) N_1 \\ \partial_t N_2 &= D_1 \nabla^2 N_2 + r(1 - N_2 - \nu_2 N_1)N_2 - \mu_2 \Phi_2(y_1) N_2 \\ \partial_t B_1 &= D_2 \nabla^2 B_1 + \beta_1 N_1 - \delta_1 B_1 - y_1 \\ \partial_t B_2 &= D_3 \nabla^2 B_2 + \beta_2 N_2 - \delta_2 B_2 - y_2, \end{cases} \tag{4.3}$$

involving the re-scaled response functions $\Phi_i(x)$ $(i = 1, 2)$ given by

$$\Phi_i(x) = \begin{cases} 0, \text{ if } x \leq 1 \\ \frac{(x-1)^2}{c_i + (x-1)^2}, \text{ otherwise.} \end{cases} \tag{4.4}$$

These Holling III functional responses assume a threshold for toxin effects and saturation of the allelopathic suppression.

In this spatially explicit model it is assumed that both species and their released allelochemicals spreads in space through normal diffusion (the terms $\nabla^2 N_1$, $D_1 \nabla^2 N_2$, $D_2 \nabla^2 B_1$, and $D_3 \nabla^2 B_2$). All the remaining terms have the same interpretations as those in equation (4.1). But a key change was introduced: only the quantities y_1 and y_2 of toxins consumed by each species can cause allelopathic suppression. Hence, the functional responses $\Phi_i(x)$ are functions of $y_j = \gamma_i N_i B_j$, $j = 1, 2$, instead of the total ammounts B_1 and B_2 of allelochemicals released into the environment, as will be discussed in the next section. Indeed, for bacteria, the secreted bacteriocin molecules bind to specific cell receptors on the target bacteria, from which they gain entry into the cell [151]. Also, in contrast to previous study [107], in which the diffusion coefficient D_N of the native plant was assumed to be a decreasing function of the invader phytotoxin concentration above its threshold, here we do not consider that the species diffusivities are directly affected by the toxins.

Specifically, our major interest is to discuss the numerical results for traveling waves solutions in two space dimensions. The invasion spreading starting from either a single or more foci was studied through numerical integration. Figures 4.1 and 4.2 partially illustrate the impact of the biochemical warfare on the interspecific competition involving two

species in a space-dependent system. The numerical integration of the system (4.3) was performed in square lattices with length $L = 200$ and null periodic boundary conditions. In both figures, the competition coefficients are in the range of values that ensure species coexistence in the homogeneous (space-independent) regime.

Figure 4.1 shows the possibility of a weaker competitor to invade and eradicate a stronger competitor since it is provided with more effective allelochemical weapons. In this example, the wavefronts exhibit constant and isotropic speeds.

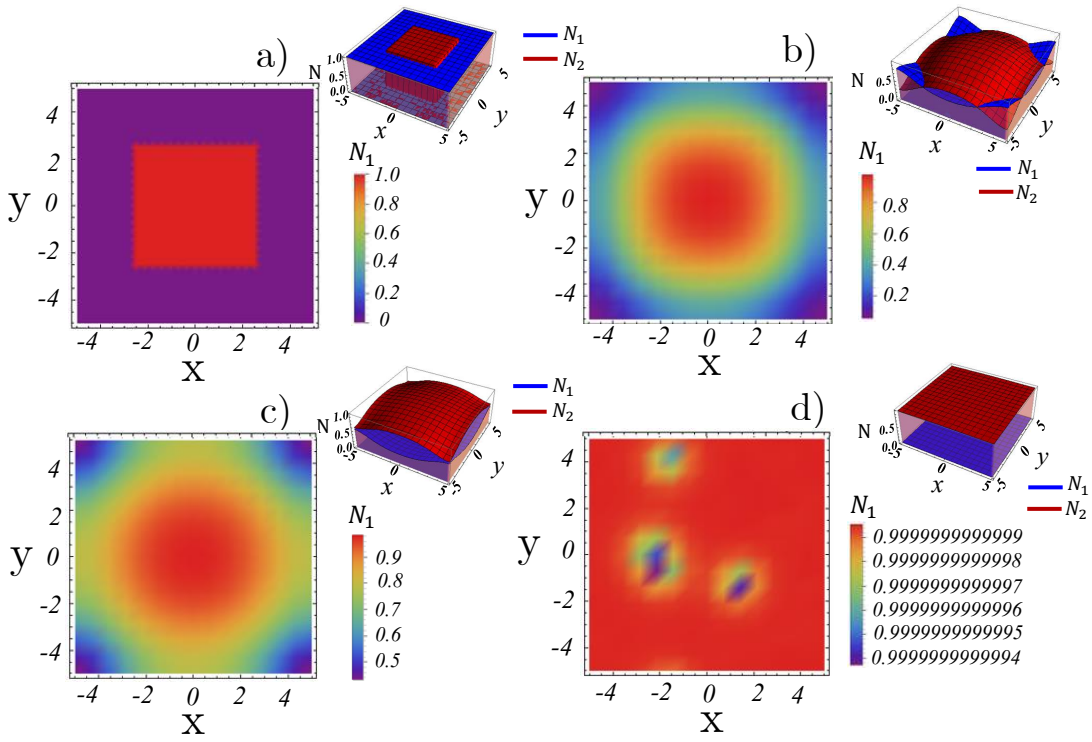

Figure 4.1: (a-d) Evolution in time of a two-dimensional invasion process with allelopathic suppression. The invader species occupies only a 100×100 central square patch. The competition coefficients used were $\nu_1 = 0.9$, $\nu_2 = 0.09$ (within the space-independent coexistence range), and the toxins have equal sensitivities ($c_1 = c_2 = 0.1$) but distinct efficacies ($\mu_1 = 0.1$ and $\mu_2 = 1$). All the other parameters are the same for both species ($r = 1$, $D_1 = D_2 = 0.1$, $\beta_1 = \beta_2 = 0.5$, $\delta_1 = \delta_2 = 0.1$, and $\gamma_1 = \gamma_2 = 1.2$). Figure taken from reference [108].

In turn, Figure 4.2 shows an unexpected and very interesting finding for the interaction between two species having equal competition and allelochemical traits. In Figure 4.2-(a) an invasion process occurs without species eradication, the predicted outcome at the coexistence regime. However, Figure 4.2-(b), in which only the initial spatial distributions of the interacting species were altered, shows an invasion process with one species eradication. Surprisingly, despite equal competition and allelochemical capacities, the coexistence outcome is replaced by one species eradication. This outcome is impossible in

classical competition, whatever be the case: space-independent or -dependent. But it is possible if, in addition to competition, allelochemical suppression and spatial heterogeneity are in action. So, our numerical analysis reveal that the present model may exhibit tristability — eradication of either species 1 or 2 and coexistence — ruled by the spatial population distributions.

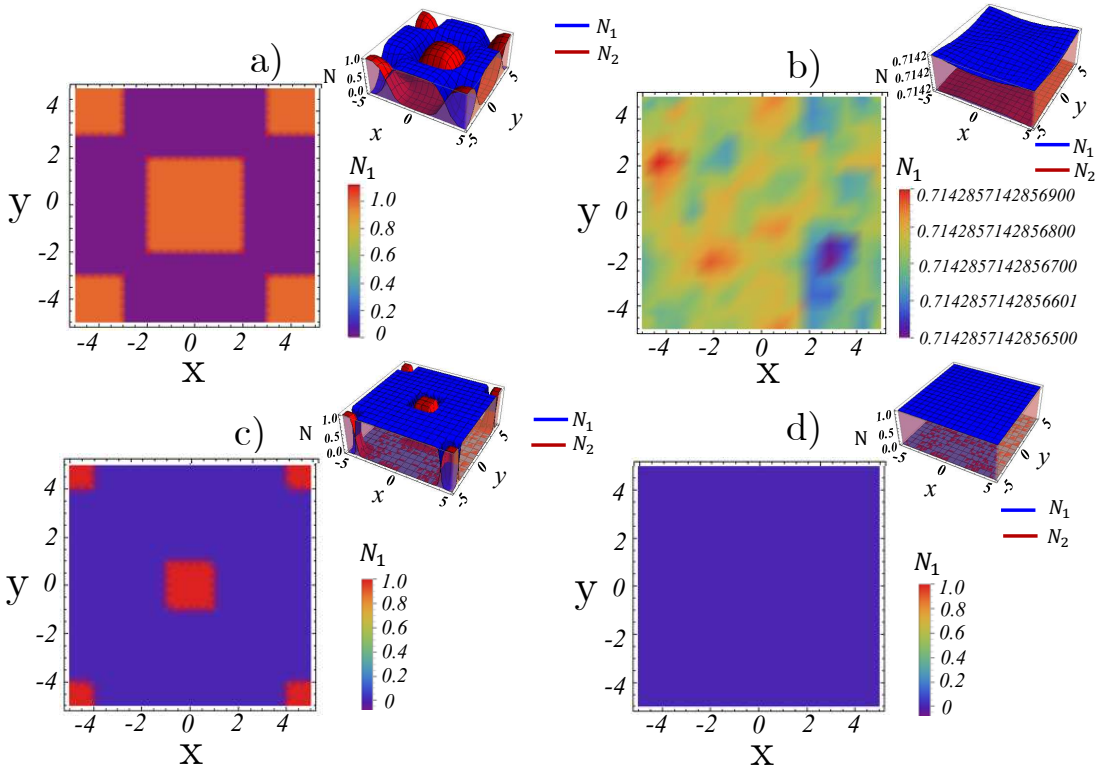

Figure 4.2: (a) The same as in Figure 4.1, but now the invasion leads to species coexistence illustrated in (b). In (c) the initial spatial area occupied by the species 1 was reduced leading to its eradication as shown in (d). The altered parameters were $\nu_1 = \nu_2 = 0.4$ and $\mu_1 = \mu_2 = 0.1$ (equal competition and allelochemical capacities). Figure taken from reference [108].

In the next section an extension for more species in heterogeneous spatial dynamics is addressed.

4.3 Game Model in Allelochemical Networks

To investigate the characteristics of the generalized spatially extended multispecies, the system (4.1) is solved numerically discretizing a square lattice of size L^2. The populations and its toxins are arranged on this square lattice. Initially was used Dirichlet null boundary conditions at the edges of the grid, i.e., $N_i(x, y, t) = B_i(x, y, t) = 0$ if $x, y = 0$

or $L+1$, which represents the lack of individuals outside the landscape borders. Two types of initial conditions were tested. The first one consists in distributing each type population in spatially separated patches which are circular in form. In turn, the toxins $\{B\}$ are initially null across space. So $N_i(x, y, t = 0) = 0.25$ and $B_i(x, y, t = 0) = 0\ \forall i$. Investigating an initial condition of this type is useful because it more accurately portrays the initial distribution of bacterial colonies performed in a laboratory experiments where usually each strain is distributed at isolated sites of the culture plate without an initial mixing between them. The second type of initial condition is generated randomly, where for each point of the space was distributed one of the species with $N_i(x, y, t = 0) \in [0.01, 1]$ (0 for toxins across space) and the others with densities equal to zero. The nonzero population allocated at each spatial point of the system is randomly decided.

It is straightforward to investigate system (4.1) to take into account any number of species engaged in a biochemical warfare. Such an extension is of paramount relevance for real ecosystems often involving interactions among more than three species. The aim is to understand the self-organized pattern formation processes leading to species coexistence, a fundamental problem in ecology and evolutionary biology [149]. To investigate the circumstances under which the species survival generates spatial patterns and how such patterns facilitate a significant improvement in ecosystem stability, the spatially extended population model(4.1) with functional response, equation (4.2), will be used. We start with the model considering competition for common resources and each species suppressing allelopathically each other using cyclic game rock-paper-scissor (RPS).

Recently, the paradigm to address the role of population mobility in coexistence and biodiversity is the three-species cyclic game model (RPS) [152]. Indeed, several models were proposed and its whole class of variants are based on individual agents and their rules for dispersion, predation, replication, etc. (the "microscopic" interactions). A hallmark result is that coexistence emerges at small mobilities from the interactions of entangled rotational spiral waves in the landscape. Since then the spiral wave patterns are thought to be the basic dynamical structure supporting coexistence.

As seen in *Chapter* 2, strains of *E. coli* can be separated into producer (C), resistant (R), and sensitive (S) allelopathyc species. The result of such a dynamics is that the resistant *E. coli* strain grow faster than the poisonous ones, as the latter are resistant and produce a poison, which is yet an extra cost [153]. Consequently, these dynamics exhibits a cyclic interaction, similar to the game RPS.

Reichenbach et al. [152] showed that when three strains (resistant, sensitive and producing) of the *E. coli* are placed on a culture medium, all three strains coexist, organizing in time-dependent spatial niches dominated by one strain. In Figure 4.3, frames of these regions monitored over various days are shown. Borders between different groups emerge, and all three strains co-evolve at comparable densities. The patterns are dynamical: Due to the nonequilibrium character of the species' interactions, groups dominated by one bac-

terial strain cyclically invade each other, resulting in an endless hunt of the three species on the plates. The scenario changes rather when the bacteria is placed in a flask with additional stirring. This scenario affect in a sizeable way the evolution of cooperation and only the resistant strain survives, while the two others die out after a short transient time. The stochastic version of the three-species (RPS) cyclic game system was studied by [152] within the formalism of an urn model which allows the investigation of finite size effects. The authors found that fluctuations around the deterministic trajectories grow in time until two species become extinct.

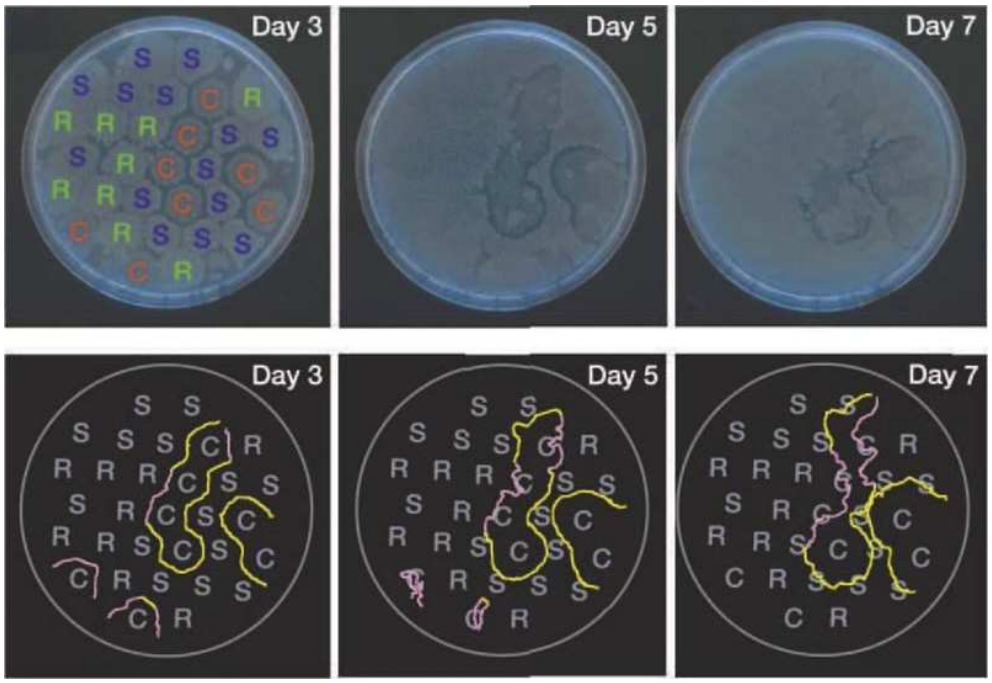

Figure 4.3: Experimental study of three strains of the *Escherichia Coli* E2 that either produce (C), are sensitive (S) to or are resistant (R) to producing molecules toxic to other cells. The system evolves into spatial patterns in a growth medium. The interactions of the three strains is cyclic (rock-paper-scissors game) and therefore of non-equilibrium in nature, leading to dynamic patterns. Source: Figure taken from Ref. [154].

Inspired by the RPS spatial patterns, will be considered here the results of numerical simulations of the model, equation (4.1), using functional responses, equation (4.2). In Figure 4.4 are shown the spatial patterns and the evolution in time of populations for three species competing for resources and allelopathically suppressing each other. The three species are linked through cyclic suppressions as shown in Figure 4.4-(A1,A2). Our results are qualitatively similar to those obtained for the rock-paper-scissor (RPS) game model to five mobile species [155, 156, 157, 158, 159], although in our graph there are no suppressive interactions connecting each species to its two next nearest neighbors. In particular, our "macroscopic" model, Eq. (4.1) extended to account for three species, reveals the coexistence of all species even at high allelopathic suppression ($\mu_i = 0.4\ \forall i$)

but small species and toxin diffusivities ($D_i = 0.005\ \forall i$). Specifically Figure 4.4 (C1-C4) shows the temporal evolution of the average spatial densities that either oscillate around an equilibrium point (C1 and C3) or converge to a stable fixed point (C2 and C3). In the same figure, one can observe two types of spatial patterns: spiral or spiral combined with antispiral (B1, B2 and B3) and pattern without specific patch forms (B4).

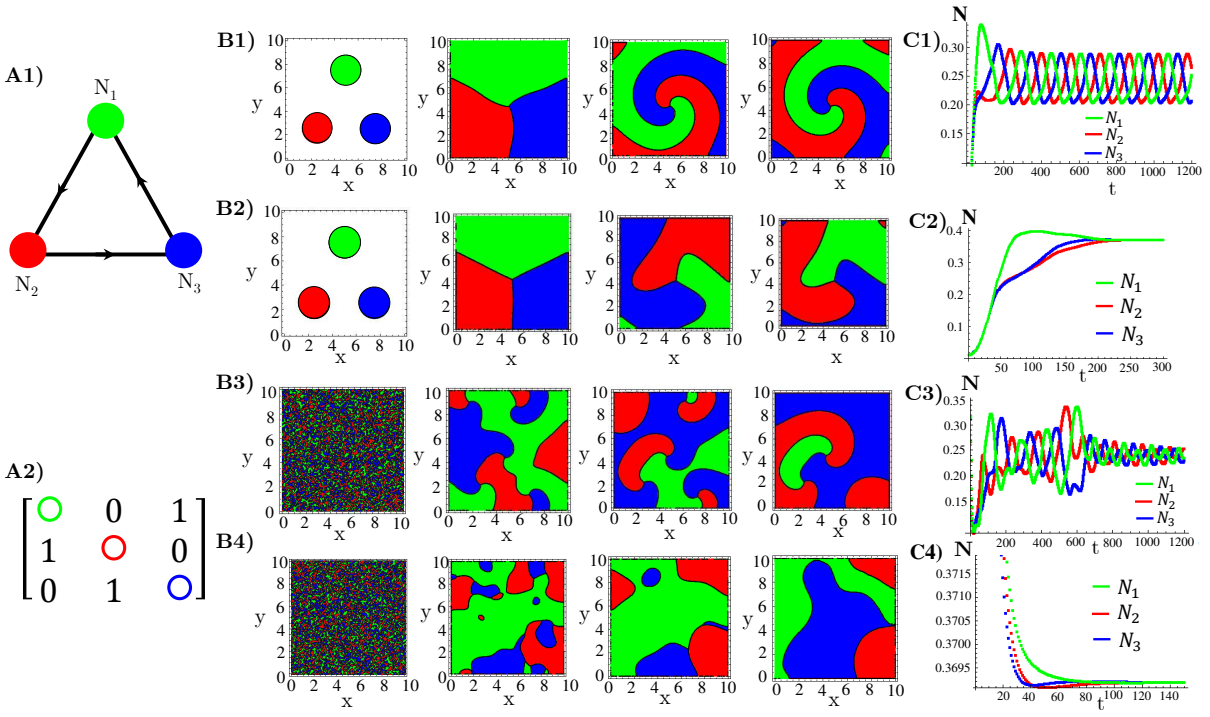

Figure 4.4: Temporal evolution of densities N_1, N_2, and N_3, of species competing for resources and with cyclic (rock-paper-scissor) allelochemical suppressions. (A1) Schematic illustration of three-species allelochemical warfare. Arrows point from suppressor to suppressed. (A2) The allelochemical interaction matrix associated to the graph in (A1). The initial populations are spatially distributed either regularly in single, disjunct, isolated, and circular patches (B1,B2) or randomly in adjacent, disjunct but disordered patches (B3,B4). The corresponding spatial distributions of the species at three distinct times are shown for each initial condition. The different colors indicate the locally dominant species. The evolution in time of the total population densities are shown in (C1-C4). The results in (B1,C1) and (B3,C3) refer to response functions dependent on the total concentration of allelochemicals, whereas those in (B2,C2) and (B4,C4) are for response only to locally uptaken toxins. The competition and allelochemical traits are the same for all species. Their values were fixed in $D_i = D = 0.005$ (small diffusivities), $r_i = r = 0.3$, $\nu_i = \nu = 0.5$, $\mu_i = \mu = 0.4$ (high allelopathy), $\beta_i = \beta = 0.5$, $\delta_i = \delta = 0.1$, and $\gamma_i = \gamma = 0.1$ $\forall\ i$.

An important issue to be analyzed in our model is the identification of the parameter sets that generate patterns and also coexistence between the populations, since both are correlated. To visualize the dependence of pattern formation (coexistence) as a function of the main parameters of the model, the reproduction rate r, mortality μ and compe-

tition ν were varied as a function of the diffusion coefficient D. Figure 4.5 shows these scenarios when we use the functional response $\Phi^{(1)}$ and initial conditions in which the populations are arranged in circular patches that form an equilateral triangle as shown in Figure 4.4-A1. For diffusion parameters $D_i \ll 1 \ \forall i$, spiral patterns are formed in the coexistence scenario ($\nu_i < 1 \ \forall i$). These parameter spaces show that there are very small regions of parameters that support the formation of patterns and coexistence between the three species. We can conclude from these figures that the greater the mobility of individuals is, the more susceptible to extinction are allelopathic species, and smaller the range of parameters where the model agrees with the experimentally observed coexistence [153, 160].

It is important to notice that species diffusion is responsible for coexistence, since for null diffusion coefficients we would have a temporal evolution ruled exclusively by ODEs, which generate competitive exclusion with the survival of only one species. However, the diffusion coefficient cannot exceed a certain limit because, instead of promoting the coexistence through the a rather constrained interaction between different points of the system, it would significantly increase the suppressive interactions, and impairs the coexistence, as we saw in Figure 4.5.

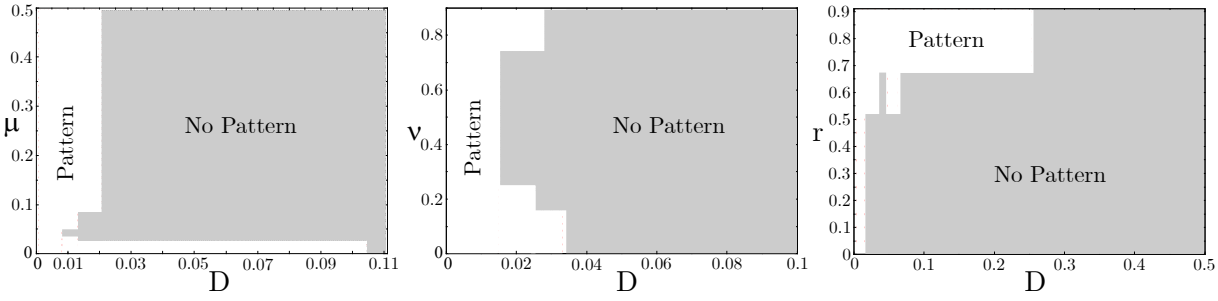

Figure 4.5: Pattern formation phase diagram in the μD, νD, rD - plane, for species competing for resources and with cyclic (rock-paper-scissor) allelochemical suppressions. The same allelochemical interaction matrix (A1) was used. Initial populations are spatially distributed in circular patches (B1) and their response functions are dependent on the local concentration of allelochemicals. Shadowed is the region where no patterns arise. In all phase diagrams, patterns emerge for $D \ll 1$. For each parameter set, the same used in Figure 4.4, we plot the results after $t = 3000$ simulation time steps.

The simultaneous time evolution of the fractional abundances of the three different species N_1, N_2 and N_3 is shown in the ternary diagram in Figure 4.6. The four scenarios described in Figure 4.4 involving two initial conditions and two response function $\Phi^{(1,2)}$ are considered. Figure 4.6 shows that for different initial conditions and mortality effect, the orbits are attracted to limit sets in different phase space (fixed point, periodic cycles, or even strange attractors). But the probability of biodiversity maintenance is relativity hight, since distinct realization of initial condition guarantees biodiversity.

In order to provide a more quantitative description of the system time evolution, the

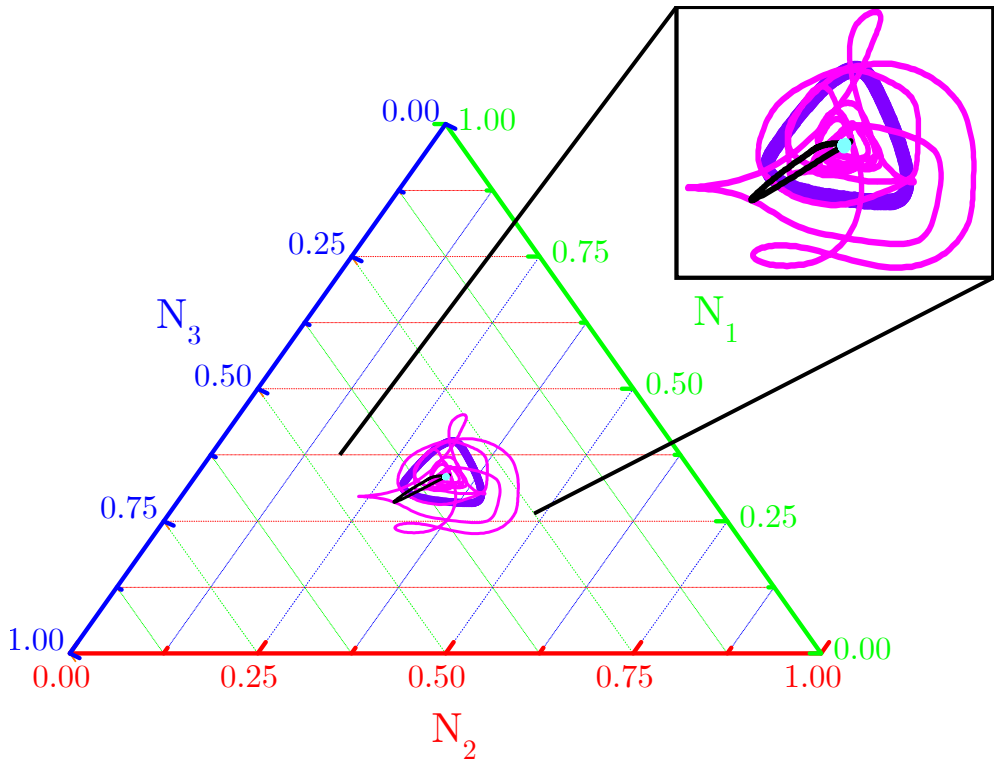

Figure 4.6: Ternary diagram for the time evolution of the spatial-density abundances of the three different species on single runs of our simulations. Different scenarios including or not the effect of absorption and two initial conditions were considered. The purple and black colours describes, respectively, the scenarios with initial conditions in the form of circle and all toxin contribute for mortality; while pink and cyan colours describes, respectively, the scenarios with random initial conditions and only absorbed toxins contributing to the mortality. In all cases, the evolution in time proceeded up to $t = 1.2 \times 10^3$ and the dynamical parameters are the same used in Figure 4.4.

Fourier transform of the fractional abundance $\rho_i(t)$ of the species i was computed. Let us define the temporal discrete Fourier transform as

$$\rho_i(f) = \frac{1}{n_i} \sum_{t=t_0}^{T} N_i(t)\, exp(-2\,\pi\, i\, f\, t) \tag{4.5}$$

where $t_0 = 50$, and $T = 1.2 \times 10^3$ generations (the first 50 generations of each simulation have been discarded in the calculation of the power spectrum).

The power spectrum of ρ_i is exhibited in Figure 4.7 for different populations and were averaged over 1.2×10^3 numerical integrations. The insets reveals the amplitudes A of the peaks varies as functions of the frequency. The power-law decay of A is similar to those observed with small amplitudes in damped harmonic oscillator systems [161].

We also investigate the temporal correlation length, ξ_i, which is extracted from the autocorrelation function $C(\tau)$, as the time for the autocorrelation to decrease to half of its value at the initial time. Accordingly closely Refs. [154, 156, 162, 163], the autocorrelation

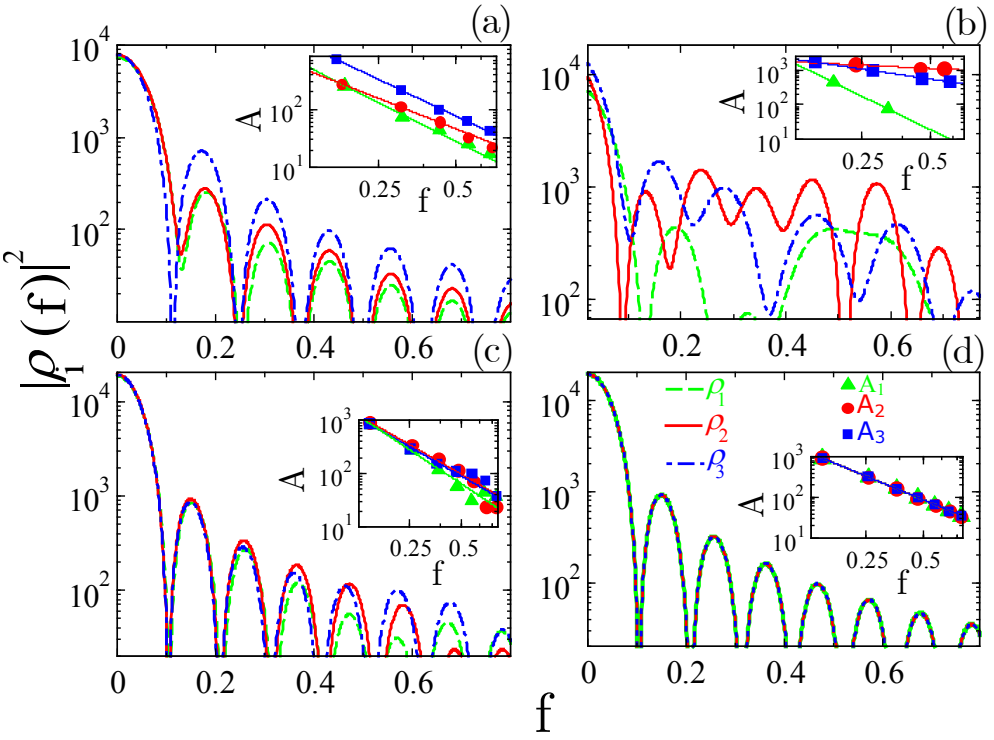

Figure 4.7: Power spectrum of the total densities ρ_1, ρ_2, and ρ_3 for the different species. The results were averaged over simulations with a time span $t = 1.2 \times 10^3$ generations each one corresponding to different initial conditions and considering the effect of absorption to mortality (the first 50 generations of each simulation have been discarded in the calculation of the power spectrum). The insets show the dependence of the frequency peaks (amplitudes) A of the total density for distinct scenarios: triangular patches and spatially random initial populational distributions considering or not the absorption to mortality. The symbols ▲, ●, and ■ describe, respectively, the amplitudes associated the frequencies ρ_1, ρ_2, and ρ_3; solid lines represent the linear fitting functions. The results for the reaction-diffusion PDE are markedly the same as those exhibited by a damped harmonic oscillator and these oscillations reflect the rotation of the spiral waves. The dynamical parameters are the same used in Figure 4.4.

function has the form

$$C_{ii}(\tau) = \frac{1}{\tau}\sum_{t=0}^{T-\tau}(\rho_i(t) - \langle\rho_i\rangle)\,(\rho_i(t+\tau) - \langle\rho_i\rangle) \tag{4.6}$$

where $\langle\rho_i\rangle$ is the average of the abundance $\rho_i(t)$, $\forall i$ species and and $T = 1.2 \times 10^3$. In Figure 4.8 the autocorrelations for case of standard mobility, circle (a,b) and random (c,d) initial conditions and effective mortality function, Eq. (4.2), $\Phi^{(1)}$ (a,c) and $\Phi^{(2)}$ (b,d) are shown. Also, the inset in Figure 4.8 shows the correlation function for τ between 0 and 1000.

Similar patterns as those exhibited in Figure 4.4 were found for Newmann null boundary conditions, $\partial_x N_i(x,y,t) = \partial_y N_i(x,y,t) = 0$ and $\partial_x B_i(x,y,t) = \partial_y B_i(x,y,t) = 0$

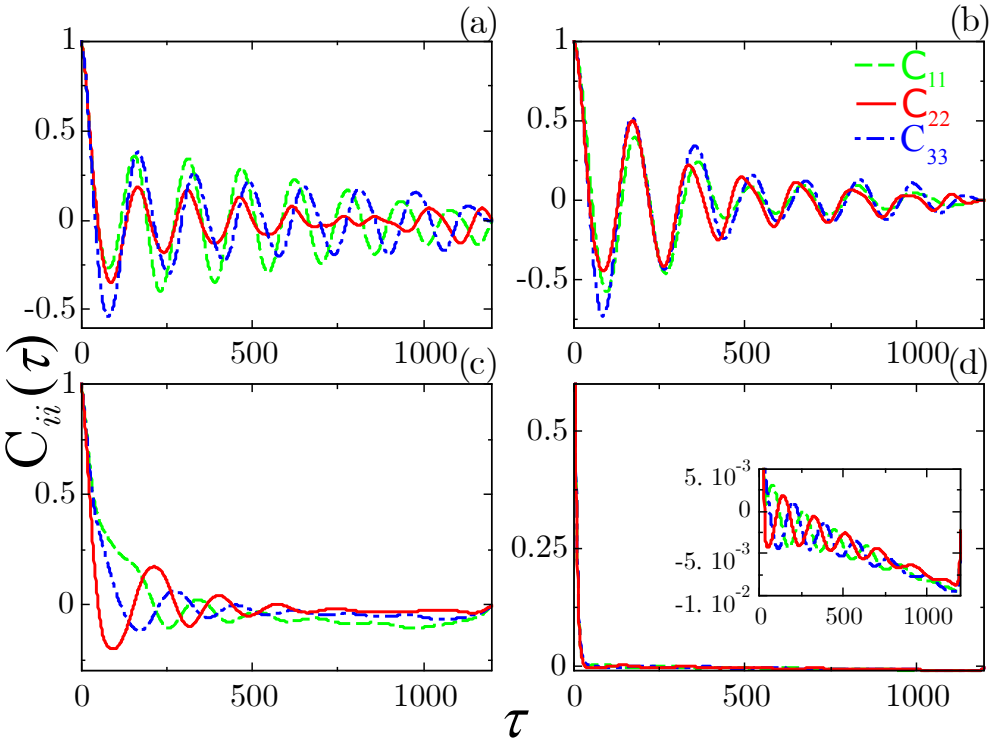

Figure 4.8: The temporal autocorrelation functions shown as functions of τ. Results obtained from reaction-diffusion PDE numerical solutions, Eq. (4.1), for three species N_1, N_2, and N_3 considering that either all toxins contribute to mortality (a,c) or only the absorbed toxins induces mortality (b,d). Moreover, initial populations are spatially distributed either in circular patches (a,b) or randomly distributed in space. Temporal correlations (right) show damped oscillations dependent on initial conditions (triangular and random) and effective mortality rate (μ and $\gamma\,\mu$). The inset in frame (d) shows the autocorrelation functions as function of $\tau \in [0,1000]$. The dynamical parameters used are the same in Figure 4.4.

if $x, y = 0$ or $L\ \forall\ i$, and periodic boundary conditions with $N_i(0, y, t) = N_i(L, y, t)$, $N_i(x, 0, t) = N_i(x, L, t)$ and the same for the toxins.

In addition, tests of other allelochemical interaction networks between three species were performed, as shown in Figure 4.9. For each case illustrated in Figure 4.9, the dynamic of system, equation (4.1), was simulated associated for initial conditions where each species occupies a circle on the vertices of an equilateral triangle. Also, the functional response correspond to $k = 1$, in equation (4.2). The results showed that these networks are not capable of generating coexistence and spiral patterns simultaneously (data not shown). Among the graphs presented in Figure 4.9, only G_3 results in coexistence, and furthermore, neither of the graphs generate spiral or other pattern type.

Next, were tested two other boundary conditions for the scenario B1) discussed in Figure 4.4: null and Newman (null flux) periodic boundaries conditions. Newman's boundary conditions do not change the results shown earlier in Figure 4.4, as can be seen in Figure 4.10-(B1,C1). However, null periodic boundary conditions, break the spiral patterns

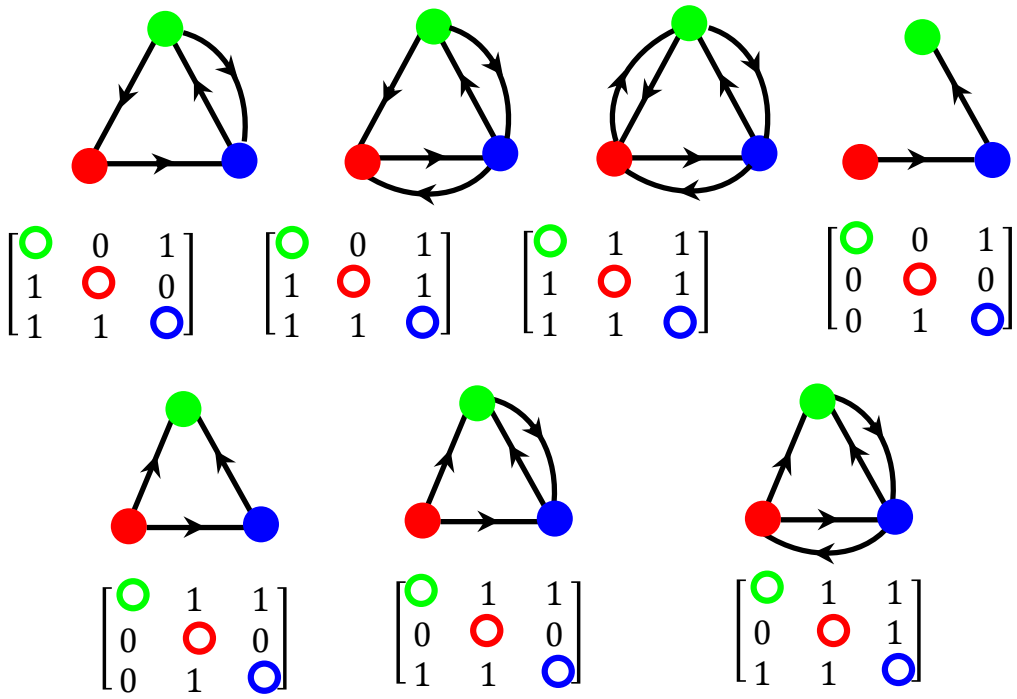

Figure 4.9: Different graphs of allelochemical interactions between 3 species.

typical of the RPS dynamics, and generate the spatial-temporal distributions shown in Figure 4.10-(B2,C2).

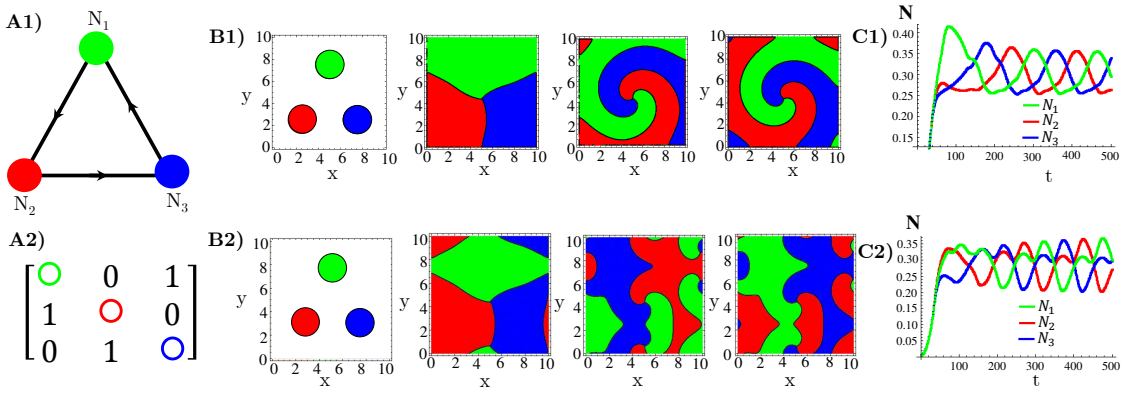

Figure 4.10: Spatial-temporal dynamics obtained by Eq. (4.1) and functional response (4.2) associated to $k = 1$, with null flux Newman (B1,C1) and periodic (B2,C2) boundary conditions in the RPS allelopathic interactions (A1,A2). The model parameters used were: $D_i = D = 0.005$ (small diffusivities), $r_i = r = 0.3$, $\nu_i = \nu = 0.5$, $\mu_i = \mu = 0.4$ (high allelopathy), $\beta_i = \beta = 0.5$, $\delta_i = \delta = 0.1$, and $\gamma_i = \gamma = 0.1$ $\forall$ i.

The spatially explicit population dynamics, Eq. (4.1) with functional response (4.2), for more species was investigated using Dirichlet boundary condition. In Figure 4.11 are shown the spatial patterns and the evolution in time of populations for five species

competing for resources and allelopathically suppressing each other. The five species are linked through cyclic suppressions as shown in Figure 4.11-A1. The results are qualitatively similar to those previously discussed (for 3 species in RPS allelochemical network) and also to those obtained for the rock-paper-scissor-lizard-Spock (RPSLS) game model including five mobile species [164]. However, in our graph there are no suppressive interactions connecting each species to its two next nearest neighbors. In particular, our "macroscopic" model, Eq. (4.1), extended to account for five species, reveals the coexistence of all species even at high allelopathic suppression ($\mu = 0.4$) but small species and toxin diffusivities. For large diffusivities species are led to extinction, as illustrated in Figure 4.12, and eventually one species dominates the entire landscape (see Figure 4.12). Again, as in the RPSLS model, the coexistence or extinction is generated through the interaction of five distinct local spiral wave patterns. At last, the ecosystem dynamics is attracted (converges) to either a limit cycle, as illustrated in Figure 4.11-C1,C3 or a fixed point, as seen in Figure C2,C4. Particularly, the RPSLS model can generate extinction of at least two species over a time interval (see Figure 4.13-C1). Extinct species may reappear, leading other species to extinction. In the case of all the allelochemical parameters maintained fixed, the warfare's outcomes will depend on the way toxins affect the species. If all the local amount of a toxin inhibits its target, the stationary state is either a limit cycle or stable focus. In turn, if only the locally uptaken toxin affects its target, the time evolution is driven to a fixed point. Communities assembly for more species are considered in Appendix C.

4.4 Discussion

Nowadays, two distinct mathematical approaches are widely employed to describe the evolution in time and space of biological populations. The first one, called macroscopic models, are based on coupled partial differential equations for continuous time, space, and state variables. The second one relies at the opposite extreme: totally discrete, agent-based models, as the evolutionary game dynamics [152, 105] recently proposed. In such microscopic models, species interactions are implemented at the individual level via a set of mechanistic action rules. The key lesson of this subsection is that macroscopic models can provide results qualitatively consistent with those obtained using microscopic models. This is true except nearby the critical values of the model's parameter values as, for instance, the diffusivities on the onset of species extinctions. Inside these critical regions, the nature of spatio-temporal correlations and fluctuations in individual-based models is very distinct from those present in continuous models. Consequently, the correct critical (scaling) behavior is not captured by macroscopic models.

In a heteogenous enviromnt, our results for the 1-1 biochemical warfare reveal that,

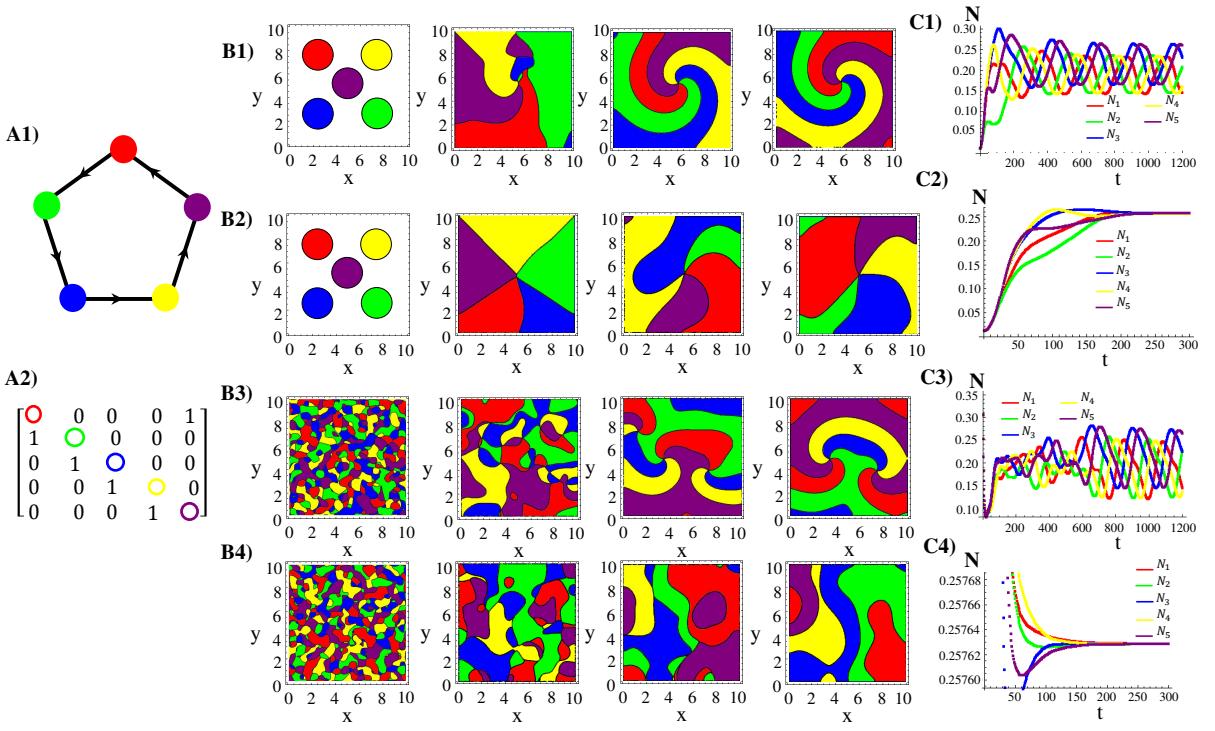

Figure 4.11: Five species competing for resources and with cyclic allelochemical suppressions. (A1) Schematic illustration of five-species allelochemical warfare. Arrows point from suppressor to suppressed. (A2) The allelochemical interaction matrix associated to the graph in (A1). The initial populations are spatially distributed either regularly in single, disjunct, isolated, and circular patches (B1,B2) or randomly in adjacent, disjunct but disordered patches (B3,B4). The corresponding spatial distributions of the species at three distinct times are shown for each initial condition. The different colors indicate the locally dominant species. The evolution in time of the population densities are shown in (C1C4). The results in (B1,C1) and (B3,C3) refer to response functions dependent on the local concentration of allelochemicals, whereas those in (B2,C2) and (B4,C4) are for responses only to locally uptaken toxins. The competition and allelochemical traits are the same for all species. Their values were fixed in $D = 0.005$ (small diffusivities), $r = 0.3$, $\nu = 0.5$, $\mu = 0.4$ (high allelopathy), $\beta = 0.5$, $\delta = 0.1$, and $\gamma = 0.1$

depending on the initial population distributions in space, the invasion process can lead to three outcomes, namely, the eradication of the invader organism, or the extinction of the native species, or yet the coexistence of both invader and native organisms. Such unexpected tristability was observed even for two species sharing the same competition coefficients and allelochemical traits. Such major finding is consistent with the bahvior of recently studied ecosystems in which interactions involve the coordinate social behaviour of the species as, for instance, gather and hunt in herds [150], i. e., nonclassical 1-1 interactions among competing individuals. Indeed, since it is assumed that the individuals in both populations stick together, the interactions occur mainly via those individuals living at the perimeter of the territory occupied by the herds [108].

In system (4.3) there is no social behavior. Instead, the toxins released by each in-

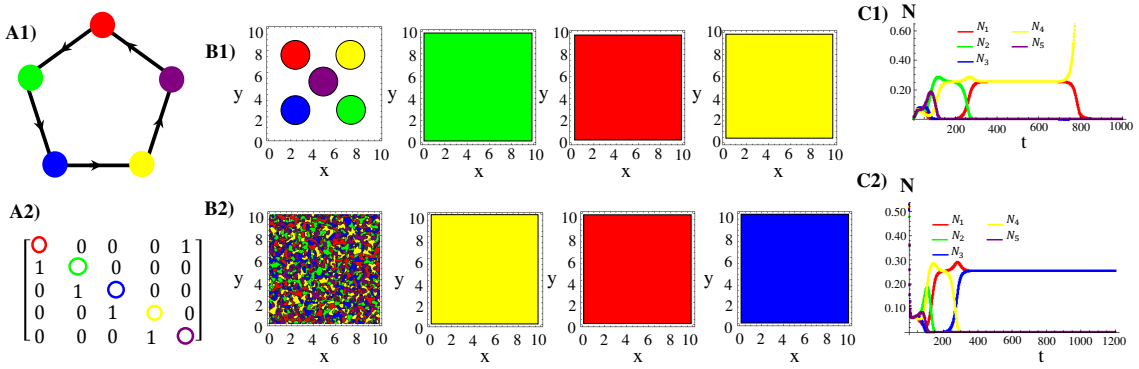

Figure 4.12: The same as in Figure 4.11, but for large diffusivities $D = 0.5$ and response functions dependent on the total local concentration of allelochemicals.

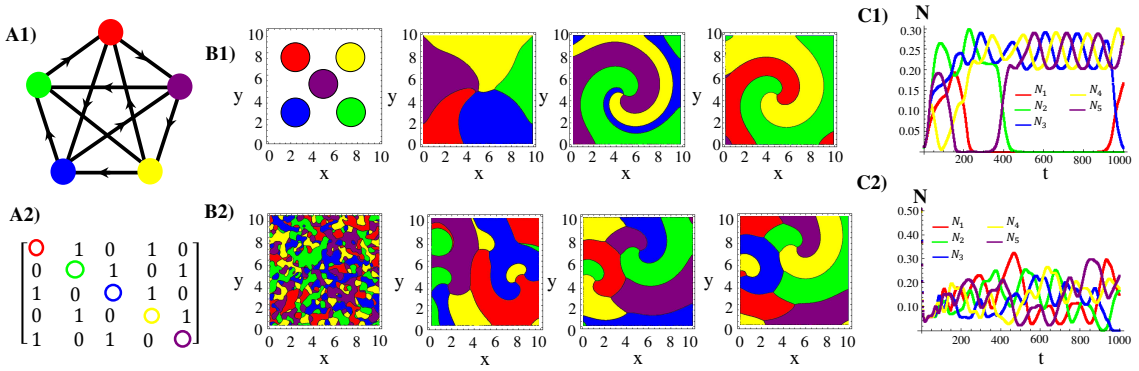

Figure 4.13: The same as in Figure 4.11, but for five species that, in addition to RPSLS allelochemical suppressions, suppress one and is suppressed by others of its two next nearest neighboring species (A1). In (C1) and (C2) the extinction of respectively, two and one species occurs. The data refers to response functions dependent on the total local concentration of allelochemicals.

dividual effectively diffuse throughout an area with a characteristic radius fixed by their diffusivities and degradation rates. Only within this area allelopathic suppression can be relevant. So, in the case of an invasion focus, the mutual allelopathic suppressions effectively occur into a rim around the focus. Again, interfacial or peripheral interactions are established, but without socialized behavior. These interfacial interactions emerge from the combination of allelopathy and patchy population distributions in space. It is just this combination that is lost in the regime of pure competition in which allelopathy is absent. Accordingly, the tristability is impossible in classical pure competition. Therefore, our model provides a distinct mechanism for an emergent tristability independent of social behaviors as those discussed in reference [150, 108].

In general, communities with more species have been studied and local correlations have significant influence on spatial distribution and coexistence of species. Our model

can exhibit pattern formation and coexistence of species since diffusion coefficients are low and species interact cyclically with each other (RPS for three species) in allelochemical networks with odd species number. The temporal oscillations observed in this dynamics originate from models involving cyclic interaction such as May and Leonard [165] and are related to oscillation of population densities.

The loss of coexistence and spatial patterns is observed in scenarios with high diffusion coefficients and is an expected effect in the model so that it satisfactorily reproduces interactions between strains of *E. coli*. Loss of coexistence through increased mobility of individuals is not an effect that occurs only in allelopathy-mediated competition observed between *E. coli* species, but is generally an inherent effect of cyclic competition models [152]. This can be observed in biological experiments when interactions between far-reaching individuals occurs, that is, when a form of mixing brings individuals closer to different spatial regions. Increasing the diffusion coefficient generates a greater mix between individuals occupying different spatial regions with local dynamics, thereby promoting the loss of coexistence.

Investigation of microbial self-organization in bacterial strains reveal simple patterns of bacterial colonies when there are optimal growth conditions. Low nutrient concentration, or environments on which the carrying capacity for bacteria growth has heterogeneities, or yet when the bacteria are exposed to antibiotics can generates complex fractal patterns [166, 167, 168]. Other aspects that influence the spatial distributions of species comprise motility [169], the kind of bacterial movement, such as, swimming [170], swarming, or gliding [171, 172], in addition to chemotaxis and external heterogeneities [173]. Also, patterns of multiple co-evolving bacterial strains of *E. coli* can be segregated into well-defined regions due to enviromental flutuations [174, 175].

Chapter 5

Structural Stability of Ecological Complex Network

One of the main goals of theoretical ecology consists in determining which properties of ecosystems favor or disfavor the maintenance of biodiversity in the face of environmental perturbations. For this goal, the concept of complexity have an important role, since the idea proposed by MacArthur, that the complexity of ecosystems favors their stability [7]. Later May proposal [9] challenges this conjecture. On the other hand, Rohr [176] and Bastolla [177] have proposed another way to resolve the apparent contradiction between stability and complexity by focusing on structural stability, i.e., the stability of the model ecosystem with respect to changes in its parameters. In order to study analytically structural stability, Bastolla [130, 129, 177] proposed model ecosystems consisting of two groups of species, denominated animals and plants, interacting through interspecific competition, inter-group competition, predation and mutualism. More recently, this approach leads them to conclude that mutualism supports biodiversity when the competition is weak and favors structural stability [129]. In addition, these authors determined regimes in which either the nestedness or the connectance are the properties of mutualistic networks that most affect structural stability. In this *Chapter*, the Bastolla's ecosystem model is presented and the initial numerical results for structural stability considering the intergroup competition, predation and mutualism are briefly reported.

5.1 Model

To describe the emergence of stable networks topologies in ecological communities, two groups of $S^{(P)}$ plants and $S^{(A)}$ animal species are governed by the following multispecies

dynamical system:

$$\frac{1}{N_i^{(P)}}\frac{\mathrm{d}N_i^{(P)}}{\mathrm{d}t} = \alpha_i^{(P)} - \sum_{j\in P}\beta_{ij}^{(P)}\,N_j^{(P)} + \sum_{k\in A}\frac{\gamma_{ik}^{(P)}\,N_k^{(A)}}{1+g_j^{(A)}\sum_{j\in P}|\gamma_{kj}^{(A)}|\,N_j^{(P)} + h_i^{(P)}\sum_{l\in A}|\gamma_{il}^{(P)}|\,N_l^{(A)}}$$
$$\frac{1}{N_i^{(A)}}\frac{\mathrm{d}N_i^{(A)}}{\mathrm{d}t} = \alpha_i^{(A)} - \sum_{j\in A}\beta_{ij}^{(A)}\,N_j^{(A)} + \sum_{k\in P}\frac{\gamma_{ik}^{(A)}\,N_k^{(P)}}{1+g_j^{(P)}\sum_{j\in A}|\gamma_{kj}^{(P)}|\,N_j^{(A)} + h_i^{(A)}\sum_{l\in P}|\gamma_{il}^{(A)}|\,N_l^{(P)}} \tag{5.1}$$

where $N_i^{(P)}$ and $N_i^{(A)}$ represent, respectively, plant and animal abundances; $\alpha_i^{(P)}$ and $\alpha_i^{(A)}$ are the model parameters that measure the intrinsic growth rates associated to species i of plant/animal in the absence of other species (or death rate if i is not a primary producer), and $\beta_{ij}^{(P)}$, $\beta_{ij}^{(A)}$ is the interspecific competitive interaction matrices associated to plants and animals, respectively. In this case, competition matrices are described by Lotka-Volterra (LV) terms with intraspecific competition $\beta_{ii}^{(P)}$,$\beta_{ii}^{(A)} = 1$ for all species and interspecific competition is represented by $\rho_{i,j}^{(P)}$ and $\rho_{i,j}^{(A)}$. Moreover, the links between the groups of plants and animals are mediated by the matrices $\gamma_{ik}^{(P)}$ (i =plant, k =animal) and $\gamma_{ij}^{(A)}$ (i =animal, j =plant), respectively. We set $\gamma_{ik} = \gamma_0\, g_{ik}$, where γ_0 denotes the scale of mutualistic, competitive or predatory interactions. Note that if the two groups of species compete with each other, the signs of the inter-group interaction parameters $\gamma_0^{(P)}$,$\gamma_0^{(A)}$ are negative. The qualitative interpretation is that shared competitors of the other group tend to reduce the effective competition between species of the same group exactly as shared mutualistic partners [129]. For the case of predatory interactions, the interaction is positive for one group and negative for the other group, so that we have to use $\gamma_0^{(A)} > 0$ and $\gamma_0^{(P)} < 0$. So predatory inter-group interactions increase the productivity of predators but decrease the productivity of preys. In the mutualistic interactions $\gamma_0^{(P)}, \gamma_0^{(A)} > 0$. Thus, in this case both species are benefited by the interaction.

The Holling II functional response present in equation (5.1) has the following properties:

1. In the mutualistic case, the functional response is recovered with a term that describes the effective competition between species that share a mutualistic interaction;

2. In the case of predation, the denominator in the functional response introduces effective competition between predators of the same prey, and effective mutualism between prey of the same predators, which is something that is observed in the compartments of herds of herbivores and birds. In addition, the case $g = h = 0$, in which the denominator is equal to 1, recover the LV system;

3. In the case of competition, an effective mutualism is introduced between species that compete with the same species;

4. The functional response is invariant with respect to the splitting of a species N_j in two populations with identical properties, N_j^P and N_j^A.

5.2 Numerical measure of structural stability

To measure the structural stability associated with ecological interactions β_{ij} and γ_{ik} following the steps were performed. First, we fixed the number of species $S^{(A)}$, $S^{(P)}$ and we set the elements of the interspecific competition matrix as $\beta_{ii}^{(P)} = \beta_{ii}^{(P)} = 1$, $\beta_{ij}^{(P)} = \rho^{(P)}$, and $\beta_{ij}^{(A)} = \rho^{(A)}$ for $i \neq j$ and $\rho^{(P)}, \rho^{(A)} > 0$.

Once the ecological interactions are defined, the model is constructed by assuming that a coexistence equilibrium exists and it is dynamically stable, as in ref. [129]. In other words, we choose the growth rates $\alpha_i^{(P)}$ and $\alpha_i^{(A)}$ so that the equilibrium abundances are positive and we choose the interaction parameters in such a way that the system is dynamically stable. We then impose perturbations to the growth rates, let the system to evolve according to their dynamical equations, and we record extinctions. In this way, we can measure the structural stability as the maximum perturbation compatible with the maintenance of all species (more precisely, as the perturbation for which the probability that at least one species gets extinct is 0.5), and we can investigate which are the properties of the ecological interactions that promote or hinder structural stability.

Following this protocol, we set the unperturbed grow rates $\bar{\alpha}_i^{(P)}, \bar{\alpha}_i^{(A)}$ to the values,

$$\begin{aligned}
\bar{\alpha}_i^{(P)} &= \sum_{j\in P} \beta_{ij}^{(P)}\, \bar{N}_j^{(P)} - \sum_{k\in A} \frac{\gamma_{ik}^{(P)} \bar{N}_k^{(A)}}{1 + g_i^{(P)} \sum_{j\in P} |\gamma_{ij}^{(A)}| \bar{N}_j^{(P)} + h_i^{(P)} \sum_{l\in A} |\gamma_{il}^{(P)}| \bar{N}_l^{(A)}} \\
\bar{\alpha}_i^{(A)} &= \sum_{j\in A} \beta_{ij}^{(A)}\, \bar{N}_j^{(A)} - \sum_{k\in P} \frac{\gamma_{ik}^{(A)} \bar{N}_k^{(P)}}{1 + g_i^{(A)} \sum_{j\in A} |\gamma_{ij}^{(P)}| \bar{N}_j^{(A)} + h_i^{(A)} \sum_{l\in P} |\gamma_{il}^{(A)}| \bar{N}_l^{(P)}}.
\end{aligned} \tag{5.2}$$

that result in equilibrium abundances $\bar{N}_i^{(P)} = \bar{N}_i^{(A)} = 1$ for all species, a fixed point of equation (5.1). These conditions guarantee that the equilibrium is feasible and has large structural stability. Then, these growth rates are perturbed as

$$\begin{aligned}
\alpha_i^{(P)} &= \bar{\alpha}_i^{(P)} \,(1 + \Delta\, \epsilon_i^{(P)}) \\
\alpha_i^{(A)} &= \bar{\alpha}_i^{(A)} \,(1 + \Delta\, \epsilon_i^{(A)}),
\end{aligned} \tag{5.3}$$

where ϵ_i are random numbers $\in [-1, 1]$ generated by a uniform distribution with $\bar{\epsilon}_i = 0$, $\bar{\epsilon}_i^2 = 1/\sqrt{3}$ for plants and animal species.

We numerically measure the structural stability associated with an ecological interaction considering ecological networks consisting of $S^{(A)} = S^{(P)} = 20$ animal and plant species, and competition matrices $\beta_{ii}^{(P)} = \beta_{ii}^{(A)} = 1$, $\beta_{ij}^{(P)} = \rho^{(P)}, \beta_{ij}^{(A)} = \rho^{(A)} > 0$ for $i \neq j$.

The fourth-order Runge-Kutta method applied to integrate the ecological dynamics after 500 random perturbations of the intrinsic growth rate with a species whose abundance falls below 10^{-8} of the initial value is considered extinct. As initial conditions, it is assumed that $N_i^{(P)}(t=0), N_i^{(A)}(t=0)$ are random independent numbers uniformly distributed between 0 and 1.

Initially, we performed this computation for several values of the parameter ρ in the absence of interactions between the groups of plants and animals ($\gamma^{(P)} = \gamma^{(A)} = 0$). For each set of system parameters system, and Δ, 500 realizations of the perturbed growth rates ϵ_i were randomly drawn. We recorded the probabilities for which there is at least one extinction as a function of Δ. These probabilities are shown in Figure 5.1, and they follow a characteristic sigmoidal form. The critical value Δ_c is defined as the value of Δ for which the probability for at least one extinction is 0.5 (dashed line). The value of Δ_c is obtained for each parameter set by interpolating the extinction curve. Figure 5.1-a) exhibit the extinction probability as a function of Δ for distinct values for $\rho^{(A)} = \rho^{(P)}$. Figure 5.1-b) shows the results for $\rho^{(A)} \neq \rho^{(P)}$. Error bars quantify the standard deviations obtained from 200 realizations of the parameters and the ecological dynamics.

Figure 5.2 shows that mutualistic, competitive and predatory interaction affects the structural stability of ecological networks in a complex way dependent on different regimes of parameters. In this figure are considered sets of networks with homogeneous and equal strength interactions ($\left|\gamma^{(P)}\right| = \left|\gamma^{(A)}\right|$) as well as plant strength interactions stronger than that of the animals ($\left|\gamma^{(P)}\right| = 2\left|\gamma^{(A)}\right|$). We look at four scenarios for weak interspecific competition ($\rho^{(P)} = \rho^{(A)} = 0.05$, $\rho^{(P)} = \rho^{(A)} = 0.3$, $\rho^{(P)} = 0.05$ and $\rho^{(A)} = 0.3$ and vice-versa). Also, four different saturation and large saturated interactions growth rates $(1/h, 1/g)$ ($h = g = 0$, $h = g = 0.1$, $h = 0.1$ and $g = 0$ and vice-versa) were considered. Our results reveal that mutualism tends to increase the structural stability, but competition decreases structural stability, while predation can increase (if $\rho^{(A)} > \rho^{(P)}$) or decrease (if $\rho^{(A)} \leq \rho^{(P)}$) structural stability, depending on the strength of competition.

In this chapter, we briefly reported our initial results for the structural stability of competing species networks. The major goal of this study is to identify possible structures of ecological networks (connectivity, ecological overlap - nestedness) that guarantee structural stability and complexity of model ecosystems involving mutualism, predation, and competition interactions.

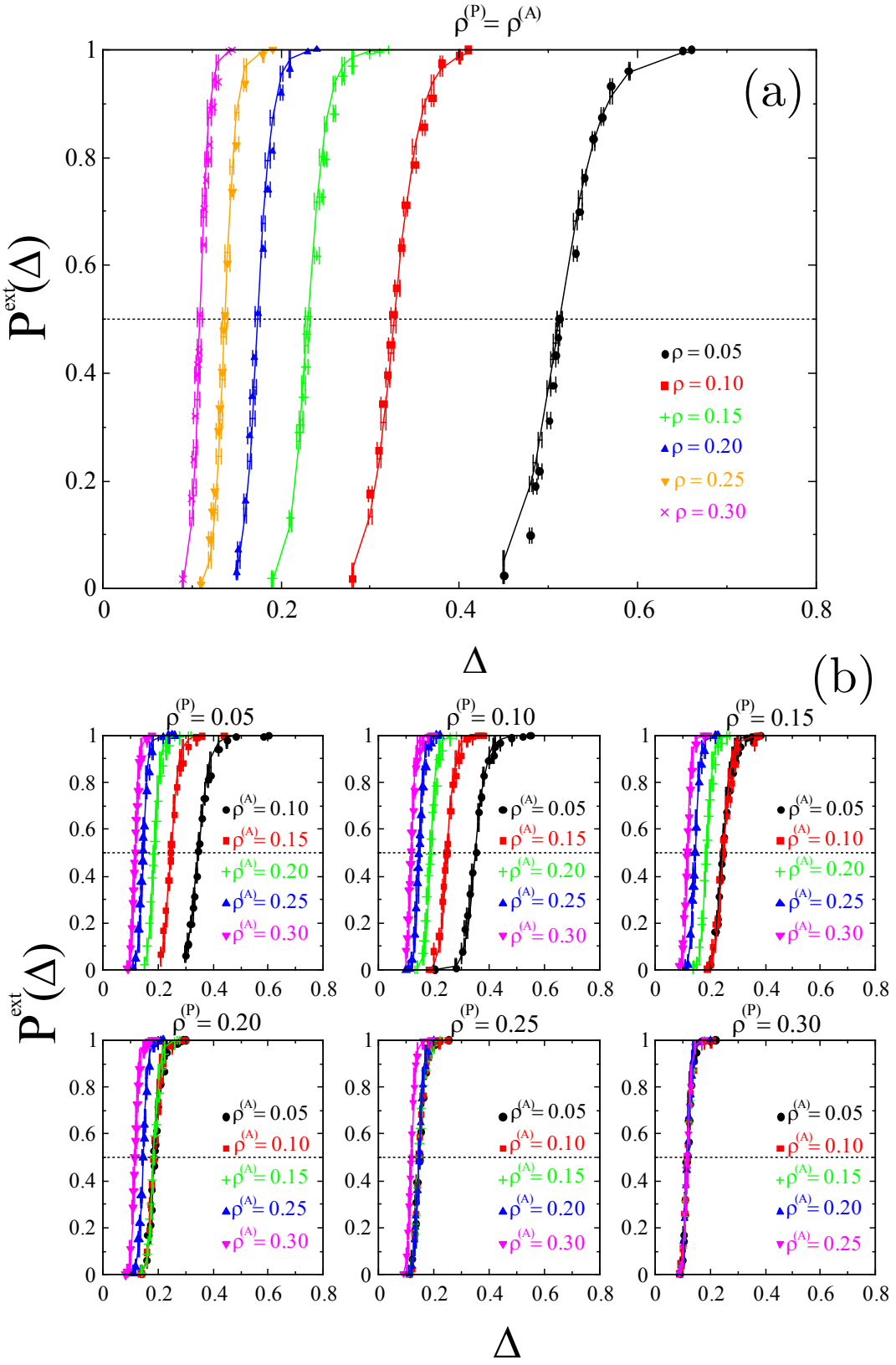

Figure 5.1: Probability of at least one species extinction as a function of the relative fluctuations Δ of the intrinsic growth rates for (a) $\rho^{(A)} = \rho^{(P)}$ and (b) $\rho^{(A)} \neq \rho^{(P)}$. In both cases, $S^{(P)} = S^{(A)} = S = 20$ were assumed. Solid curves correspond to the logistic equation fitting $\frac{(\Delta/\Delta_c)^n}{1+(\Delta/\Delta_c)^n}$, with $n \sim S$ for all cases.

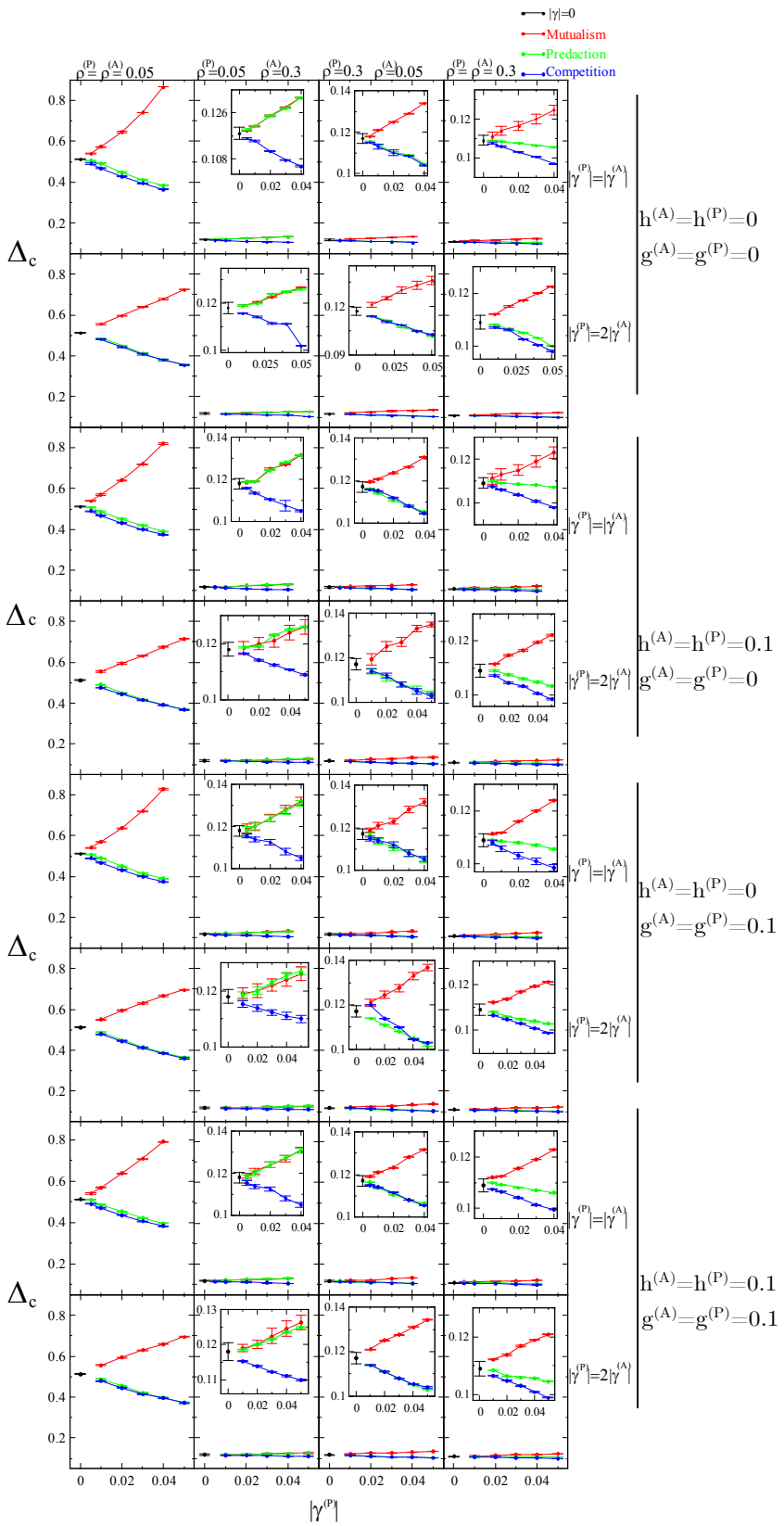

Figure 5.2: Structural stability Δ_c as a function of interaction strength. Each point represents different competition, predation, mutualistic and no inter-group interaction networks with $\left|\gamma^{(P)}\right| = \left|\gamma^{(A)}\right|$ and $\left|\gamma^{(P)}\right| = 2\left|\gamma^{(A)}\right|$. The values Δ_c are defined as the relative perturbations of intrinsic growth rates that produce at least one species extinction with a probability 0.5. Were tested different parameters regimes when $g = h = 0$, $g = 0$ and $h = 0.1$ (and vice-versa), and $g = h = 0.1$.

Chapter 6

General Conclusions

The complexity and diversity of phenomena underlying species interactions, coexistence, evolution and invasions; the range of spatial and temporal scales over which they act, extending from the molecular to the ecological levels; and the intricate way in which they are interwoven make practically unfeasible the understanding of the biochemical warfare between living organisms through intuition alone. The development of quantitative theoretical models for these phenomena, such as the one presented in this *thesis*, might be a very useful approach to deduce how distinct mechanisms interact to generate community stability and biodiversity, to integrate the rapidly increasing amount of accurate information obtained at the macroscopic scales, and to predict the macroscopic response of ecological systems to control interventions. Such mechanistic models can provide real insights into critical traits that regulate invasion success, coexistence, and diversity in eco-evolutionary systems. They can also guide the design of new essays by indicating relevant processes for further investigation and prevent excessive experimentation needed to develop effective control strategies [146].

The major part of these thesis focused on the LVM dynamics considering competition, allelopathy, predation and mutualism to address stability and complexity in ecological networks. Specifically, invasions and branching processes have been studied for assembling species communities that compete for resources and interact through allelopathy. Also, structural stability was applied to the study of mutualism, competition, and predation. In this final *Chapter*, I would like to start by addressing the themes of ecology and physics in a broader context, trying to get an idea of the similarities between these research fields. Figure 6.1 summarizes some similarities and differences in approaches to physics and ecology.

In physics, the solution of motion equations for two bodies using the Newtonian formalism of classical mechanics is analytically possible given the initial conditions for velocities (or momenta) and positions. The three-body dynamics, the Euler problem, is highly complex, non-soluble analytically for general initial conditions (except for specific config-

urations). Furthermore, the three-boy dynamics is often chaotic. Similarly, the evolution equations for two species competing for resources in the Lotka-Volterra continuous model are analytically soluble and easy to understand because systems will always converge to fixed points or limit cycles. The dynamics for three or more species are highly complex when considering distinct interspecific competition coefficients. In the case of three or more competing species, their densities can oscillate [165, 180, 181] or exhibit deterministic chaos [182, 183]. Figure 6.1 shows comparative between the Newtonian approach to these two and three body problem and LVM to describe species competition between two and three species [144].

For understanding the behavior of large systems containing $N \sim 10^{23}$ particles, statistical physics is the traditional approach from physics. Particularly, for network theory and non-equilibrium process in complex systems (ecology, epidemic spreading, power grids, etc.). In this way, statistical physics becomes one of the most fundamental tools of modern science to address multidisciplinarity. In analogy with the statistical approach in physics, one might not wonder whether a mechanistic view of the interactions of multiple populations in ecology will also give rise to simple statistical rules. Ecological communities are highly complex, yet they also display consistent spatial and temporal patterns that seem to be quite robust, independently on many details. The second decade of the 21st century is ending, and the debate that began in the second half of the 1950s about stability and complexity yet is open; if in on hand MacArthur found that complexity increases with biodiversity, or in other words, $S \sim C^z$ where z is a scaling exponent [7, 12], on the other hand, May and Damuth's found that $S \sim C^{-z}$ [9, 13]. Both MacArthur and May approaches have power-laws, but the former proposes an increase and the last a decrease of stability with complexity.

Motivated by this debate, in the first part of this thesis we proposed and studied, through analytical and numerical methods, the basic ideas of a model for the assembly of species communities that interact by competition and allelopathy based on two cases, namely, invasion processes and speciation. The model proposed contains $2N$ ODE's that describe the population dynamics of species and their toxins. Its main terms take into account competition for resources, species mortality, exudation, consumption and natural degradation of toxins. We included in our multispecies LVM competitive dynamics and an increase in mortality due to allelopathy given by Holling type I, II and III functional responses and distinct toxin uptakes regimes. We then applied network theory to both cases aiming to evaluate the outcomes for different network architectures. We found three types of distributions associated with the topology of the emerging networks. A weak allelopathic suppression allows stable species communities with increasing complexity, or biodiversity, as presented by MacArthur [7]. In this case, the network degree distribution is Gaussian or Normal. For intermediate allelopathic strengths, the degrees are distributed according to power laws truncated with stretched exponentials, but there

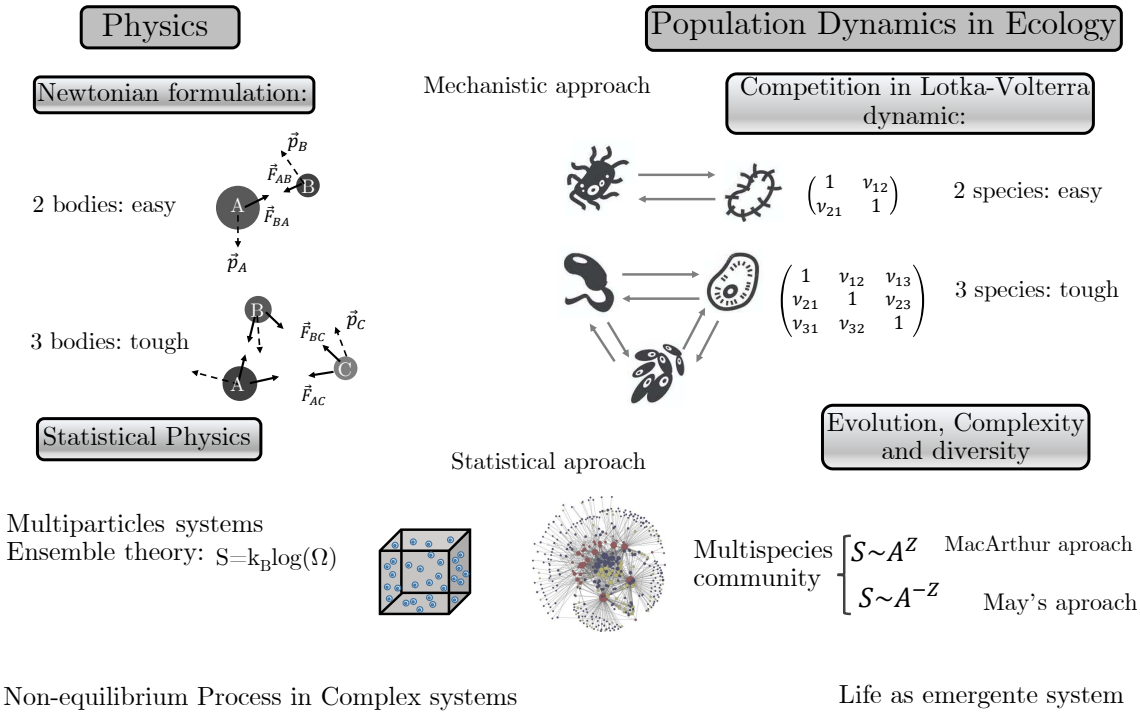

Figure 6.1: In Newtonian physics and ecology, it is relatively simple to solve analytically two bodies/species problems, but very hard approach the problem of three or more bodies/species general initial conditions. Statistical physical, however, it is nevertheless possible to analyze large multiparticle systems, as it happens with the ideal gas. In ecology, we face a similar challenge. There are large scale patterns, like species-area relationships, yet there is no firm theory that explains how these patterns arise as a consequence of ecological interactions among the many components of an ecosystem. The link of thermodynamics and statistical mechanics is mediated by Legendre transformation of the entropy ($S = k_B log(\Omega)$, where Ω is an appropriate partition function). In ecology, the complexity-stability debate focuses on $S \sim C^z$ or $S \sim C^{-z}$. Figure inspired in [144].

is a threshold for complexity. For stronger allelopathic effects, the communities exhibit statistical properties in which the stability is negatively correlated with complexity. In this case, the network degree distribution is of a Weibull type. Strong allelopathy effect is supported by May theory [9] while intermediate allelopathy still increases complexity for small events and tends to saturate. In addition, allelochemical interactions tend to be arranged in modules or hierarchies with low clustering coefficients, disassortative behavior, and homogeneous or heterogeneous degree distributions in order to ensure community stability. In a homogeneous environment, species-rich communities can be assembled only in the context of weak biochemical warfare between organisms, and even under this regime species interact with a few others.

Although ecologists are claiming for a possible solution of great stability-complexity debate, our results indicate that in allelopathic dynamics the outcome is neither increase of stability with complexity nor decrease of stability with complexity only, it depends as

the competition parameters. This behavior is analogous to the debate about the nature of light, wave-particle, ruled by Newton and Huygens. Surprisingly, the ultimate argument was revolutionary. Light is a quantum system and, accordingly, its wave - or particle-like behavior is determined by the measurement (interaction) process. Moreover, positive non-trophic interactions, as well as a weak negative effect or yet strong but heterogeneous environments can increase biodiversity, complexity, and stability contrary to May's approach [9].

In our model, the ecological dynamics are described by deterministic ODE's, as rules the "Newtonian tradition". However, the random effects of competitive and/or allelopathic networks introduced into the model via invasion or speciation events (the evolutionary dynamics) demand the ensemble hypothesis to address multispecies communities. Thus statistical averages are used to characterize complex network properties. The major limitation of ODEs to treat the problem of stability in ecological communities is that even without the toxin-mediated interaction, species abundances are inversely proportional to the number of species in the community. Therefore it is arbitrary and imprecise to define the surviving and extinct species. Indeed, if the community has 1000 species, the expected average abundance of each species is $N_i(\infty) \sim 10^{-4}$. In in our case, populations smaller than 10^{-8} were considered extinct. However, such a threshold is a parameter of our model that has not been tested. We will explore this parameter in future simulations.

As a general rule, network analysis has shown that there is a significant difference between the topological properties measured in communities obtained via speciations and invasions. Network comparison indicates the presence of specialist and generalist species. The introduction of stochasticity in competitive and allelopathic parameters in the communities obtained by the branching process can lead to mass extinctions. In a weak allelopathic regime for SIE events were shown that diversity increases with the number of invasion events. It is not clear for us if there is bordering the regions of diversity increase and decrease at a larger number of invasion events, i.e., for $n_{SIE} \gg 100$. Future, we intent to simulate many more than 100 invasions in order to clarify this point, and verify if alternatively, biodiversity reaches a stationary state. Also, we will try to develop more analytical insights about the ecologically relevant regime in which the dynamics of the chemicals is much faster than that of the species. In this regime, the toxins B_i can be assumed to reach an equilibrium and the population dynamics equations proposed in *Chapter 3* can be rewritten in terms of an additional competitive interaction mediated by the toxins plus an effective mutualistic interaction between species that absorb the same toxin. Our measure of structural stability of interactions as mutualism, competition, and predation shows that increasing biodiversity can be observed in mutualistic species (when the interspecific competition is weak) but is impaired when intragroup competition is considered. In turn, predation interactions can increase or decrease the biodiversity (if the interspecific competition is weak or strong). We will continue to study how a com-

bination of mutualism and prey-predator interactions influences the structural stability of the model ecosystem, and which is the topology of the combined interaction network that better supports structural stability. In other words, we shall try to identify possible structures of ecological networks (connectivity, ecological overlap - nestedness) that guarantee structural stability and complexity of model ecosystems involving distinct types of interactions. Applications in microbial communities and mass extinctions are imperative issues.

Finally, environmental heterogeneities in spatial distribution were studied to describe the establishment of species that compete for the same resources and can suppress each other allelopathically. We found tristability in the dynamics LVM for two species. This tristability depends on the initial spatial distributions of the species, not only on their poisoning forces. We consider different allelopathic interaction networks for more than 2 species and found that biodiversity and the formation of atypical spatial patterns can be obtained with low diffusivities when allelopathic interaction networks are cyclic and the number of interacting species is odd. These conditions may result in patterns that take the forms of a spiral, spiral combined with antispiral, and spatially disordered species groups without specific form. Spiral patterns can be broken when mortality is low, diffusivities are high or even when the number of interacting species is even. The PDE's system discussed in this thesis provide a sufficient approximation for smaller ecosystems but needs to be refined for large and realistic communities.

Moreover, is approaches are inevitable the overlapping of populations at a network site (species would occupy the same place in space), which can be unrealistic in the real world. But a few real-world systems could be represented in this way and can I mention two examples: species placed in reactors or aquatic ecosystems. In such systems, there is no evidence supporting our findings. In addition, we would like to be able to answer the question about the role played by the number of species in allelochemical networks, i.e., why the undoing the observed patterns are destroyed when the number of species is odd. For this purpose, we intend to make an analytical analysis. Lastly, space has a very important function for ecosystems maintenance of ecosystems, hence it seems imperative to consider spatial heterogeneity in the stability-complexity debate is necessary.

Bibliography

[1] *Post-war reconstruction and development in the Golden Age of Capitalism*. World Economic and Social Survey 2017: Reflecting on Seventy Years of Development Policy Analysis, 2017. DOI:https://dx.doi.org/10.18356/a15c28ca-en

[2] Landi, P. et. al; *Complexity and stability of ecological networks: a review of the theory*. Population Ecology, **60**, 319-345, 2018.

[3] A-L. Barabási; *Network science*. Cambridge University Press, 2016.

[4] D. Pimentel. *Species diversity and insect population outbreaks*. Ann. Entomol. Soc. Am., **54**, 76-86, 1961

[5] S. L. Pimm; *The complexity and stability of ecosystems*. Nature, **307**, 321-326, 1984.

[6] G. E. Hutchinson; *The paradox of the plankton*. Am. Nat., **95**, 137-145, 1961.

[7] R. MacArthur; *Fluctuations of animal populations and a measure of community stability*. Ecol., **36(3)**, 533-536, 1955.

[8] K. S. McCann; *The diversity-stability debate*. Nature, **405**, 228-233, 2000.

[9] R. M. May; *Will a large complex system stable?*. Nature, **238**, 413, 1972.

[10] R. M. May; *Stability and complexity in model ecosystem*. Princeton Univ. Press, 1974.

[11] M. R. Gardner, W. R. Ashby; *Connectance of large dynamic (Cybernetic) systems: critical values for stability*. Nature, **228**, 784, 1970.

[12] R. H. MacArthur, E. O. Wilson; *The Theory of Island Biogeography*. Princeton University Press, Princeton, 1967.

[13] J. Damuth; *Population density and body size in mammals*. Nature, **290**, 699-700, 1981.

[14] R. R. Williams, et. al; *Two degrees of separation in complex food webs*. PNAS, **99**, 12913-12916, 2002.

[15] T. Gross, et. al; *Generalized models reveal stabilizing factors in food webs*. Science, **325**, 747-750, 2009.

[16] R. W. Brooker et. al; *Facilitation in plant communities: the past, the present, and the future*. J. Ecol., **96**, 18-34, 2008.

[17] M. G. A. Van der Heijden, T. R. Horton; *Socialism in soil? The importance of mycorrhizal fungal networks for facilitation in natural ecosystems*. J. Ecol., **97**, 1139-1150, 2009.

[18] R. V. Solé, J. Valls; *On structural stability and chaos in biological systems*. J. Theor. Biol., **155**, 87-102, 1992.

[19] R. P. Rohr, S. Saavedra, J. Bascompte; *On structural stability and chaos in biological systems*. Science, **345**, 1253497, 2014.

[20] M. S. Araujo, et. al; *Network analysis reveals contrasting effects of intraspecific competitions on individual vs. population diets*. Ecology, **89**, 1981-1993, 2008.

[21] J. M. Smith; *The game lizard play*. Nature, **380**, 198-199, 1996.

[22] J. B. C. Jackson, L. W. Buss; *Allelopathy and competition among coral-reef invertebrates*. Proc. Natl. Acad. Sci. USA, **72**, 5160-5163, 1975.

[23] D. D. Cameron, A. White, J. Antonovies; *Parasite-grass-forb interactions and rock-paper-scissor dynamics: predicting Rhinanthus minor on host plant communities*. J. Ecol., **97**, 1131-1319, 2009.

[24] B. C. Kirkup, M. A. Riley; *Antibiotic-mediated antagonism leads to a bacterial game of rock-paper-scissor in vivo*. Nature, **428**, 412-414, 2004.

[25] E. D. Kelsic, J. Zhao, K. Vetsigian, R. Kishony; *Counteraction of antibiotic production and degradation stabilizes microbial communities*. Nature, **521**, 516-521, 2015.

[26] O. Gillor, B. C. Kirkup, M. A. Riley; *Colicins and microcins: The next generation antimicrobials*. Adv. Appl. Microbiol., **54**, 129-146, 2004.

[27] A. P. Müller, J. A. Gallas; *How community size affects survival chances in cyclic competition games that microorganisms play*. Phys. Rev. E Stat. Nonlin. Soft. Matter Phys., **82(5)**, 052901, 2010.

[28] A. P. O. Müller; *Impacto da tamnho da comunidade em modelos de competição cíclica*. Tese apresentada ao Programa de Pós-Graduação do Instituto de Física da Universidade Federal do Rio Grande do Sul, 2012.

[29] A. R. Ives, S. R. Carpenter; *Stability and diversity of ecosystems*. Science, **19**, 58-62, 2007.

[30] N. E. Stork; *Re-assessing current extinction rates*. Biodiversity and Conservation, **19**, 357-371, 2010.

[31] A. L. Barabsi, Z. N. Oltvai; *Network biology: understanding the cell's functional organization*, Nature Reviews, **5**, 101-113, 2004.

[32] J. E. Cohen, D. W. Stephens; *Food webs and niche space*. Princeton University Press, 1978.

[33] M. Begon, C. R. Townsend, J. L. Harper; *Ecology: from individuals to ecosystems*. Blackwell, Malden, MA, 4 edition, 2006.

[34] J. I Perotti, O. V. Billoni, F. A. Tamarit, D. R. Chialvo, S. A. Cannas; *Emergent self-organized complex network topology out of stability constraints*. Phys. Rev. L, **103(10)**, 108701, 2009.

[35] S. A. Carvalho, M. L. Martins; *Community structures in allelopathic interaction networks: an eco-evolutionary approach*, https://arxiv.org/abs/1812.00052, 2018.

[36] A-L. Baraási; *Scale-free networks: A decade and beyond*. Sci., **325**, 412-413, 2009.

[37] A. Barrat, M. Barthélemy, A. Vespignani; *Dynamical processes on complex networks*. Cambridge University Press, 2008.

[38] M. E. J. Newman; *Networks: An introduction*. Oxford University Press, 2010.

[39] N. Boccara; *Modeling complex systems*. Springer New York, 2010.

[40] A. Viol and et. al; *Shannon entropy of brain functional complex networks under the influence of the psychedelic Ayahuasca*. Sci. Rep., **7388(7)**, 1-13, 2017.

[41] F. Picard, V. Miele, J. J. Daudin, L. Cottret, S. Robin; *Deciphering the connectivity structure of biological networks using MixNet*. BMC Bioinf., **10(6)**, 1-11, 2009.

[42] D. J. Watts, S. H. Strogatz; *Collective dynamics of 'small-world' networks*. Nature, **393**, 440-442, 1998.

[43] E. Ravasz, A-L. Barabási; *Hierarchical organization in complex networks*. Phys. Rev. E. Stat. Nonlin. Soft Matter Phys., **67**, 026112, 2003.

[44] E. Ravasz, A. L. Somera, D. A. Mongru, Z. N. Oltvai, A-L. Barabási; *Hierarchical organization of modularity in metabolic networks*. Sci., **297**, 1551-1555, 2002.

[45] M. E. J. Newman; *Assortative mixing in networks*. Phys. Rev. Lett., **89**, 208701, 2002.

[46] S. A. Carvalho; *Um modelo de interação entre bactérias alelopáticas*. Dissertação apresentada ao Programa de Pós-Graduação em Física da Universidade Federal de Viçosa, 2015.

[47] S. N. Dorogovtsev; *Lectures on complex networks*. Oxford University Press, 2010.

[48] R. Pastor-Satorras, A. Vázquez, A. Vespignani; *Dynamical and correlation properties of the Internet*. Phys. Rev. Lett., **87**, 258701, 2001.

[49] A. Vázquez, R. Pastor-Satorras, A. Vespignani; *Large-scale topological and dynamical properties of Internet*. Phys. Rev. E, **65**, 066130, 2002.

[50] C. Shannon; *A mathematical theory of communication*. Bell System Tech. Jou., **379(423)**, 623656, 1948.

[51] T. G. Lewis; *Network science: theory and applications*. Wiley-Blackwell, 2009.

[52] T. M. Cover, J. A. Thomas; *Elements Of Information Theory Notes*. Wiley Series in Telecommunications and Signal Processing, 2006.

[53] P. Erdös, A. Rényi; *On the evolution of random graphs*. Publ. Math. Inst. Hung. Acad. Sci., **5**, 17-61, 1960.

[54] N. D. Martinez; *Artifacts or Attributes? Effects of Resolution on the Little Rock Lake Food Web*. Ecol. Monogr., **61**, 367-392, 1991.

[55] J. M. Montoya; *Small world patterns in food webs*. J. Theor. Biol., **214**, 405-412, 2002.

[56] A-L. Barabási, R. Albert; *Emergence of scaling in random networks*, Sci., **286**, 509-512, 1999.

[57] A-L. Barabási, R. Albert, H. Jeong; *Mean-field theory for scalefree random networks*, Phys. A, **272**, 173-187, 1999.

[58] R. Albert, A-L. Barabási; *Statistical mechanics of complex networks*, Rev. Mod. Phys., **74**, 47, 2002.

[59] J. M. Montoya, S. L. pimm, R. V. Solé; *Ecological networks and their fragility*, Nature, **442**, 259, 2006.

[60] P. Chesson; *Mechanisms of maintenance of species diversity*. Annu. Rev. Ecol. Sys., **31**, 343-366, 2005.

[61] D. Tilman; *Resource competition and community structure*. Princeton University Press.

[62] S. Depuydt; *Arguments for and against self and non-self root recognition in plants*. Front. Plant Sci., **5(614)**, 1-7, 2014.

[63] J. F. C. Jr, G. M. Gordon; *The behavioral ccology of nutrient foraging by plants*. Front. Annu. Rev. Ecol. Evol. Syst., **42**, 289-311, 2011.

[64] M. Liesje, V. R. Jasper, J. Corien, M. V. S. Harry, K. Hans; *Interactive effects of nutrient heterogeneity and competition: implications for root foraging theory*? Func. Ecol., **26(1)**, 66-73, 2012.

[65] S. Mariana, S. Sirgi, L. Anu; *Plant root exudates mediate neighbour recognition and trigger complex behavioural change*. New Phytotologist, **204**, 631-637, 2014.

[66] J. F. Cahill, G. G. McNickle, J. J. Haag, E. G. Lamb, S. M. Nyanumba, C. C. S. Clair; *Plants integrate information about nutrients and neighbors*. Science, **328**, 1657, 2010.

[67] O. X. Cordero, H. Wildschutte, B. Kirkup, S. Proehl, L. Ngo, F. Hussain, F. Le Roux, T. Mincer, M. F. Polz; *Ecological populations of bacteria act as socially cohesive units of antibiotic production and resistance*. Sci., **337(6099)**, 1228-31, 2012.

[68] W. T. Starmer, P. F. Ganter, V. Aberdeen, M. A. Lachance, H. J. Phaff; *The ecological role of killer yeasts in natural communities of yeasts*. Can. J. Microbiol., **33(9)**, 783-96, 1987.

[69] J. Berdy; *Recent developments of antibiotic research and classification of antibiotics according to chemical structure*. Adv. Appl. Microbiol.,**18**, 309-402, 1974.

[70] H. P. Bais, S. W. Park, T. L. Weir, R. M. Callaway, J. M. Vivanco; *How plants communicate using the underground information superhighway*. Trends Plant Sci., **9(1)**, 26-32, 2004.

[71] R. A. Gatenby, E. T. Gawlinski, A. F. Gmitro, B. Kaylor, R. J. Gillies; *Acid-mediated tumor invasion: a multidisciplinary study*. Cancer Res., **66(10)**, 5216-23, 2006.

[72] R. James, C. Kleansthous, G. R. Moore; *The biology of E colicins: paradigms and paradoxes*. Microbiology, **142**, 1569-1580, 1996.

[73] Y. Iwasa, M. Nakamarum, S. A. Levin; *Allelopathy of bacteria in lattice population: competition between colicin-sensitive and colicin-producing strain*. Evol. Ecol., **12**, 785-802, 1996.

[74] A. P. Pugsley; *The ins and outs of colicins. Part II. Lethal action, immunity and ecological implications*. Microb. Sci., **8**, 203-205, 1984.

[75] M. A. Riley, D. M. Gordon; *The ecology and evolution of bacteriocins*. J. Ind. Microbiol., **17**, 151-158, 1996.

[76] V. Braun, S. I. Patzer, K. Hantke; *Ton-dependent colicins and microcins: modular design and evolution*. Biochimie, **84**, 365-380, 2002.

[77] D. M. Gordom, C. L. O'brien; *Bacteriocin diversity and the frequency of multiple bacteriocin production in Escherichia coli*. Microbiology, **152**, 32393244, 2006.

[78] R. Y. Morita; *Bioavailability of energy and its relationship to growth and starvation survival in nature*. Can. J. Microbiol., **34**, 436-441, 1988.

[79] E. R. Zinzer, R. Kolter; *Escherichia coli evolution during stationary phase*. Res. Microbiol., **155**, 328-336, 2004.

[80] S. E. Finkel; *Long-term survival during stationary phase: evolution and the GASP phenotype*. Nat. Rev. Microbiol., **4**, 113-120, 2006.

[81] I. Bjedov, O. Tenaillon, B. Grard, V. Souza, E. Denamur, M. Radman, F. Taddei, I. Matic; *Stress-induced mutagenesis in bacteria*. Science, **300**, 1404-1409, 2003.

[82] O. Tenaillon, E. Denamur, I. Matic; *Evolutionary significance of stress-induced mutagenesis in bacteria*. Trends Microbiol., **12**, 264-270, 2004.

[83] M. M. Zambrano, D. A. Siegele, M. Almirón, A. Tormo, R. Kolter; *Microbial competition: Escherichia coli mutants that take over stationary phase cultures*. Science., **259**, 1757-1760, 1993.

[84] S. E. Finkel, R. Kolter; *Evolution of microbial diversity during prolonged starvation*. Proc. Natl. Acad. Sci. USA, **96**, 4023-4027, 1999.

[85] E. R. Zinzer, R. Kolter; *Mutation enhancing amino acid catabolism confer a growth advantage in stationary phase*. J. Bacteriol., **181**, 5800-5807, 1999.

[86] E. R. Zinzer, R. Kolter; *Prolonged stationary-phase incubation selects for lrp mutations in Escherichia coli K-12*. J. Bacteriol., **182**, 4361-4365, 2000.

[87] J. E. Keymer, M. A. Fuentes, P. A. Marquet; *Diversity emerging: from competitive exclusion to neutral coexistence in ecosystems*. Theor. Ecol., **5(3)**, 457-463, 2011.

[88] J. L. Round, S. K. Mazmanian; *The gut microbiota shapes intestinal immune responses during health and disease*. Nat. Rev. Immunol., **9**, 313-323, 2009.

[89] M. J. Richards, J. R. Edwards, D. H. Culver, R. P. Gaynes; *Nosocomial infections in combined medical-surgical intensive care units in the United States*. Infect. Control Hosp. Epidemiol., **21**, 510-515, 2000.

[90] M. S-C, S-P. Nuccio, H. Liu, D. Hernandez, C. T. Vu, A. A. Takahashi, R. A. Edwards, M. Raffatellu; *Microcins mediate competition among Enterobacteriacae in the inflamed gut*. Nature, **540**, 280-283, 2016.

[91] E. Braganhol, M. R. Wink, G. Lenz, A. M. O. Battastini; *Purinergic signaling in glioma progression. In: Baranska J (ed) Glioma signaling, Advances in experimental medicine and biology, vol 986*. Springer, Dordrecht.

[92] J. D. Bever, *et al*; *Rooting theories of plant community ecology in microbial interactions*. Trends Ecol. Evol., **25**, 468-478, 2010.

[93] H. P. Bais, *et al*; *How plants communicate using the underground information superhighway*. Trends Plant Sci., **9**, 26-32, 2004.

[94] H. E. Flores, *et al*; *'Radicle' biochemistry: the biology of root-specific metabolism*. Trends Plant Sci., **4**, 220-226, 1999.

[95] R. D. Morton, R. Law; *Regional species pool and the assembly of local ecological communities*. J. Theor. Biol., **187**, 321-331, 1997.

[96] K. Shea, P. Chesson; *Community ecology theory as a framework for biological invasions*. Trends Ecol. Evol., **17**, 170-176, 2002.

[97] C. Chou; *Roles of allelopathy in plant biodiversity and sustainable agriculture*. Crit. Rev. Plant Sci., **18**, 609-636, 1999.

[98] W. R. J. Dean; *Space invaders: modeling the distribution, impacts and control of alien organisms*. Tends Ecol. Evol., **13**, 256-258, 1998.

[99] J. A. Drake, H. A. Mooney, *et al*; *Biological invasions: a global perspective*. Wiley, Chichester, 1989.

[100] N. Shigesada, K. kawasaki; *Biological invasions: theory and practice*. Oxford University Press, 1997.

[101] D. R. de Souza, M. L Martins, F. M. S. Carmo; *A multiscale model for plant invasion through allelopathic suppression*. Biol. Invasi., **12**, 1543-1555, 2010.

[102] A. J. Lotka; *Elements of Physical Biology*. Williams & Wilkins Company, Baltimore, 1925.

[103] V. Volterra; *Fluctuations in the abundance of a species considered mathematically.* nature, **118**, 558-560, 1926.

[104] R. Durret, S. Levin; *Allelopathy in Spatially Distributed Populations.* J. Theor. Biol., **185**, 165, 1997.

[105] P. Szabó, T. Czárán, and G. Szabó; *Competing associations in bacterial warfare with two toxins.* J. Theor. Biol., **248**, 736, 2007.

[106] M. F. Weber, G. Poxleitner, E. Hebisch, E. Frey, M. Opitz; *Chemical warfare and survival strategies in bacterial range expansions.* J. R. Soc. Interface, **11**, 20140172, 2014.

[107] A. C. Fassoni, M. L. Martins; *Mathematical analysis of a model for plant invasion mediated by allelopathy.* Ecol. Comp., **18**, 4958, 2014.

[108] S. A. Carvalho, M. L. Martins; *Invasion waves in the biochemical warfare between living organisms.* Phys. Rev. E, **97**, 042403, 2018.

[109] P. Mercedes; *Computational ecology: from the complex to the simple and back.* PLoS Comp. Biol., **1(2)**, e18, 2005.

[110] J. A. Dunne; *Food webs, In: Encyclopedia of complexity and systems science*, Ed. R. A. Meyers, 3661, Springer, New York, 2009.

[111] J. Camacho, R. Guimerá, L. A. N. Amaral. *Robust patterns in food web structure.* Phys. Rev. Let., **88**, 1-4, 2002.

[112] M. Jenny, et. al; *Connectance in stream food webs.* J. of An. Ecol., **71(6)**, 1056-1062, 2002.

[113] K. Arii, L. Parrott; *Emergence of non-random structure in local food webs generated from randomly structured regional webs.* J. Theor. Biol., **227**, 327-333, 2004

[114] L. A. N. Amaral, A. Scala, M. Barthélémy, H. E. Stanley; *Classes of small-world networks.* Proc. Natl. Acad. Sci. USA, **97**, 11149-11152, 2000.

[115] W. Feng, K. Takemoto; *Heterogeneity in ecological mutualistic networks dominantly determines community stability.* Sci. Rep., **4**, 5912, 2014.

[116] T. Okuyama, J. N. Holland; *Network structural properties mediate the stability of mutualistic communities.* Ecol. Lett., **11**, 208-216, 2008.

[117] P. Jordano, J. Bascompte, J. M. Olesen; *Invariant properties in coevolutionary networks of plantanimal interactions.* Ecol. Lett., **6**, 69-81, 2003.

[118] N. T. Wheelwright, W. A. Haber, K. G. Murray, C. Guindon; *Tropical fruit eating birds and their food plants: a survey of a Costa Rican lower montane forest.* Biotropica, **16**, 173-192, 1984.

[119] T. Inoue, M. Kato, T. Kakutani, T. Suka, T. Itino; *Insect-flower relationship in the temperate deciduous forest of Kibune, Kyoto: an overview of the flowering phenology and the seasonal pattern of insect visits.* Contrib. Biol. Lab. Kyoto Univ., **27**, 377-463, 1990.

[120] R. V. Solé, D. Alonso, A. McKane; *Scaling in a network model of multiespecies ecosystem.* Phys. A, **286**, 337, 2000.

[121] M. B. Daniel, S. Suweis, J. Hidalgo, A. Maritan; *Explorability and the origin of network sparsity in living systems.* Sci. Rep., **7**, 12323, 2017.

[122] J. I. Perotti, O. V. Billoni, F. A. Tamarit, S. A. Cannas; *Stability as a natural selection mechanism on interacting networks.* Papers in Physics, **2**, 020005, 2010.

[123] F. E. Kyle, et. al; *Evolutionary stable communities: a framework for understanding the role of trait evolution in the maintenance of diversity.* Ecol. Lett., **21**, 1853-1868, 2018.

[124] N. D. Martinez. *Constant connectance in community food webs.* Am. Nat., **139**, 1208-1218, 1992.

[125] J. A. Dunne, R. J. Williams, N. D. Martinez. *Food-web structure and network theory: the role of connectance and size.* Proc. Natl. Acad. Sci. USA, **99**, 12917-12922, 2002.

[126] K. Havens; *Scale and structure in natural food webs.* Science, **257**, 1107-1109, 1992

[127] C. Banasek-Richter, et. al; *Complexity in quantitative food webs.* Ecology, **90**, 1470-1477, 2009.

[128] M. E. J. Newman; *Mixing patterns in networks.* Phys. Rev. E, **67**, 026126, 2003.

[129] A. Pascual-Garcia, U. Bastolla; *Mutualism supports biodiversity when the direct competition is weak.* Nat. Commun., **8**, 1-13, 2017.

[130] U. Bastolla, et. al; *The architecture of mutualistic networks minimizes competition and increases biodiversity.* Nature, **458**, 1018-1020, 2009.

[131] D. P Reagan, R. B. Waide; *The Food Web of a Tropical Rain Forest.* Univ. Chicago Press, Chicago, 1996.

[132] C. Melia, J. Bascompte; *Food web cohesion.* Ecology, **85**, 352, 2004.

[133] M. José, P. L. Stuart, R. V. Solé; *Ecological networks and their fragility.* Nature, **442**, 259-264,2006.

[134] J. B. Hughes, J. Roughgarden; *Species diversity and biomass stability*, Am. Nat., **155**, 618627, 2000.

[135] G. F. Gause; *The Struggle for Existence*, Williams & Wilkins, Baltimore, MD, 1934.

[136] D. Tilman; *Resource competition between planktonic algae: an experimental and theoretical approach*, Ecology, **58**, 338348, 1977.

[137] A. R. Tomas, F. J. Weissing; *Commonalities and discrepancies among multispecies competition models*, Groningen: s.n., 2010.

[138] I. Rozdilsky, L. Stone; *Complexity can enhance stability in competitive systems*, Ecol. Lett., **4**, 397400, 2001.

[139] L. Stone; *Some Problems of Community Ecology: Processes, Patterns and Species Persistence in Ecosystems*, PhD dissertation Dept. of Physics, (Monash University, 1988).

[140] A. Robers; *When will a large complex system be viable?*, Environmental Discussion Paper - Graduate School of Environmental Science, Monash University, 1989.

[141] L. Stone, A. Robers; *Conditions for a species to gain advantage from the presence of competitors*, Ecology, **72**, 19641972, 1991.

[142] V. A. A. Jansen, G. D. Kokkoris; *Complexity and stability revisited*, Ecol. Lett., **6**, 498502, 2003.

[143] M. A. Huston; *A general hypothesis of species diversity*, Am. Nat., **113**, 81-101, 1979.

[144] T. A. R. Rimbach; *Multispecies Resource Competition.* Thesis Presented at University of Groningen, 2010.

[145] M. Brede, S. Sinha; *Assortative mixing by degree makes a network more unstable*, arXiv:cond-mat/0507710, 2005.

[146] S. A. Carvalho, M. L. Martins;*Biochemical Warfare Between Living Organisms for Survival: Mathematical Modelling.* In: *Reference Series in Phytochemistry.* Springer Nature Switzerland, pp. 1-38, 2019.

[147] G. D. Smith;*Numerical solutions of partial differential equations - finite difference methods.* Oxford University Press, 1985.

[148] C. Grossmann, H. Roos, M. Stynes ;*Numerical treatment of partial differential equations*. Springer, 2007.

[149] R. M. May;*Stability and complexity in model ecosystems*. Princeton University Press, Princeton, 1973.

[150] D. Melchionda, E. Pastacaldi, C. Perri, M. Banerjee, E. Venturino;*Social behavior-induced multistability in minimal competitive ecosystems*. J. Theor. Biol., **439**, 24, 2018.

[151] D. M. Gordon, C. L. O'Brien;*Bacteriocin diversity and the frequency of multiple bacteriocin production in Escherichia coli*. Microbiology, **152**, 3239-3244, 2006.

[152] T. Reichenbach, M. Mobilia, E. Frey;*Mobility promotes and jeopardizes biodiversity in rock-paper-scissors games*. Nature, **448**, 1046-1049, 2007.

[153] B. Kerr, M. A. Riley, M. W. Feldman, B. J. M. Bohannan;*Local dispersal promotes biodiversity in a real-life game of rock-paper-scissors*. Nature, **418**, 171-174, 2002.

[154] E. Frey;*Evolutionary game theory: Theoretical concepts and applications to microbial communities*. Physica A, **389**, 4265-4298, 2010.

[155] T. Reichenbach, M. Mobilia, E. Frey;*Noise and correlations in a spatial population model with cyclic competition*. PRL, **99**, 238105, 2007.

[156] Q. He, M. Mobilia, U. C. Täuber;*Spatial rock-paper-scissors models with inhomogeneous reaction rates*. PRE, **82**, 051909, 2010.

[157] P. P. Avelino, D. Bazeia, L. Losano, J. Menezes, B. F. de Oliveira, M. A. Santos; *How directional mobility affects coexistence in rock-paper-scissors models*. PRE, **97**, 032415, 2018.

[158] P. P. Avelino, , D. Bazeia, L. Losano, J. Menezes, B. F. de Oliveira; *Spatial patterns and biodiversity in off-lattice simulations of a cyclic three-species Lotka-Volterra model*. EPL, **121**, 48003, 2018.

[159] P. P. Avelino, , D. Bazeia, L. Losano, J. Menezes, B. F. de Oliveira; *Spatial patterns and biodiversity in off-lattice simulations of a cyclic three-species Lotka-Volterra model*. EPL, **121**, 48003, 2018.

[160] K. G. Károlyi, Z. Neufeld, I. Scheuring; *Rock-scissors-paper game in a chaotic flow*. J. Theor. Biol., **236(1)**, 12-20, 2005.

[161] S. T. Thornton, J. B. Marion; *Classical dynamics of particles and systems*. 5th Edition, California: Thomson Books/Cole, 2004.

[162] T. Reichenbach, M. Mobilia, E. Frey;*Self-organization of mobile populations in cyclic competition*. J. Theor. Biol., **254**, 368-383, 2008.

[163] D. Groselj, F. Jenko, E. Frey ;*How turbulence regulates biodiversity in systems with cyclic competition*. PRE, **91**, 033009, 2015.

[164] H. Cheng, N. Yao, Z. G. Huang, J. Park, Y. Do, Y. C. La ;*Mesoscopic interactions and species coexistence in evolutionary game dynamics of cyclic competitions*. Sci. Rep., **4**, 7486, 2014.

[165] R. M. May, W. J. Leonard ;*Nonlinear aspects of competition between three species*. SIAM J. Appl. Math., **29**, 243-253, 1975.

[166] E. B. Jacob, I. Cohen, H. Levine ;*Cooperative self-organization of microorganisms*. Adv. Phys., **49**, 395-554, 2000.

[167] E. B. Jacob, I. Cohen, I. Golding, D. L. Gutnick, M. Tcherpakov, D. Helbing, I. G. Ron Open; *Bacterial cooperative organization under antibiotic stress*. Phys. A, **282**, 247-282, 2000.

[168] M. Matsushita, H. Fujikawa; *Diffusion-limited growth in bacterial colony formation*. Phys. A, **168**, 498-506, 1990.

[169] R. Rudner, O. Martsinkevich, W. Leung, E. D. Jarvis; *Classification and genetic characterization of pattern-forming bacilli*. Mol. Microbiol., **27**, 687-703, 1998.

[170] M. Eisenbach; *Functions of the flagellar modes of rotation in bacterial motility and chemotaxis*. Mol. Microbiol., **4**, 161-167, 1990.

[171] J. Henrichsen; *Gliding and twitching motility of bacteria unaffected by Cytochalasin B*. A. Pathol. Microbiol. Scand. B B, **80**, 623, 1972.

[172] J. Henrichsen, L. O. Froholm, K. Bovre; *Studies on bacterial surface translocation. 2. Correlation of twitching motility and fimbriation in bolony variantsof Moraxella-Nonliquefaciens, M-Bovis, and M-Kingii*. A. Pathol. Microbiol. Scand. B B, **80**, 445, 1972.

[173] P. M. Park, E. A. Wolanin, H. Yuzbashyan, N. C. Lin, J. B. Darnton, P. Stock, R. Silberzan; *Influence of topology on bacterial social interaction*. Proc. Natl. Acad. Sci. USA, **100**, 1391-13915, 2003.

[174] O. Hallatschek, P. Hersen, S. Ramanathan, D. R. Nelson; *Genetic drift at expanding frontiers promotes gene segregation*. Proc. Natl. Acad. Sci. USA, **104**, 19926-19930, 2007.

[175] O. Hallatschek, D. R. Nelson; *Gene surfing.* Theor. Pop. Biol., **73**, 158, 2008.

[176] R. P. Rohr, S. Saavedra, J. Bascompte; *Ecological networks. On the structural stability of mutualistic systems.* Science, **345**, 1253497, 2014.

[177] U. Bastolla, M. Fortuna, A. Pascual-Garcia, A. Ferrera, B. Luque, J. Bascompte; *The architecture of mutualistic networks minimizes competition and increases biodiversity.* Nature, **458**, 1018-1020, 2009.

[178] S. R. Proulx, D. E. L. Promislow, P. C. Phillips; *Network thinking in ecology and evolution.* Trends Ecol. Evol., **20**, 345, 2005.

[179] G. Caldarelli; *Scale-free Networks - complex webs in nature and technology.* Oxford University Press, 2007.

[180] M. E. Gilpin; *Limit cycles and competition in communities.* American Naturalist, **109**, 51-60, 1975.

[181] M. L. Zeeman; *Hopf bifurcations in competitive three-dimensional Lotka-Volterra systems.* Dynamics and Stability of Systems, **8**, 189-216, 1993.

[182] S. Smale; *On the differential equations of species in competition.* Journal of Mathematical Biology, **3**, 5-7, 1976.

[183] A. Arneodo, P. Coullet, J. Peyraud, C. Tresser; *Strange attractors in volterra equations for species in competition.* Journal of Mathematical Biology, **14**, 153-157, 1982.

Appendix A

Statistical Properties of a Degree Distribution

A.1 Shape Characteristics of Probability Distributions

In most complex networks nodes tend to not have equal connectivity, and certainly, there are nodes more connected than others. Information about how the connectivity is distributed between the nodes in a network can be obtained from the distribution of degrees $P(k)$, or by calculating of the distribution moments,

$$\langle k^n \rangle = \sum_k k^n P(k). \tag{A1.1}$$

The first moment, $\langle k \rangle$, is the expected value (mean) of the degree distribution. The second moment measures the fluctuations of the degree distribution. Larger order moments are useful for calculating asymmetry of distributions and their tails.

The variance, σ^2, measures the spread of the distribution around its mean using the function $g(k) = (k - \langle k \rangle)^2$. If most values of k are close to $\langle k \rangle$ then on average $(k - \langle k \rangle)^2$ will be small. Indeed, if many values of k are far below and/or far above $\langle k \rangle$ then on average $(k - \langle k \rangle)^2$ will be large. Squaring the deviations about $\langle k \rangle$ guarantees a positive value. The variance is defined as

$$\sigma^2 = \sum_k (k - \langle k \rangle)^2 P(k). \tag{A1.2}$$

Because σ^2 represents an average squared deviation, it is not in the same units as k. The standard deviation of k denoted σ is the square root of the variance and is in the same

units as k.

The asymmetry S, also called *Skewness*, measures the symmetry of a distribution around its mean value using the function $g(k) = (k - \langle k \rangle)^3/\sigma^3$, where σ^3 is just the standard deviation raised to the third power. Thus, *Skewness* can be calculated by,

$$S = \frac{\sum_k (k - \langle k \rangle)^3 \, P(k)}{\sigma^3} \tag{A1.3}$$

When k is far below its mean, the term $(k - \langle k \rangle)^3$ is a big negative number, ergo $S < 0$ guarantees a negative asymmetric distribution (long left tail). Otherwise, when S is far above its mean $(k - \langle k \rangle)^3$ is a big positive number then $S > 0$ (positive asymmetry with long right tail). If k are close to the mean ($S \sim 0$) then the distribution is symmetric, since positive and negative values in the equation A1.3 cancel out.

The kurtosis measures the thickness in the tails of a distribution and is based on $g(k) = (k - \langle k \rangle)^4/\sigma^4$. If a frequency curve is flattened relative to a normal reference curve, kurtosis can be measured from the following coefficient:

$$K = \frac{\sum_k (k - \langle k \rangle)^4 \, P(k)}{\sigma^4} \tag{A1.4}$$

where σ^4 is just standard deviation raised to the fourth power. Since kurtosis is based on deviations from the mean raised to the fourth power, large deviations get lots of weight.

Hence, distributions with large kurtosis values are ones where there is the possibility of extreme values. In contrast, if the kurtosis is small then most of the observations are tightly clustered around the mean and there is very little probability of observing extreme values. The reference for the kurtosis coefficient is calculated from the Gaussian (or Normal) distribution whose value is $K = 3$ (see subsection A.2). This value defines a mesokurtic distribution. If for a given distribution, $K > 3$, then its tail will be thicker than Normal and it will be called leptokurtic distribution. Finally, if the distribution has tail thinner than Normal, $K < 3$, and it is said that the distribution is platykurtic.

A.2 Degree Distribution in Complex Networks

From the degree distribution $P(k)$ exhibited by a complex network, one can distinguish two classes of networks: *homogeneous* and *heterogeneous*. In the *homogenenous* networks, it is observed that the connectivities are distributed around a typical value, the mean value $\langle k \rangle$, vanishing at the extreme $P(+\infty) \to 0$. For *homogeneous* networks the degree distribution $P(k)$ decreases rapidly to large values of k (a distribution of this type is called "light tailed"), as for instance the Gaussian or Poisson degree distributions (see figure A.1-a and b). However, in the second class, the network nodes have very distinct

connectivities without any typical scale for the characteristic degree. This scale-free nature leads to a power-law decay of the distribution $P(k)$. In this case, it's said that the distribution is "heavy tailed". This statistical heterogeneity indicates that few nodes have many connections while most nodes have low connectivities, but the frequency of highly connected nodes is not exponentially rare and thus such rare nodes are very relevant.

To obtain a better understanding of the heterogeneity, consider the ratio κ between the first and second moments of $P(k)$:

$$\kappa = \frac{\langle k^2 \rangle}{\langle k \rangle}. \tag{A2.1}$$

The homogeneous networks are characterized by $\kappa \sim \langle k \rangle$, while scale-free networks has $\kappa \to \infty$. For this reason, one can generalize and refer to scale-free networks as all networks that have the parameter $\kappa \gg \langle k \rangle$ because the real networks are finite [179].

From now on some of the most common types of distributions present in the study of complex networks will be discussed.

- The *Poisson Distribution* is given by:

$$P(k) = \frac{e^{-\langle k \rangle} \langle k \rangle^k}{k!} \tag{A2.2}$$

where $\langle k \rangle$ is mean connectivity. Random networks have $P(k)$ described by Poisson distribution when the node's number tend to infinity and mean connectivity, $\langle k \rangle$ is fixed. The graphical representation of this distribution for different values of mean and standard deviation can be visualized in the Figure (A.1-a). The second moment of this distribution is:

$$\begin{aligned} \langle k^2 \rangle &= \sum_{k=0}^{\infty} k^2 \frac{e^{-\langle k \rangle} \langle k \rangle^k}{k!} \\ &= \langle k \rangle + \langle k \rangle^2, \end{aligned} \tag{A2.3}$$

which produces a variance $\sigma^2 = \langle k \rangle$ and a standard deviation $\sigma = \sqrt{\langle k \rangle}$. The ratio $\kappa = \frac{\langle k^2 \rangle}{\langle k \rangle} \sim \langle k \rangle$, a signature of homogeneous networks.
Its *Skewness* is

$$\begin{aligned} s &= \sum_{k=0}^{\infty} \frac{(k - \langle k \rangle)^3}{\sigma^3} \frac{e^{-\langle k \rangle} \langle k \rangle^k}{k!} \\ &= \frac{1}{\sqrt{\langle k \rangle}}. \end{aligned} \tag{A2.4}$$

Finally, its *Kurtosis* is

$$\begin{aligned} K &= \sum_{k=0}^{\infty} \frac{(k-\langle k\rangle)^4}{\sigma^4} \frac{e^{-\langle k\rangle}\langle k\rangle^k}{k!} \\ &= 3 + \frac{1}{\langle k\rangle}. \end{aligned} \tag{A2.5}$$

- The *Normal (Gaussian) Distribution* has a "bell-shaped" (see Figure A.1-b) whose probability density is given by:

$$P(k) = \frac{1}{\sqrt{2\pi\,\sigma^2}}\, e^{-\frac{1}{2\sigma^2}(k-\langle k\rangle)^2}. \tag{A2.6}$$

Therefore, the Normal distribution is parametrized by its mean (real number $\langle k\rangle$) and standard deviation (positive real number σ). For simplicity k was considered a continuous variable and the discrete sum was replaced by an integral. So, the second moment is

$$\begin{aligned} \left\langle k^2\right\rangle &= \int_{-\infty}^{+\infty} k^2 \frac{1}{\sqrt{2\pi\,\sigma^2}} e^{-\frac{1}{2\sigma^2}(k-\langle k\rangle)^2} dk \\ &= \langle k\rangle^2 + \sigma^2 \end{aligned} \tag{A2.7}$$

and variance $\sigma^2 = \langle k^2\rangle - \langle k\rangle^2$. Thus, the ratio $\kappa = \frac{\langle k^2\rangle}{\langle k\rangle} \sim \langle k\rangle$, again a homogeneous network signature.
The asymmetry is zero:

$$\begin{aligned} S &= \int_{-\infty}^{+\infty} \frac{(k-\langle k\rangle)^3}{\sigma^3} \frac{1}{\sqrt{2\pi\,\sigma^2}} e^{-\frac{1}{2\sigma^2}(k-\langle k\rangle)^2} dk \\ &= 0 \end{aligned} \tag{A2.8}$$

In turn, the kurtosis is

$$\begin{aligned} K &= \int_{-\infty}^{+\infty} \frac{(k-\langle k\rangle)^4}{\sigma^4} \frac{1}{\sqrt{2\pi\,\sigma^2}} e^{-\frac{1}{2\sigma^2}(k-\langle k\rangle)^2} dk \\ &= 3. \end{aligned} \tag{A2.9}$$

- The *Power Law Distribution* is expressed by:

$$P(k) \propto k^{-\gamma} \tag{A2.10}$$

with $k \neq 0$ and $\gamma > 0$ the exponent of the distribution. In contrast to the Poisson or Normal distributions, networks with Power Law distributed $P(k)$ don't exhibit a characteristic scales for their connectivities. This "connection free" makes such net-

works known as scale-free. Figure *A*.1-c shows typical curves for this distribution. The mean value of this distribution is

$$\begin{aligned}\langle k\rangle &= \int_m^{k_c} k\,A\,k^{-\gamma}dk \\ &= \frac{\gamma-1}{m^{1-\gamma}}\,\frac{k^{2-\gamma}}{2-\gamma}\,\Big|_m^{k_c} \\ &= \frac{\gamma-1}{\gamma-2}\left(m^{2-\gamma}-k_c^{2-\gamma}\right) \\ &= \frac{\gamma-1}{\gamma-2}\,m \end{aligned} \tag{A2.11}$$

where $\langle k\rangle$ and the normalizing constant $A=\frac{\gamma-1}{m^{-\gamma+1}}$ were obtained in the asymptotic limit of infinite networks $k_c\to\infty$ and $\gamma>2$. So, the mean degree of this distribution is defined and finite. The variance of the distribution $\sigma^2/\langle k\rangle^2$ measures the strength of stochastic fluctuations present in the system. The variance $\sigma^2=\langle k^2\rangle-\langle k\rangle^2$ is dominated by the second moment of the distribution

$$\begin{aligned}\left\langle k^2\right\rangle &= \int_m^{k_c} k^2\,A\,k^{-\gamma}dk \\ &\sim k_c^{3-\gamma} \end{aligned} \tag{A2.12}$$

In the asymptotic limit of infinite networks, one has $\langle k^2\rangle\to\infty$, and , the fluctuations diverge when $\gamma<3$. The absence of any characteristic scale to such degree fluctuations, within the range defined by $2<\gamma\leq 3$, implies that the mean value is not a characteristic scale for the system. Hence, such networks are referred as *scale-free networks*. As previously mentioned, if the network is *scale-free*, $\kappa\to\infty$.

- The *Weibull Distribution* is given by

$$P(k)=\begin{cases}\alpha\left(\frac{k-\lambda}{\eta}\right)^{\alpha-1}e^{-\left(\frac{k-\lambda}{\eta}\right)^{\alpha}}, & \text{se}\quad k>\lambda \\ 0, & \text{otherwise.}\end{cases} \tag{A2.13}$$

This distribution exhibit different shapes depending on the parameter values, as shown in Figure *A*.1-d. The mean value of a Weibull distribution is

$$\begin{aligned}\langle k\rangle &= \int_0^{\infty} k\,P(k)dk \\ &= \lambda+\eta\,\Gamma\left[1+\frac{1}{\alpha}\right]. \end{aligned} \tag{A2.14}$$

Its second moment is

$$\begin{aligned} \left\langle k^2 \right\rangle &= \int_0^\infty k^2 \, P(k) dk \\ &= \lambda^2 + 2\,\eta\,\lambda\,\Gamma\left[1+\frac{1}{\alpha}\right] + \eta^2\,\Gamma\left[1+\frac{2}{\alpha}\right] \end{aligned} \tag{A2.15}$$

Also, the *Skewness* is

$$S = \frac{2\,\Gamma\left[1+\frac{1}{\alpha}\right]^3 - 3\,\Gamma\left[1+\frac{1}{\alpha}\right]\,\Gamma\left[1+\frac{2}{\alpha}\right] + \Gamma\left[1+\frac{3}{\alpha}\right]}{\left(-\Gamma\left[1+\frac{1}{\alpha}\right]^2 + \Gamma\left[1+\frac{2}{\alpha}\right]\right)^{\frac{3}{2}}}, \tag{A2.16}$$

while the *Kurtosis* is

$$K = \frac{\left(-3\,\Gamma\left[1+\frac{1}{\alpha}\right]^4 + 6\,\Gamma\left[1+\frac{1}{\alpha}\right]^2\,\Gamma\left[1+\frac{2}{\alpha}\right] - 4\,\Gamma\left[1+\frac{1}{\alpha}\right]\,\Gamma\left[1+\frac{3}{\alpha}\right] + \Gamma\left[1+\frac{4}{\alpha}\right]\right)^{\alpha}}{\left(-\Gamma\left[1+\frac{1}{\alpha}\right]^2 + \Gamma\left[1+\frac{2}{\alpha}\right]\right)^2} \tag{A2.17}$$

A.3 The Cumulative Distribution Function

The Cumulative Distribution Function (CDF) $F(k)$, provides the probability of a node has a degree smaller or equal to k. The CDF is represented by

$$F(k) = \sum_{k_i<k} P(k_i), \tag{A2.18}$$

where $P(k_i)$ is the fraction of nodes in the network degree with degree k. By definition $F(k)$ is a monotonically increasing function of k (see Figure A.2), with $F(-\infty) = 0$ and $F(\infty) = 1$.

Also, the Cumulative Complementary Distribution Function (CCDF), defined as,

$$G(k) = 1 - \sum_{k_i<k} P(k_i), \tag{A2.19}$$

is frequently used. This distribution is showed in Figure (A.2).

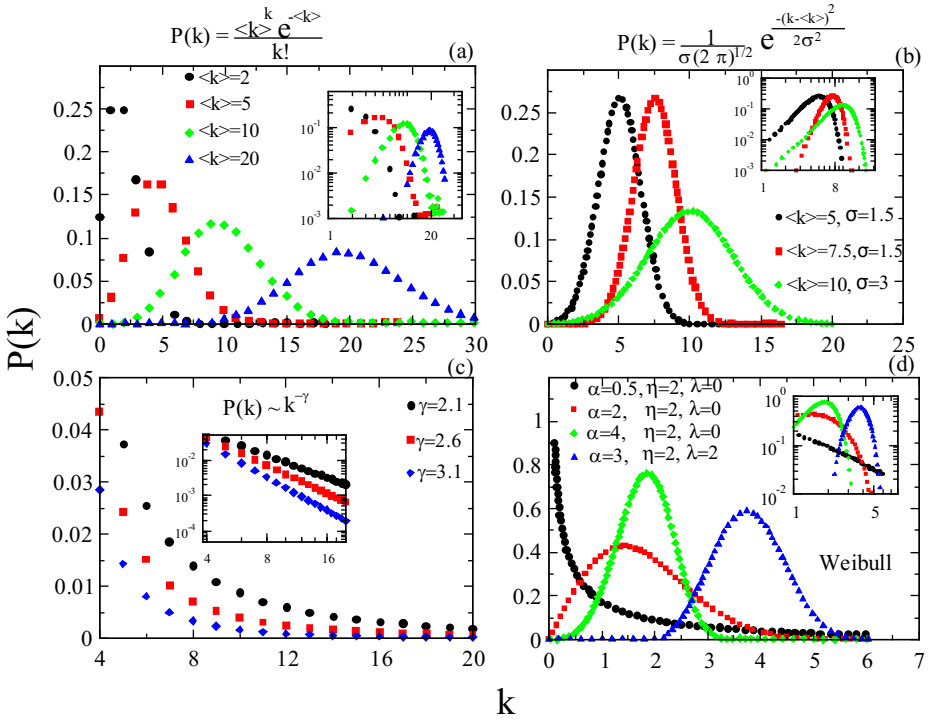

Figure A.1: Probability density function: a) Poisson, b) Normal (Gaussian), c) Power Law, and d) Weibull.

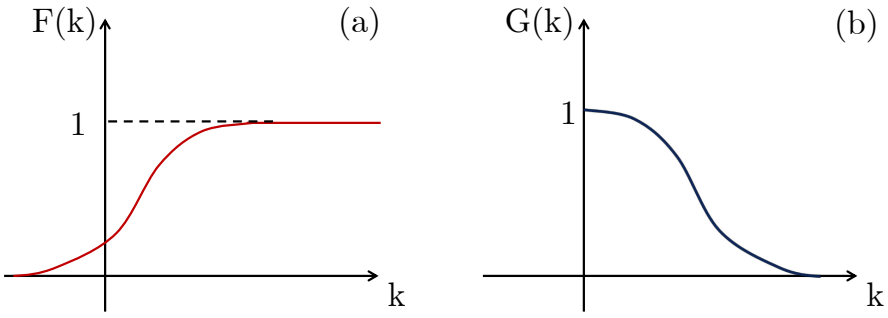

Figure A.2: Typical (a) cumulative and (b) cumulative complementary probability distribution functions.

Appendix B

Ecological and Evolutionary Dynamic in Allelopathic Systems

B.1 Dynamical System

To extend the models proposed in Refs. [107, 108, 146], the multi-species population dynamics is governed by the ordinary differential equations

$$\begin{aligned} \frac{\mathrm{d}N_i}{\mathrm{d}t} &= r_i \left(1 - \sum_{j=1}^{l} \nu_{ij} N_j\right) N_i - \sum_{j \neq i}^{l} \mu_{ij} \Phi_{ij}^{(k)}(y_j)\, N_i \\ \frac{\mathrm{d}B_i}{\mathrm{d}t} &= \beta_i\, N_i - \delta_i\, B_i - \sum_{j \neq i}^{l} \gamma_{ji}\, N_j\, B_i, \end{aligned} \tag{B.1}$$

where N_i and B_i denotes, respectively, the species i population and the concentration of its allelochemicals; r_i is its intrinsic growth rate, ν_{ij} are the inter-and intraspecific competition coefficients, μ_{ij} is the matrix element associated to species mortality due allelopathic suppression, and γ_{ij} is the allelochemical absorption matrix element. Moreover, β_i and δ_i are, respectively, release and natural toxins degradation rates. Here we extended the set of functional responses Φ introduced in the main text to evaluate the effect of mortality induced only by the absorbed toxins. The increase in mortality rates by allelopathic suppression are governed by response functions of the Holling types

$$\Phi_{ij}^{(k)} = \begin{cases} \frac{B_j}{B_0} & (k=1) \\ \frac{B_j}{c_i+B_j} & (k=2) \\ \frac{B_j^2}{c_i+B_j^2} & (k=3) \\ \gamma_{ij}N_iB_j & (k=4) \\ \frac{\gamma_{ij}N_iB_j}{c_i+\gamma_{ij}N_iB_j} & (k=5) \\ \frac{(\gamma_{ij}N_iB_j)^2}{c_i+(\gamma_{ij}N_iB_j)^2} & (k=6). \end{cases} \tag{B.2}$$

The parameters $B_0 \equiv 1$ is the slope of the linear response and make it dimensionless. In turn, c_i control the toxins efficiencies in poison their competing species. All these response functions assume null thresholds for toxin effects, but those with $k = 2, 3, 5, 6$ impose saturation to the allelopathic suppression. Also, the response functions indexed by $k = 1, 2, 3$ involve the total toxin concentration, in contrast to those indexed by $k = 4, 5, 6$ for which only the absorbed toxins can induce responses. In the main text, we used only the three first response functions.

B.2 Statistical Metrics Concerning the Functional Responses $\Phi^{(1-3)}$

Tables B.1 and B.2 describe the main statistical traits and fitting parameters for the degree distributions shown in Figures 3.12 and 3.18 in Sections 3.3.1 and 3.3.1, respectively. In Table B.3 are listed the fitting parameters for clustering coefficients plotted in Figure 3.20, Section 3.3.1.

Functional Responses $\Phi^{(4-6)}$ - Only absorbed toxins contribute to mortality

Different functional responses of the Holling types *I*, *II*, and *III* were assumed if one considers that only the absorbed toxins can induce mortality. The qualitative behaviors for the cases SIE and BP are the same discussed in the Section 3.3.

SIE - dynamics						
	$\mu = 0.1$			$\mu = 0.5$		
	$\Phi^{(1)}$	$\Phi^{(2)}$	$\Phi^{(3)}$	$\Phi^{(1)}$	$\Phi^{(2)}$	$\Phi^{(3)}$
$\langle k_{in} \rangle$	49.56	16.51	49.50	4.23	1.55	1.71
$\langle k_{in}^2 \rangle$	2480.89	282.40	2474.28	21.62	3.21	3.91
κ_{in}	50.06	17.11	49.99	5.11	2.07	2.28
σ_{in}^2	24.46	9.93	24.39	3.71	0.81	0.98
σ_{in}	4.95	3.15	4.94	1.93	0.90	0.99
S_{in}	0.01	0.09	0.01	0.48	0.09	0.24
K_{in}	2.95	3.04	2.96	3.19	2.52	2.84
α_{in}	-	-	-	2.42	2.08	2.08
η_{in}	-	-	-	4.74	2.00	2.16

Table B.1: The statistical metrics and degree distribution exponents associated to Figure 3.12 (a) weak ($\mu = 0.1$) and (b) strong ($\mu = 0.5$) allelopathic effect in the Section 3.3.1: first moment ($\langle k_{in} \rangle$), second moment ($\langle k_{in}^2 \rangle$), ratio $\kappa_{in} = \langle k_{in} \rangle / \langle k_{in} \rangle$, variance ($\sigma_{in}^2$), standard deviation ($\sigma_{in}$), skewness ($S_{in}$), and kurtosis ($K_{in}$). The exponents of the Weibull degree distributions are α_{in}, η_{in}, and $\lambda = 0$.

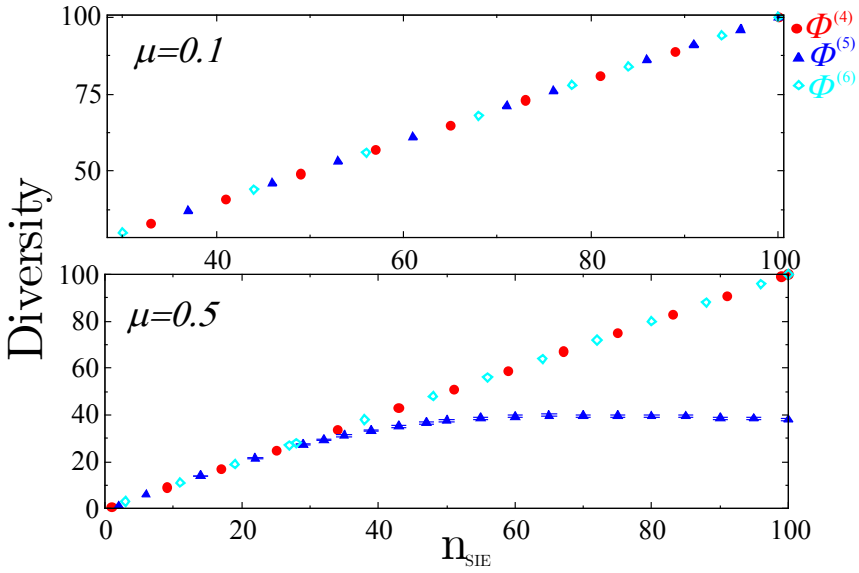

Figure B.1: Average diversity for 200 independent SIE dynamics observed after successive invasion events. The top and bottom plots refer, respectively, to weak ($\mu = 0.1$) and strong ($\mu = 0.5$) allelopathic effects using functional response (B.2) associated to $k = 4 - 6$. All the other model parameters are those used in Figure 3.10 in the Section 3.3.1.

BP - dynamics									
	Scenario 1			Scenario 2			Scenario 3		
	$\Phi^{(1)}$	$\Phi^{(2)}$	$\Phi^{(3)}$	$\Phi^{(1)}$	$\Phi^{(2)}$	$\Phi^{(3)}$	$\Phi^{(1)}$	$\Phi^{(2)}$	$\Phi^{(3)}$
$\langle k_{in} \rangle$	24.708	1.1820	33.678	0.0973	0.0630	0.0945	0.0057	0.0065	0.0120
$\langle k_{in}^2 \rangle$	986.80	7.8543	1583.9	0.3549	0.2115	0.3393	0.0098	0.0120	0.0240
κ_{in}	39.938	6.6450	47.032	3.6485	3.3559	3.5928	1.7177	1.8437	2.0045
σ_{in}^2	307.75	5.4427	438.20	0.3363	0.2036	0.3218	0.0097	0.0120	0.0237
σ_{in}	17.543	2.3330	20.933	0.5799	0.4513	0.5673	0.0987	0.1093	0.1539
S_{in}	1.1260	3.6365	0.5399	8.0924	9.5926	8.0661	23.063	22.437	17.634
K_{in}	3.5269	16.485	2.5337	78.885	109.56	77.693	686.27	637.12	404.13
α_{in}	-0.003	-0.256	-0.003	-0.174	-0.554	-0.174	1.2979	1.2979	1.5561
η_{in}	2.3×10^{-6}	6.1×10^{3}	2.95×10^{-6}	0.0781	0.0235	0.0721	3.8631	3.8631	3.8
λ_{in}	3.2322	2.4023	3.0922	1.8313	2.3828	1.9213	0.6732	0.6332	0.6288
$\langle k_{out} \rangle$	24.708	1.1820	33.978	0.0973	0.0630	0.0945	0.0057	0.0065	0.0120
$\langle k_{out}^2 \rangle$	1081.5	20.444	1562.6	0.3497	0.2091	0.3374	0.0120	0.0132	0.0303
κ_{out}	43.769	17.296	46.398	3.5948	3.3178	3.5724	2.1058	2.0210	2.5336
σ_{out}^2	398.14	17.934	416.91	0.3311	0.2012	0.3199	0.0120	0.0132	0.0300
σ_{out}	19.954	4.2349	20.418	0.5754	0.4486	0.5656	0.1094	0.1147	0.1732
S_{out}	1.1711	6.9845	0.5124	7.9691	9.7468	8.0706	27.668	24.588	20.377
K_{out}	3.3085	59.779	2.5701	75.755	115.03	78.005	996.94	769.22	517.63
α_{out}	-0.003	1.1398	-0.003	-0.174	0.5543	-0.104	1.5261	1.2979	1.5556
η_{out}	2.3×10^{-6}	5.4115	2.3×10^{-6}	0.0821	0.0236	0.0721	2.3826	3.8631	3.6
λ_{out}	3.2322	0.3241	3.1322	1.8313	2.3828	1.9213	0.6088	0.6332	0.6288

Table B.2: The main statistical traits and fitting parameters for the stretched exponential truncated by power law degree distribution: σ^2 - variance, σ - standard deviation, S - *skewness*, K - *kurtosis*, κ - ratio between first and second moments, and exponents α, η and λ in Figure 3.18 in the Section 3.3.1. Scenarios 1, 2 and 3 describe, respectively, (c) homogeneous, (d) competition heterogeneous, and (e) completely heterogeneous cases.

BP dynamic - scenario 1						
	α_{in}	η_{in}	λ_{in}	α_{out}	η_{out}	λ_{out}
$\Phi^{(1)}$	0.35089	3.8×10^{-7}	3.4822	0.3508	3.8×10^{-7}	3.4822
$\Phi^{(2)}$	-0.0039	7.2×10^{-6}	3.2822	0.7051	7.8×10^{-5}	3.48
$\Phi^{(3)}$	0.35080	3.8×10^{-7}	3.4822	0.3508	3.8×10^{-7}	3.4822
BP dynamic - scenario 2						
$\Phi^{(1)}$	-0.2856	1.7469	-0.215	0.3868	8.5×10^{-5}	4.5368
$\Phi^{(2)}$	0.00464	2.9×10^{-5}	5.0438	0.2745	6.5×10^{-5}	4.9179
$\Phi^{(3)}$	0.32646	2.9×10^{-5}	5.0438	-1.309	4.77605	-0.520
BP dynamic - scenario 3						
$\Phi^{(1)}$	17.2623	9.3354	0.9298	15.77	9.70117	0.8164
$\Phi^{(2)}$	15.7938	0.997452	2.0432	0.6339	1.98495	0.3803
$\Phi^{(3)}$	-1.0219	4.05067	7.9×10^{-8}	11.9773	7.7238	0.7703

Table B.3: The exponents of the clustering coefficient associated to Figure 3.20 presented in the Section 3.3.1. Scenarios 1, 2 and 3 describe, respectively, (a) homogeneous, (b) competition heterogeneous, and (c) completely heterogeneous cases. The parameters α, η, and λ are associated to stretched exponential truncated by power law degree distributions.

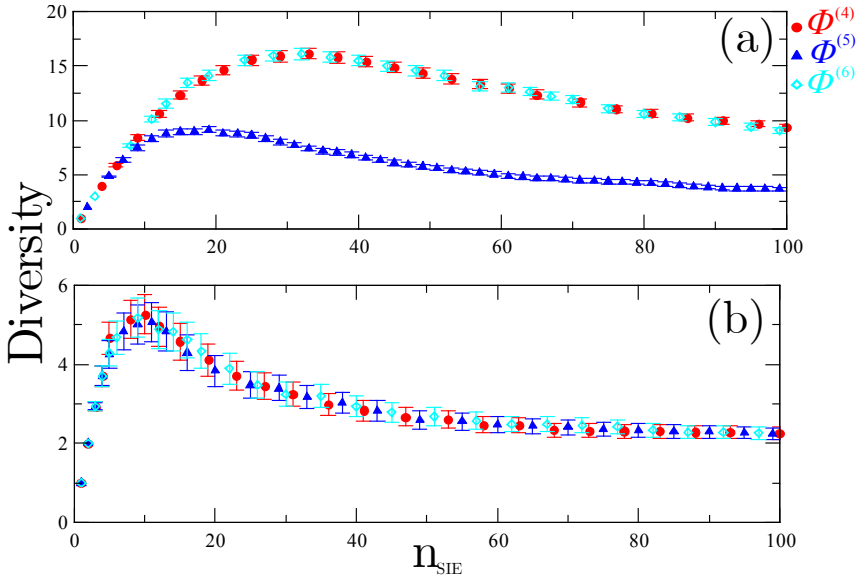

Figure B.2: Average diversity for 200 independent SIE simulations. In (a) only the competition coefficients are heterogeneous and the allelopathic traits are the same for all species. The value $\mu = 0.1$ was used (weak allelopathy). In (b) competition and allelochemical parameters are both heterogeneous, i.e., randomly chosen from uniform distributions in $(0, 1]$. All the other model parameters are those used in Figure 3.14 in the Section 3.3.1.

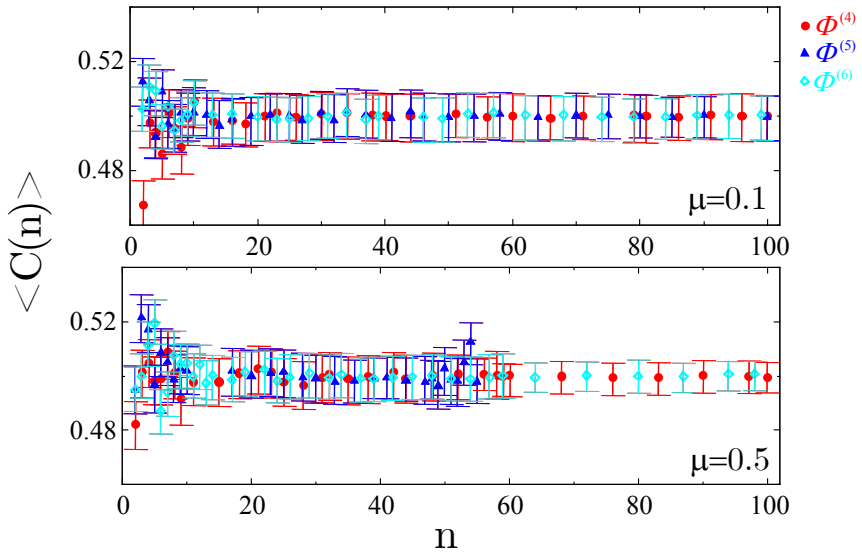

Figure B.3: Average network connectivity $C(n)$ in communities containing n species after a SIE using functional response (B.2) for $k = 4 - 6$. The results for weak ($\mu = 0.1$) and strong ($\mu = 0.5$) allelopathic suppression are shown in the top and bottom frames, respectively. All the other model parameters are those used in Figure 3.11 in the Section 3.3.1.

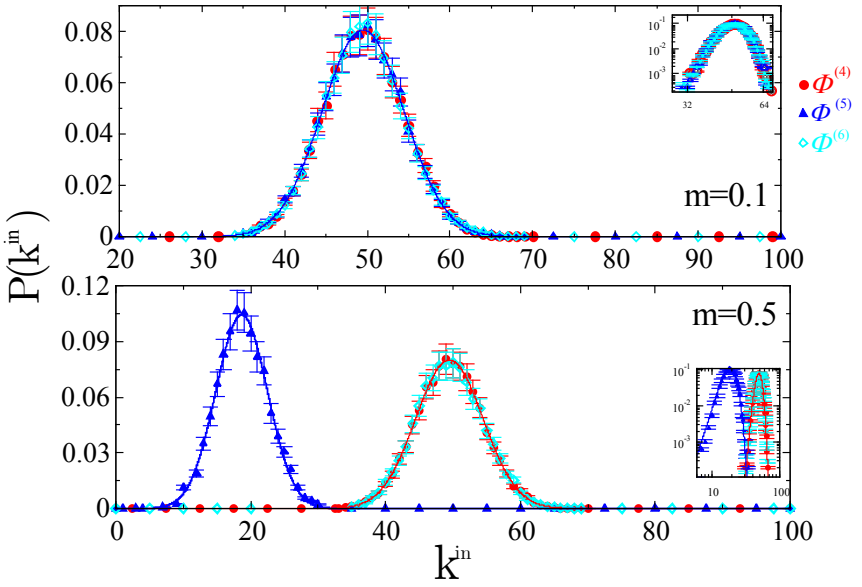

Figure B.4: Degree distribution $P(k^{in})$ for SIE allelochemical interaction networks in which the competition and allelochemical traits are the same for all species. The top and bottom frames correspond, respectively, to weak ($\mu = 0.1$) and strong ($\mu = 0.5$) allelopathic suppression using functional response (B.2) for $k = 4 - 6$. All curves were fitted by Gaussian distributions for which the parameters are listed in Table B.4. All the other model parameters are those used in Figure 3.12 in the Section 3.3.1.

SIE - dynamics						
	$\mu = 0.1$			$\mu = 0.5$		
	$\Phi^{(4)}$	$\Phi^{(5)}$	$\Phi^{(6)}$	$\Phi^{(4)}$	$\Phi^{(5)}$	$\Phi^{(6)}$
$\langle k_{in} \rangle$	49.51	49.47	49.49	49.47	18.84	49.46
$\langle k_{in}^2 \rangle$	2475.42	2471.23	2474.16	2472.12	369.59	2471.13
κ_{in}	50.00	49.96	49.99	49.97	19.62	49.97
σ_{in}^2	24.46	24.58	24.65	24.96	14.68	25.18
σ_{in}	4.95	4.96	4.97	4.99	3.83	5.02
S_{in}	0.00	0.00	0.04	0.01	0.17	0.03
K_{in}	2.97	2.99	3.12	2.98	3.03	2.95

Table B.4: Parameters of the Gaussian degree distributions associated to the Figure B.4: first moment ($\langle k_{in} \rangle$), second moment ($\langle k_{in}^2 \rangle$), ratio $\kappa_{in} = \langle k_{in} \rangle / \langle k_{in} \rangle$, variance ($\sigma_{in}^2$), standard deviation ($\sigma_{in}$), skewness ($S_{in}$), *and kurtosis* ($K_{in}$).

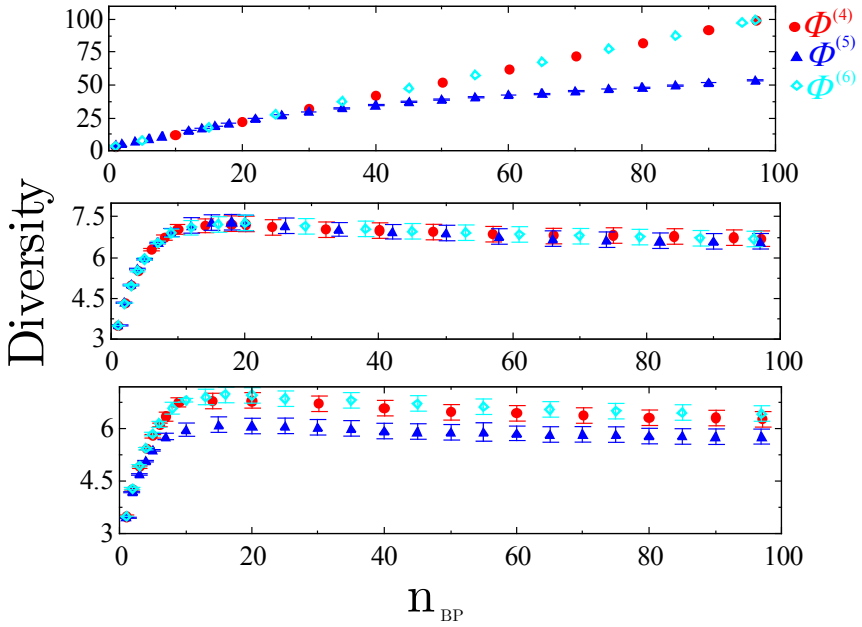

Figure B.5: Average diversity for 200 independent BP eco-evolutionary histories as function of the number n of speciation events. The top, middle, and bottom plots refer, respectively, to homogeneous, heterogeneous competition, and completely heterogeneous (both competition and allelopathy) scenarios. All model parameters are those used in Figure 3.16 in the Section 3.3.1.

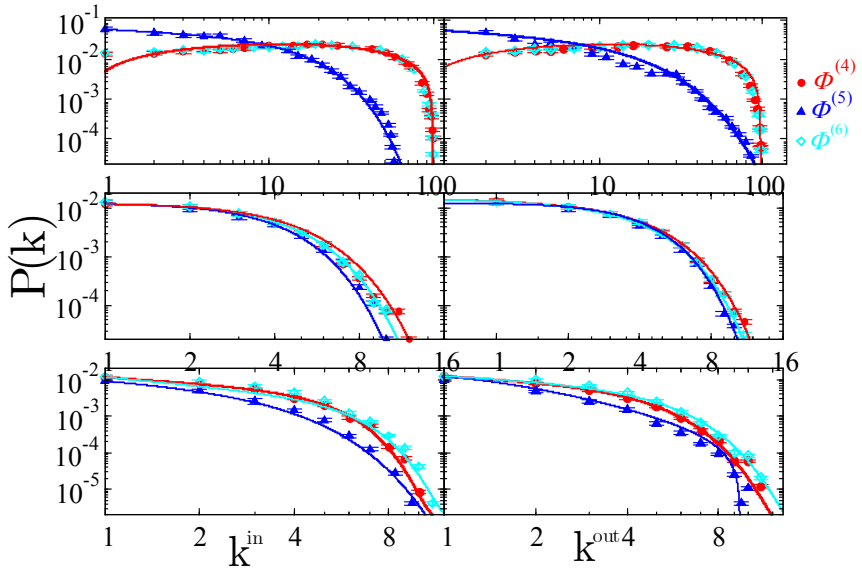

Figure B.6: In- and out-degree distribution functions for directed allelochemical networks generated by BP dynamics (see figure 1 in the main text) averaged over 200 independent simulations. The top, middle, and bottom plots refer, respectively, to homogeneous, heterogeneous competition, and completely heterogeneous scenarios. All curves were fitted by stretched exponentially truncated power laws, whose parameters are described in Table B.5. All model parameters are those used in Figure 3.18 in the Section 3.3.1.

BP - dynamics									
	Scenario 1			Scenario 2			Scenario 3		
	$\Phi^{(4)}$	$\Phi^{(5)}$	$\Phi^{(6)}$	$\Phi^{(4)}$	$\Phi^{(5)}$	$\Phi^{(6)}$	$\Phi^{(4)}$	$\Phi^{(5)}$	$\Phi^{(6)}$
$\langle k_{in} \rangle$	33.217	4.3402	33.326	0.1135	0.0900	0.1130	0.0771	0.0397	0.0972
$\langle k_{in}^2 \rangle$	1526.6	89.466	1549.1	0.4367	0.3618	0.4243	0.2702	0.1156	0.3586
κ_{in}	45.959	20.614	46.485	3.8495	3.6541	3.7571	3.5058	2.9125	3.6905
σ_{in}^2	412.71	59.941	427.41	0.4115	0.3426	0.3995	0.2585	0.1125	0.3401
σ_{in}	20.315	7.7422	20.674	0.6415	0.5853	0.6321	0.5084	0.3354	0.5832
S_{in}	0.5736	4.3968	0.5524	7.6293	7.8797	7.5071	8.8479	11.563	8.0466
K_{in}	2.6555	26.217	2.5594	70.316	73.129	66.956	93.965	163.37	77.356
α_{in}	0.1127	-0.213	0.1127	0.0465	0.0465	0.0465	-0.564	-0.548	0.7940
η_{in}	0.1466	0.0223	0.1466	0.0707	0.0707	0.0707	0.0083	0.1448	0.0058
λ_{in}	0.3359	1.4075	0.3359	1.8244	1.9944	1.8944	2.8798	1.6679	2.8799
$\langle k_{out} \rangle$	33.217	4.3402	33.326	0.1135	0.0900	0.1130	0.0771	0.0397	0.0972
$\langle k_{out}^2 \rangle$	1513.9	142.06	1543.9	0.4315	0.3561	0.4253	0.2664	0.1154	0.3565
κ_{out}	45.578	32.732	46.328	3.8033	3.5968	3.7638	3.4563	2.9066	3.6691
σ_{out}^2	400.62	110.58	422.81	0.4063	0.3369	0.4003	0.2547	0.1123	0.3380
σ_{out}	20.016	10.516	20.562	0.6374	0.5804	0.6327	0.5047	0.3351	0.5814
S_{out}	0.5290	3.8870	0.5417	7.6510	7.8119	7.5391	8.9649	11.696	8.0659
K_{out}	2.5910	17.345	2.5603	70.640	71.975	67.914	97.647	168.74	78.155
α_{out}	0.1127	-0.214	0.1127	-0.093	0.0465	-0.093	-0.441	-3.096	-0.441
η_{out}	0.1466	0.0613	0.1466	0.0772	0.0674	0.0797	0.0397	4.5106	0.0317
λ_{out}	0.3359	1.0675	0.3359	1.8322	1.9944	1.8322	2.1392	-0.531	2.1393

Table B.5: Parameters of the stretched exponentially truncated power law degree distributions associated to the Figure B.4: first moment ($\langle k_{in} \rangle$), second moment ($\langle k_{in}^2 \rangle$), ratio $\kappa_{in} = \langle k_{in} \rangle / \langle k_{in} \rangle$, variance ($\sigma_{in}^2$), standard deviation ($\sigma_{in}$), skewness ($S_{in}$), and kurtosis ($K_{in}$). Also, the exponents α, η and λ fitting such distributions are listed. Scenario 1, 2 and 3 describe, respectively, (a) completely homogeneous, (b) competition heterogeneous, and (c) completely heterogeneous.

BP dynamic - scenario 1						
	α_{in}	η_{in}	λ_{in}	α_{out}	η_{out}	λ_{out}
$\Phi^{(4)}$	0.1508	1.4×10^{-7}	3.6622	0.1508	1.4×10^{-7}	3.6822
$\Phi^{(5)}$	0.0351	3.8×10^{-7}	3.6222	0.3508	6.2×10^{-7}	3.8222
$\Phi^{(6)}$	0.1508	1.4×10^{-7}	3.6622	0.1508	1.4×10^{-7}	3.6862
BP dynamic - scenario 2						
$\Phi^{(4)}$	-0.289	1.7169	-0.2148	0.3868	8.5×10^{-5}	4.3368
$\Phi^{(5)}$	-0.296	1.7189	-0.2148	0.3868	8.5×10^{-5}	4.5368
$\Phi^{(6)}$	-0.285	1.7469	-0.2148	0.3868	8.5×10^{-5}	4.4368
BP dynamic - scenario 3						
$\Phi^{(4)}$	0.3867	1.1×10^{-4}	4.5368	-0.0697	1.1×10^{-4}	4.4368
$\Phi^{(5)}$	-0.069	1.1×10^{-4}	4.6368	-0.0697	1.1×10^{-4}	4.8368
$\Phi^{(6)}$	0.3868	8.5×10^{-5}	4.4368	-0.0697	1.1×10^{-4}	4.1368

Table B.6: The exponents α, η, and λ fitting the clustering coefficient distributions associated to Figure (B.7).

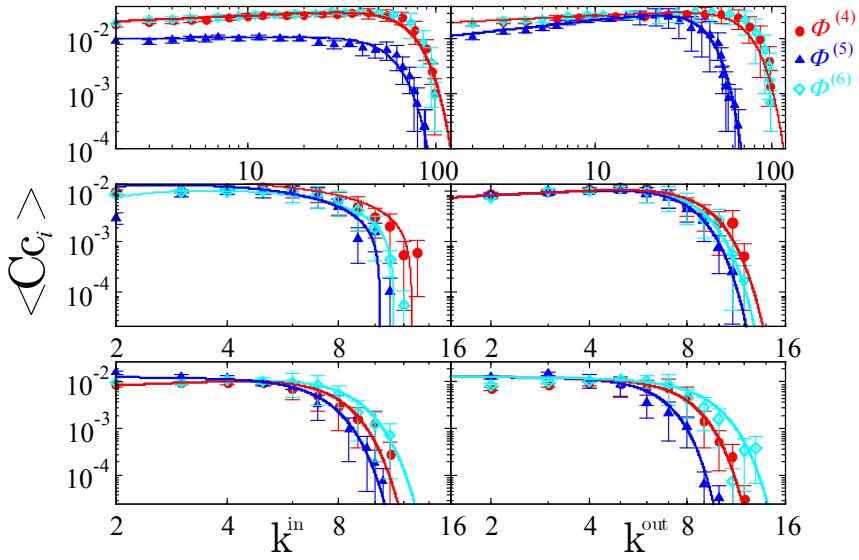

Figure B.7: Average local clustering coefficients as function of in- and out-degrees. These distributions were fitted using power law truncated by stretched exponential. The fitting parameters are listed in Table B.6. The top, middle, and bottom plots correspond to the homogeneous, heterogeneous competition, and completely heterogeneous scenarios, respectively. All model parameters are those used in Figure 3.20 in the Section 3.3.1.

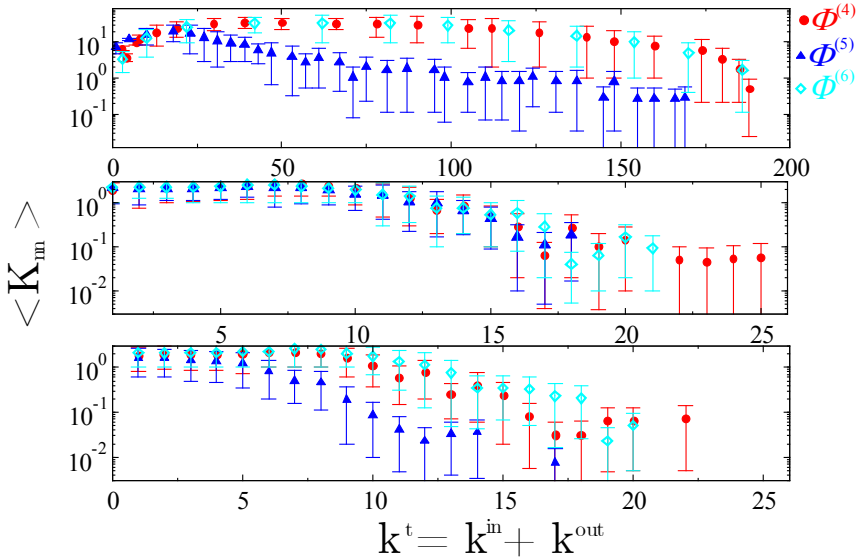

Figure B.8: Average nearest neighbours degree $K_{nn}(k)$ of a node with total degree k^t for the homogeneous (top), heterogeneous competition (middle), and completely heterogeneous (bottom) scenarios, respectively. The model parameters are those used in Figure 3.22 in the Section 3.3.1.

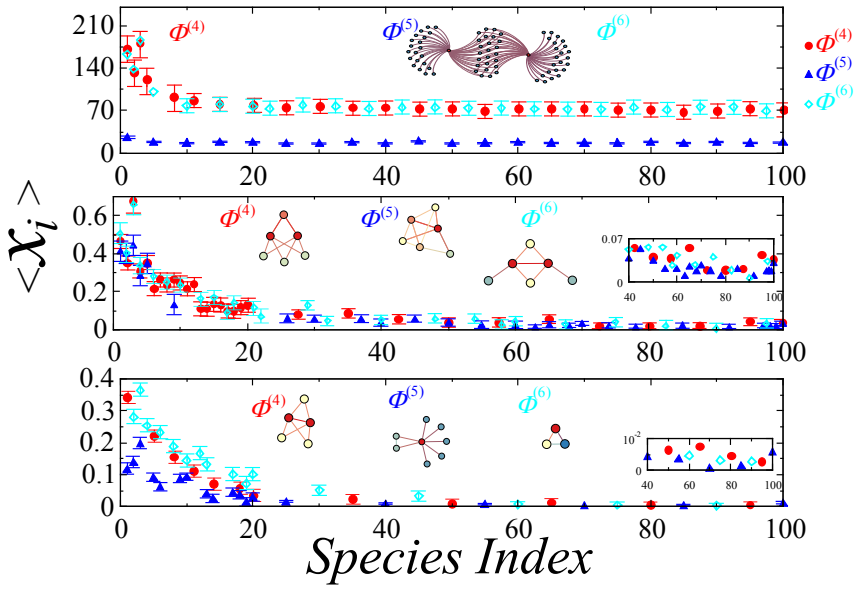

Figure B.9: Average betweenness centrality for each node (surviving species) in communities generated after 100 BP events starting from the initial graphs shown at Figure 3.9 in the Section 3.3.1. 200 independent simulations were performed for each initial graph. (a) homogeneous, (b) competition heterogeneous, and (c) completely heterogeneous scenarios. The model parameters are those used in Figure 3.17 in the Section 3.3.1.

Appendix C

Pattern Formation in Allelopathic Species Communities

In this Appendix the role played by cyclic dominance in allelochemical scenario is briefly reported. The networks of cyclic chemical interactions and its matrices of mortality are shown in Figure C.1 for communities with 4, 7 and 9 species. Qualitative changes in the dynamics emerge in communities with an even number of species.

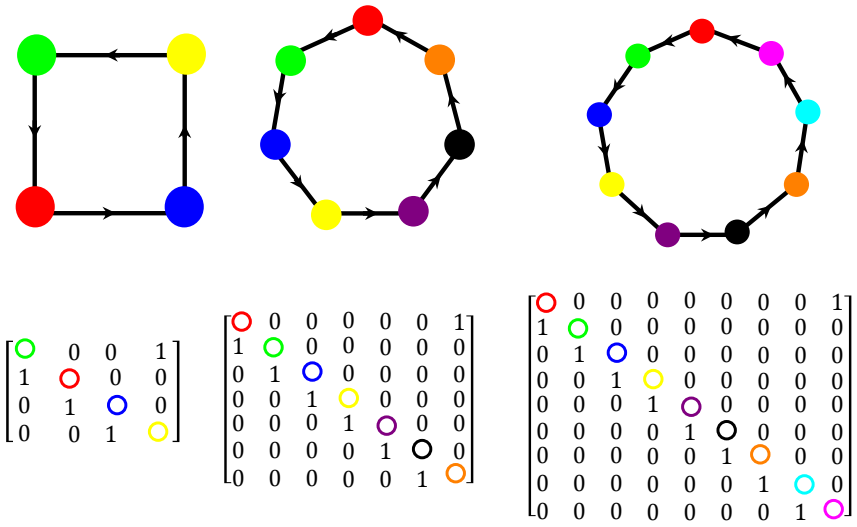

Figure C.1: Allelochemical networks used in our model with cyclic interactions. All graphs with, respectively, a) 4, b) 7, c) 9 species were tested. In special, the graphs highlight generalizations of interactions of cyclic dominance (rock-paper-scissor game) of three species (N_1 - • - outperforms N_2 - •, N_2 poisons N_3 - •, and N_3 in turn dominates over N_1. In all cases, arrows point from suppressor to suppressed.

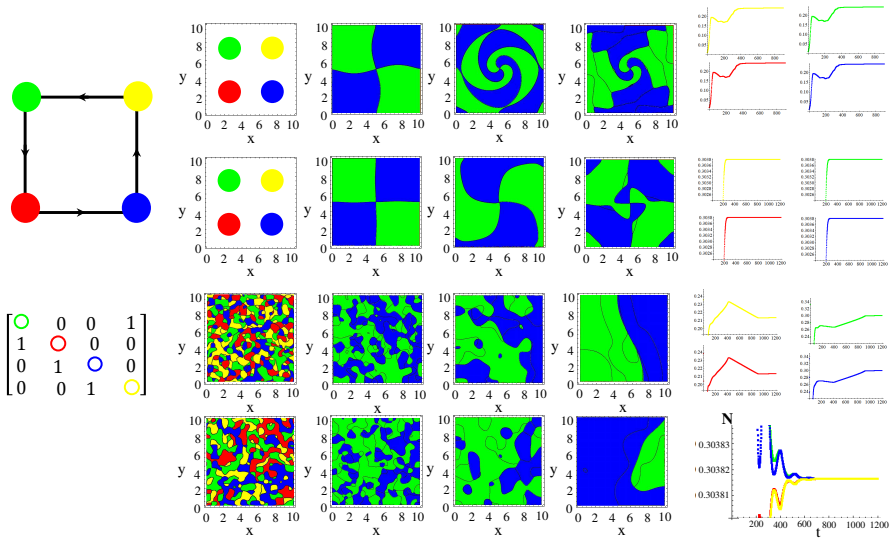

Figure C.2: Four species competing for resources and with cyclic allelochemical suppressions. (A1) Schematic illustration of four-species allelochemical warfare. Arrows point from suppressors to suppresseds. (A2) The allelochemical interaction matrix associated to the graph in (A1). The initial populations are spatially distributed either regularly in single, disjunct, isolated, and circular patches (B1,B2) or randomly in adjacent, disjunct but disordered patches (B3,B4). The corresponding spatial distributions of the species at three distinct times are shown for each initial condition. The different colors indicate the locally dominant species. The evolution in time of the population densities are shown in (C1C4). The results in (B1,C1) and (B3,C3) refer to response functions dependent on the local concentration of allelochemicals, whereas those in (B2,C2) and (B4,C4) are for responses only to locally uptaken toxins. The competition and allelochemical traits are the same for all species. Their values were fixed in $D = 0.005$ (small diffusivities), $r = 0.3$, $\nu = 0.5$, $\mu = 0.4$ (high allelopathy), $\beta = 0.5$, $\delta = 0.1$, and $\gamma = 0.1$. Null-Dirichlet boundary conditions were considered.

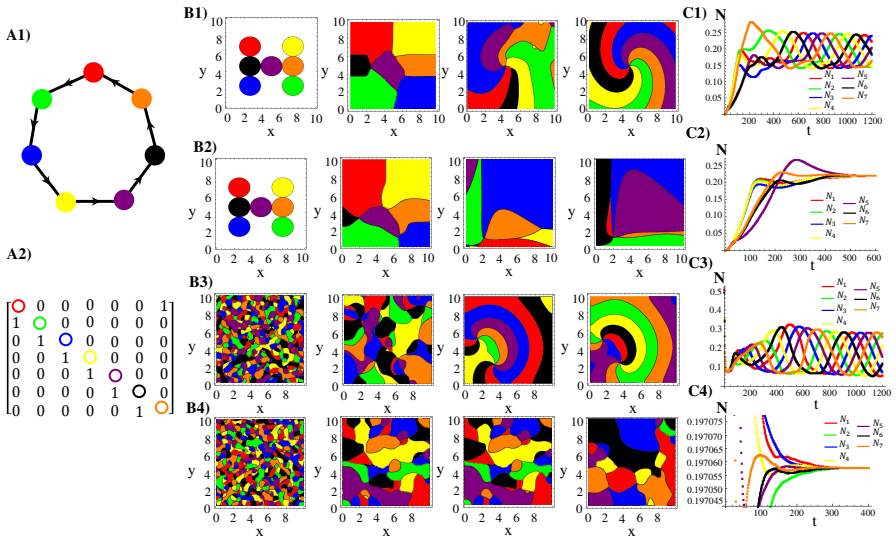

Figure C.3: The same of Figure C.2 but considering 7 species.

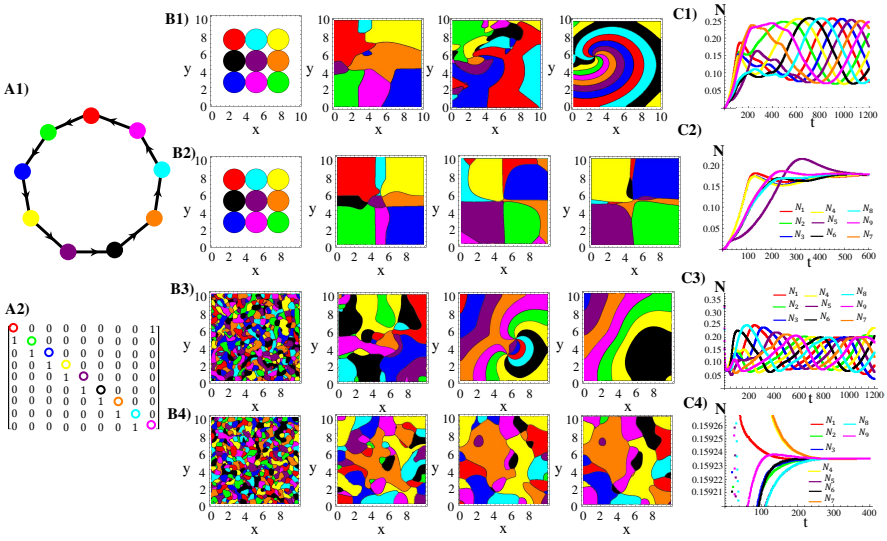

Figure C.4: The same of Figure C.2 but considering 9 species.